Dynamics and Thermodynamics of the Arabian Sea Warm Pool

Thesis submitted to the

COCHIN UNIVERSITY OF SCIENCE AND TECHNOLOGY

in partial fulfilment of the degree of

DOCTOR OF PHILOSOPHY IN MARINE SCIENCE

under the

FACULTY OF MARINE SCIENCES

by

P. SABU, M.Sc, B.Ed

NATIONAL INSTITUTE OF OCEANOGRAPHY

REGIONAL CENTRE, KOCHI-682018

January 2009

Certificate

I hereby certify that the thesis entitled "**Dynamics and Thermodynamics of the Arabian Sea Warm Pool**" submitted by P.Sabu, Research Scholar (Reg. No. 2733), National Institute of Oceanography, Regional Centre, Kochi -18, is an authentic record of research carried out by him under my supervision, in partial fulfilment of the requirement for the Ph.D degree of Cochin University of Science and Technology in the faculty of Marine Sciences and that no part thereof has previously formed the basis for the award of any degree, diploma or associateship in any university.

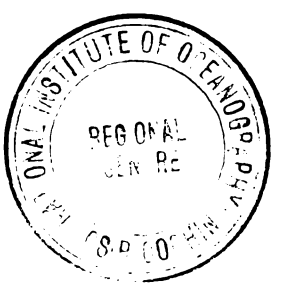

Kochi-18
19.01.2009

Dr. C. Revichandran
Supervising Guide, Scientist
National Institute of Oceanography
Regional Centre, Kochi-18
Kerala, India.

Declaration

I hereby declare that the thesis entitled "**Dynamics and Thermodynamics of the Arabian Sea Warm Pool**" is an authentic record of the research carried out by me, under the supervision of Dr. C. Revichandran, Scientist, Regional Centre of National Institute of Oceanography, Kochi - 18, in partial fulfilment of the requirement for the Ph.D degree of the Cochin University of Science and Technology in the faculty of Marine Sciences and that no part of this has been presented before for any other degree, diploma or associateship in any university.

Kochi-18
19.01.2009

(P. Sabu)

Acknowledgement

I am deeply indebted to my supervising guide Dr. C. Revichandran, Senior Scientist, National Institute of Oceanography, Regional Centre, Kochi for his guidance and constant encouragement, which enabled me to complete this thesis. Without his support and scientific advices this thesis would not have materialized.

I am thankful to the Director, National Institute of Oceanography, Goa for providing the facilities during the study. I am indebted to Dr. N. Bahulayan, Scientist - in - Charge, National Institute of Oceanography, Regional Centre, Kochi for providing me with a conducive working environment.

My sincere gratitude to the Director and staff of Centre for Marine Living Resources and Ecology (CMLRE), Kochi, for the financial and scientific support to the national programme 'Marine Research - Living Resources (MR - LR) Assessment' to which the present thesis is associated.

I express my sincere thanks to Dr. Vinu. K. Valsala, National Institute of Environmental Studies, Tsukuba, Ibaraki, Japan for his help and suggestions. I sincerely thank Dr. K. K. Balachandran, Technical Officer, NIO RC Kochi for his immense help and support.

I record my sincere thanks to all scientific and administrative staff of National Institute of Oceanography, Regional Centre, Kochi for their help and co-operation during the study. On this occasion, I thankfully recollect the moral and scientific support given my friends and colleagues during this study.

My deep sense of gratitude and love to my mother, brothers for their immense support and encouragement at all times. I thank my wife and son for their inspiration and moral support.

The financial support from Council of Scientific & Industrial Research (CSIR) as senior research fellowship is greatly acknowledged. Last but not the least, I thank each and every person who had directly or indirectly helped me to complete this thesis in time.

Most importantly, I thank Almighty God for His blessings throughout my life that enabled me to fulfil this endeavour.

P. Sabu

List of Abbreviations

AS	Arabian Sea
ASWP	Arabian Sea Warm Pool
ARMEX	Arabian Sea Monsoon Experiment
ASHSW	Arabian Sea High Salinity Water
AVISO	Archiving, Validation and Interpretation of
Satellite	Oceanographic Data
BL	Barrier Layer
BOBMEX	Bay of Bengal Monsoon Experiment
BoB	Bay of Bengal
CGCM	Coupled Ocean Circulation Model
CTD	Conductivity Temperature and Depth
EICC	East India Coastal Current
GM	Great Whirl
ILD	Isothermal Layer Depth
IOWP	Indian Ocean Warm Pool
IPWP	Indo-Pacific Warm Pool
KPP	K-profile parameterization
LH	Lakshadweep High
LL	Lakshadweep Low
ML	Mixed Layer
MLD	Mixed Layer Depth
MONEX-79	MONsoon Experiment
MSLA	Maps of Sea Level Anomaly

NCEP/NCAR	National Centre for Environmental Prediction/ National Centre for Atmospheric Research
NEAS	North Eastern Arabian Sea
NetCDF	Network Common Data Form
SEAS	Southeastern Arabian Sea
SLA	Sea Level Anomaly
SSS	Sea surface Salinity
SST	Sea Surface Temperature
TI	Temperature Inversion
TMI	Tropical Rainfall Measuring Mission/TRMM Microwave Imager
WICC	Winter Monsoon Current
WOA01	World Ocean Atlas 2001
WOA05	Wolrd Ocean Atlas 2005
XBT	eXpendable Bathy Thermograph

Contents

****

Chapter 1

Introduction

Contents

Indian Ocean is an ideal region to study the air-sea and land-sea interactions due to its small size and unique geographical location. This tropical basin, bounded in the north, comes under the influence of seasonally reversing monsoon winds that makes it unique among the world oceans. The most important climate system over the Indian Ocean region is the southwest monsoon (SWM), which evolves through the active interactions between land, atmosphere and ocean. Variations in the SWM and associated rainfall have a significant influence on the life and economy of tropical countries. The heating of the sea surface in the Indian Ocean is very important for the onset and subsequent evolution of the SWM (Webster et al., 1998). Hence, a comprehensive study on the evolution of the ocean thermal structure is necessary to understand the air-sea interaction in this region and eventually to predict the SWM.

Sea Surface Temperature (SST) is the most important oceanic parameter which controls the air-sea interaction processes. In tropical Oceans SST is of prime importance for driving the evolution of summer monsoon (Godfrey et al., 1995). The warming of the southeastern Arabian

Sea (SEAS) during pre-monsoon is important for the onset and advance of SWM along the western parts of India (Vinayachandran et al., 2007b). The variations in the warming of SST determines the intensity of the monsoon on seasonal to interannual time scales. Also, the warming of surface waters greatly influence the biosphere, especially the coral reefs (Doval and Hansell, 2000; Abram et al., 2003; Borgne et al., 2002; Sarma, 2006). Considering the location of the warm pool around Lakshadweep Sea (LS), the effect of thermal variation on the coral reefs and biological production seems to be crucial. Thus, it will be quite invoking to identify the causative factors for warming of the SEAS. studies conducted in the SEAS could not explain the processes behind the formation of warm pool. Recently, there has been an increased interest in understanding the role of different oceanic processes in the onset of southwest monsoon (Anonymous, 2001). The present thesis examines the dynamics and thermodynamics of the SEAS using observational and satellite data.

Large areas of warmer waters (SST > 28°C), in the surface layers of the tropical oceans strongly influence the development of depressions, cyclones, El-Nino/La-Nina, Indian Ocean Dipole and other oscillations ranging from 2-6 days and 30-60 days (Lau and Chan, 1988; Webster and Lukas, 1992; Godfrey et al., 1995; Saji et al., 1999). Thus, the 'warm pool' have special place in the context of tropical weather and climate. The largest and best studied warm pool is the Indo-Pacific warm pool.

1.1 Indo-Pacific warm pool

A large portion of tropical ocean with SST >28°C lies in the western Pacific and the eastern Indian Oceans, which is popularly known as Indo-Pacific Warm Pool (IPWP, Fig1.1). Studies shows that, it is a region of deep

atmospheric convection (Lau and Chan, 1986; Ardanuy et al., 1987), convergence of surface winds (Rasmusson and Carpenter, 1982) and high precipitation (Taylor, 1973; Weare et al., 1981). During the ElNino years, the warm pool is found to migrate towards the east by about 4000 km. Also, the SST over this region (120°-160°E; 5°-15°S) was found to be positively correlated to the Indian summer monsoon rain fall (Nicholls, 1983). The Pacific component of IPWP has been extensively studied in the TOGA-COARE (Tropical Ocean-Global Atmosphere-Coupled Ocean-Atmosphere Experiment) field program (Webster and Lukas, 1992), Godfrey et al., 1998)), which enhanced our understanding of the air-sea coupling processes in the west pacific. Compared to the Pacific counter part, the Indian Ocean component of IPWP has received little attention.

1.2 Indian Ocean warm pool

Considerable area of the tropical Indian Ocean with SST> 28°C is termed as Indian Ocean Warm Pool (IOWP). It includes the equatorial region east of 50° E, the Bay of Bengal and the eastern Arabian Sea. The IOWP is established over the northern Indian Ocean during May (SST>30°C, Fig.1.2g), which is highest anywhere in the world oceans. The Arabian Sea (AS), attains higher (28°C or above) SST during February–April and remains as the warmest spot in the northern Indian Ocean (Fig.1.2 d, e and f). This warm SST patch in the SEAS has been called as "mini warm pool" by Rao and Sivakumar (1999) and "SST High" by Shenoi et al. (1999b). In the present study, this high SST (>29.8°C) in the SEAS referred as Arabian Sea warm pool (ASWP).The warming over this region starts in February (Fig.1.2d), intensifies during March (Fig.1.2e), and reaches its peak during April–May (Figs.1.2f and g). During May, the ASWP merges with the larger IOWP and maintains

SSTs>30°C (Fig.1.2g).The strong winds during the onset and progress of SWM lowers the SST below 28°C over major part of the Arabian Sea (Fig.1.2h).

1.3 The Monsoon Onset Vortex and Arabian Sea SST

The warming of SST in the Arabian pre-monsoon during (March–May) Sea significantly affect the monsoon variability (Joseph and Pillai, 1984; Rao and Goswami, 1988; Yang and Lau, 1998; Clark et al., 2000; Li et al., 2001). The warm pool in the SEAS has a critical impact on the monsoon onset over the peninsular India during late May or early June. The cyclonic circulation associated with onset of southwest monsoon over the peninsular India is termed as "monsoon onset vortex" (Ananthakrishnan et al., 1968, Krishnamurti et al., 1981 and Vinayachandran et al., 2007b). The onset vortex forms a region of convergence over the SEAS, and in turn brings sustained rainfall over Kerala. In addition, the onset vortex also accelerate the northward advance of southwest monsoon over India. Seetaramayya and Master (1984), observed a patch of warm waters (>30.5°C) in the SEAS, one week before the formation of onset vortex during MONEX-79 (MONsoon EXperiment 1979). Kershaw (1985, 1988) has used this MONEX-79 data in an atmospheric model to show that the observed SST anomalies are useful for the prediction of the onset vortex formation (depression) rather than simulations with climatological SSTs. These studies have provided a relation between SST and monsoon onset in the SEAS. Rao and Sivakumar (1999) found a distinct correspondence between maximum SST in the SEAS and the genesis of onset vortex. Shenoi et al. (1999b) have argued that the warming of the SST in the SEAS is one of the conditions for the formation of onset vortex. Recent studies using a model (Masson et al., 2005), satellite as well as Reanalysis datasets

(Deepa et al., 2007) also suggest a relation between onset vortex and the SEAS SST. While the warm SST patch invariably forms every year, the onset vortex does not show any such regularity (Rao and Sivakumar, 1999; Deepa et al., 2007). The complex air-sea interaction associated with the formation of onset vortex are yet to be understood.

1.4 Geographic location and Characteristics of the study Area

The SEAS, the southern part of the west coast of India experiences seasonal reversal of winds and consequently, the upper layers exhibit different oceanographic characteristics. The monsoonal winds over the AS forces spectacular seasonal variations, particularly in the reversal of boundary currents and occurrence of seasonal upwelling/downwelling. During SWM, known as the Findlater jet (Findlater, 1969) extend from the African coast to India (Ratnagiri, Fig 1.3a). Seaward of the wind jet, the wind speed decreases causes negative wind-stress curl, which drives the strong Ekman pumping. Ekman convergence is dominant towards the southeast of the Findlater jet while the Ekman divergence in the northeast leads to upwelling (Bauer et al., 1991). Thus the along shore wind stress and wind stress curl (local forcings) are responsible for the occurrence of upwelling through Ekman dynamics. The upwelling first appears in the southern tip of India and progressively advances poleward in association with the northward propagating upwelling coastal Kelvin waves during the premonsoon season with a maximum off Kochi (McCreary et al., 1993; Shankar and Shetye, 1997).

With the onset of the southwest monsoon, boundary currents along the AS are reversed. The circulation in the interior AS is mainly characterized by large scale Ekman drift, which is westward during winter

and eastward during spring and summer monsoon seasons (Tomczak and Godfrey, 2001). An oceanic gyre (the monsoonal gyre) does occur in the AS basin (Schott, 1983). Two anticyclonic eddies, the Great whirl (GW) and the Socotra Eddy (SE) develop during this period (Figure 1.3b). The north equatorial current (NEC) is replaced by much stronger eastward flowing Indian Monsoon Current (IMC). Shetye and Shenoi (1988) compared the long shore wind stress and ship drift data along the west coast of India and found that during SW monsoon, the local winds drive the surface circulation. The surface currents along the west coast of India during the SW monsoon is towards the equator, which shallows the thermocline depth towards the coast (Shetye et al., 1990). During the SWM, close to the coast, the sea level anomaly is negative termed as Lakshadweep Low (Shankar and Shetye, 1997). The Lakshadweep Low (LL) shifts westward and dissipates during the later part of the summer monsoon.

During the northeast monsoon (November-February), the winds in the SEAS are generally northeasterly (Fig.1.3c). But, the coastal currents flow poleward along the west coast of India, which is peculiar because most of the eastern boundary currents normally change with the winds (Mittelstaedt, 1986). The collapse of the southwest monsoon winds trigger downwelling of coastal Kelvin waves that radiate along the Bay of Bengal. The Kelvin waves, on reaching the western Bay, force an equatorward East India Coastal Current (EICC), which turns around Sri Lanka to reach the west coast of India and flows poleward as the West India Coastal Current (WICC, Fig 1.3d). The EICC and WICC carry low salinity waters from the Bay of Bengal (BoB) into the SEAS during December-February. The intrusion of low-salinity water leads to strong

salinity stratification and development of a barrier layer (BL, layer between mixed layer and isothermal layer) in the SEAS (Rao and Sivakumar, 1999; Shenoi et al., 1999b, 2004). The vertical distribution of temperature in the SEAS also shows inversions (higher subsurface temperature than that at surface) during December–February (Thadathil and Ghosh, 1992; Shankar et al., 2004; Gopalakrishna et al., 2005; Shenoi et al., 2005a). The circulation in the SEAS during this period is anticyclonic around a high in sea level, known as the Lakshadweep High (LH, Bruce et al. (1994); Shankar and Shetye (1997)). The anticyclonic eddies, which develop in the SEAS during December, propagate westward during following months (Bruce et al., 1994; Shankar and Shetye, 1997). These eddies modify the hydrography of the region through downwelling, and play an important role in the redistribution of advected low-salinity water within the SEAS. The seasonally reversing coastal and equatorial currents present in and around SEAS (Shetye et al., 1991a; Schott and McCreary, 2001; Shankar et al., 2002) also have a major contribution in setting up the hydrography through the advection and redistribution of cold low-salinity water.

1.5 Earlier Studies

Using satellite derived weekly SST (Reynolds and Smith, 1994) for 1989, and weekly climatology, Shenoi et al., (1999b) have described the seasonal cycle of the ASWP. A blob of high SST (28.5°C) appears in the SEAS during early March, which is distinct from the larger IOWP. The localized patch of high SST warms up further during March-April and merges with the larger IOWP. However, the SST high retains its identity and maintains a SST about 0.5°C higher than surroundings. Moreover, the

SST high has its core (>30°C) in the Lakshadweep Sea during last week of May.

Shenoi et al. (1999b) argued that the downwelling associated with LH (Bruce et al., 1994; Shakar and Shetye et al., 1997) and the low salinity water in the surface layer provides the necessary background for the warming of sea surface, leading to the formation ASWP. They have observed a patch of low latent heat loss in the SEAS during January-February 1989 from the NCEP/NCAR (National Center for Environmental Prediction/ National Centre for Atmospheric Research) reanalysis data set. This patch disintegrates during March, when the blob of high SST and the latent heat loss increase in the SEAS during April. In addition, the net shortwave radiation is high along the Indian west coast during February, spread over a much larger area including SEAS, which was not present during March-April. Based on this, Shenoi et al., 1999b concluded that the salinity stratification and the barrier layer formation are the primary reasons for the development and growth of ASWP. It is worth mentioning here that, Air-sea fluxes are not the primary reason for the formation of ASWP.

Rao and Sivakumar (1999), using climatological datasets, have also showed salinity stratification to be an important factor in the formation of ASWP. They found that strong near surface stratification leads to shallow mixed layer and consequently, the net heat flux is distributed over a thin water column, resulting in the formation of warm pool. Their heat budget analysis showed that the net surface heat flux and horizontal advection are important factors. These two studies show that strong stratification and resulting BL are the reasons for the formation of the warm pool in the SEAS.

Sanilkumar et al. (2004) showed that the horizontal extent of the warm pool is controlled by the low salinity waters, while its vertical extent and stratification is controlled by the intensity of heating and thickness. The positive net heat flux in the AS results in net heat accumulation in the SEAS.

Thermal inversion (TI), where the subsurface waters are warmer is occurring at different parts of the world ocean. Inversions forming below the mixed layer (ML) can warm the overlaying water and deepen the isothermal layer depth (Smyth et al., 1996). TI's are a stable winter (December–February) features of the SEAS (Thadathil and Ghosh, 1992). The Arabian Sea Monsoon Experiment (ARMEX) observations (Durand et al., 2004; Shankar et al., 2004; Shenoi et al., 2005a; Gopalakrishna et al., 2005) have provided a larger picture of spatio–temporal evolution of TI. Based on the observations during ARMEX and a model study, Durand et al. (2004), Shankar et al. (2004) and (Shenoi et al., 2005a) have argued that the heating from subsurface lead to the formation of ASWP. According to Durand et al. (2004), the vertical processes (entrainment, mixing and vertical advection) heat mixed layer in the SEAS by 1.1°C during November–March, whereas the atmospheric forcing cools it by 0.3°C. The warming by vertical processes reaches its peak (0.4°C/month) during mid-January to mid-February. By the end of January, heating from vertical processes dominates over the cooling from atmospheric forcing, and results in a net heating of the mixed layer. They have argued that the heating via TI can explain the early appearance and warming of SST in the SEAS. According to this hypothesis, the ocean plays an active role in the formation of ASWP.

The Coupled General Circulation Model (CGCM) study by Masson et al. (2005), has not considered any contribution from TI to the warming of mixed layer. Their model has shown the maximum effect of BL on the SEAS SST (0.5°C) only in April, two months after the peak in BL thickness. The CGCM results have also shown an increase in precipitation (3 mm/day) during May, and an early (10–15 days) monsoon onset. Their salinity and mixed layer depth simulations are in poor agreement with observations, where the model had a coarse horizontal resolution of 2°C.

An Indian Ocean model of MOM4 (Modular Ocean Model version 4), suggested that salinity stratification is not responsible for the formation of ASWP (Kurian and Vinayachandran, 2007). They found that the contribution from temperature inversions to the warming of the SEAS is negligibly small. They re-examined the surface fluxes and found a low latent-heat flux over the SEAS during the winter monsoon to be responsible for the warming. The winds are blocked by the Western Ghats and consequently the latent heat loss over the SEAS is much lower than its surroundings, leading to the warming during February- March. The inter-annual variability of SST over the SEAS is mostly driven by the year-year variability of ocean-atmosphere fluxes.

Kumar et al., (2008) studied the role of heat flux and low salinity plume in the formation and dissipation of the warm pool in the SEAS using the Princeton Ocean Model (POM). They showed that the salinity stratification is a favorable to the warm pool, especially in its horizontal extent and degree of warming. Thus, the recent study also shows the importance of low saline water in the formation of ASWP.

1.6 Present Work

It is evident in the above discussion the low saline waters and stratification in the SEAS are fundamental to the formation of ASWP. Most of the earlier studies suggested that the low saline water is an important pre-requisite for the formation of warm pool. The air-sea heat fluxes are not considered to be the primary reason in the formation of ASWP, which is important only during April-May. The present study examines the importance of low saline waters and resulting barrier layer in the dynamics of the ASWP using observational data.

The oceanic general circulation models (OGCM) are very useful for exploring the processes responsible for the ASWP and their variability. The circulation and thermohaline structure stimulated by an OGCM changes a lot when the resolution is increased from mesoscale to macro scale. For a reasonable simulation of the ASWP, we must include the mesoscale turbulence in numerical models. Especially the SEAS is an eddy prominent region with a horizontal dimension of 100 to 500 km and vertical extent of hundred meters. These eddies may have an important role on the evolution of ASWP, which has not been explored so far.

Most of the earlier studies in the SEAS showed that the heat build-up in the mixed layer during the pre-monsoon (March-May) is primarily driven by the surface heat flux through the ocean-atmosphere interface, while the 3-dimensional heat budget of the ML physical processes that are responsible for the formation of the ASWP are unknown. With this background the present thesis also examines the relative importance of mixed layer processes that lead to the formation of warm pool in the SEAS. Objectives of the present work are

a) To understand the dynamics of the ASWP with particular emphasis on the role played by salinity

b) To study the importance of mesoscale features on the evolution of warm pool

c) To categorize various regions in the ASWP according to the significance of each mixed layer processes

The content of the subsequent chapters are as follows. Chapter 2 describes the materials and methods used for this study. The hydrography and circulation of the SEAS during the different stages of the ASWP is described in Chapter 3. The importance of low saline waters and barrier layer in the formation of warm pool is provided in chapter 4. The role of mesoscale features on the evolution of warm pool is investigated in Chapter 5. The processes involved in the collapse of the warm pool are described in Chapter 6. Summary and conclusions are presented in Chapter 7.

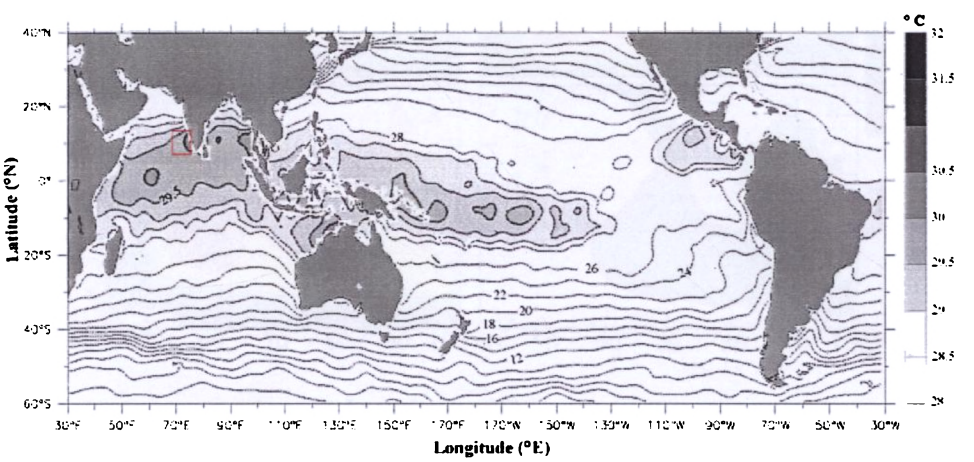

Fig.1.1. Indo-Pacific warm pool. Data shown is climatological monthly SST (°C) form world Ocean Atlas 2005 (Locarnini et al., 2006) climatology, during April. Contour interval is 2 below 28°C and 0.5 above it. SSTs above 28°C are shaded in addition to contouring. SEAS is marked by a red box.

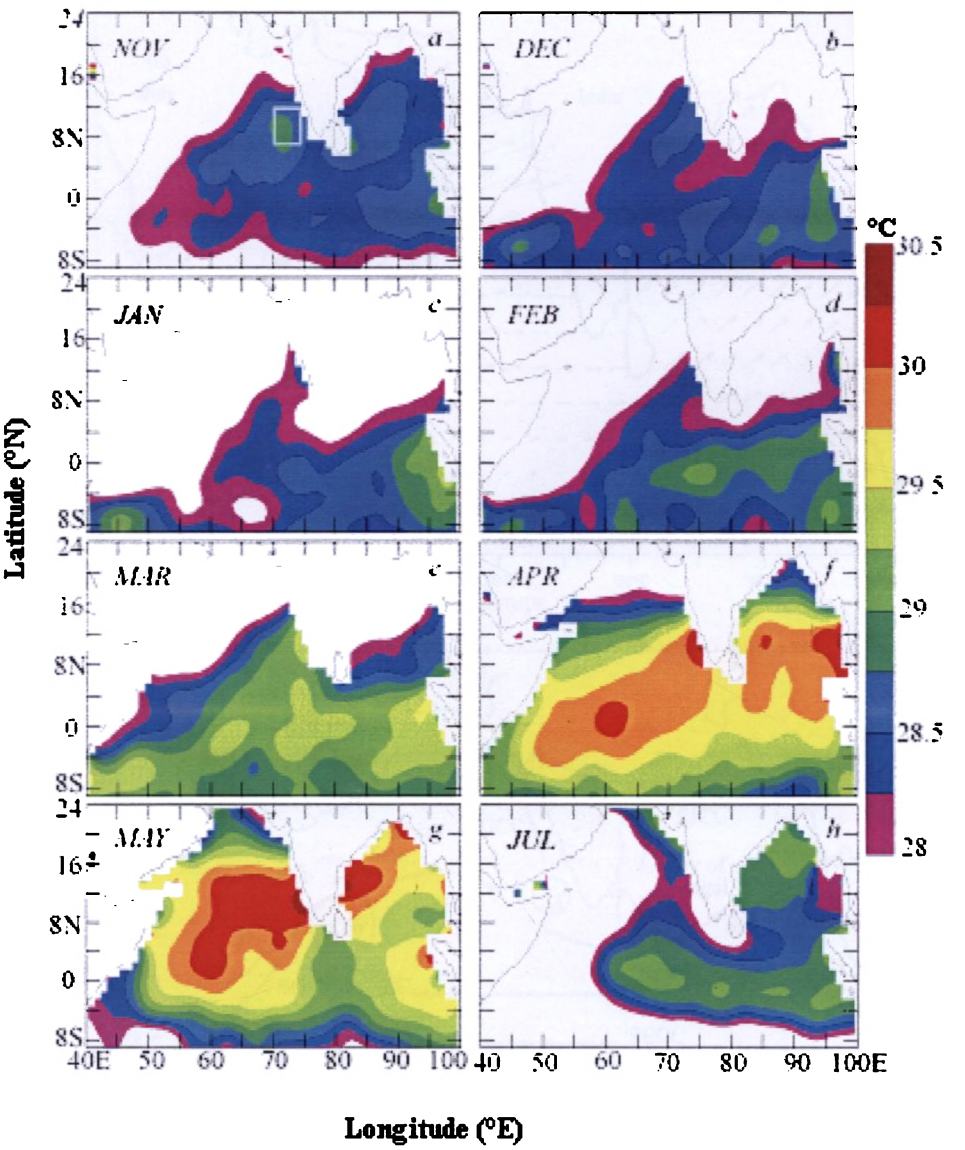

Fig.1.2. Evolution of IOWP and ASWP during January-July. Data shown is climatological monthly SST (°C) from WOA05. Only SST values above 28°C have been shown. The box in the plots 1.2 (a) shows the SEAS region.

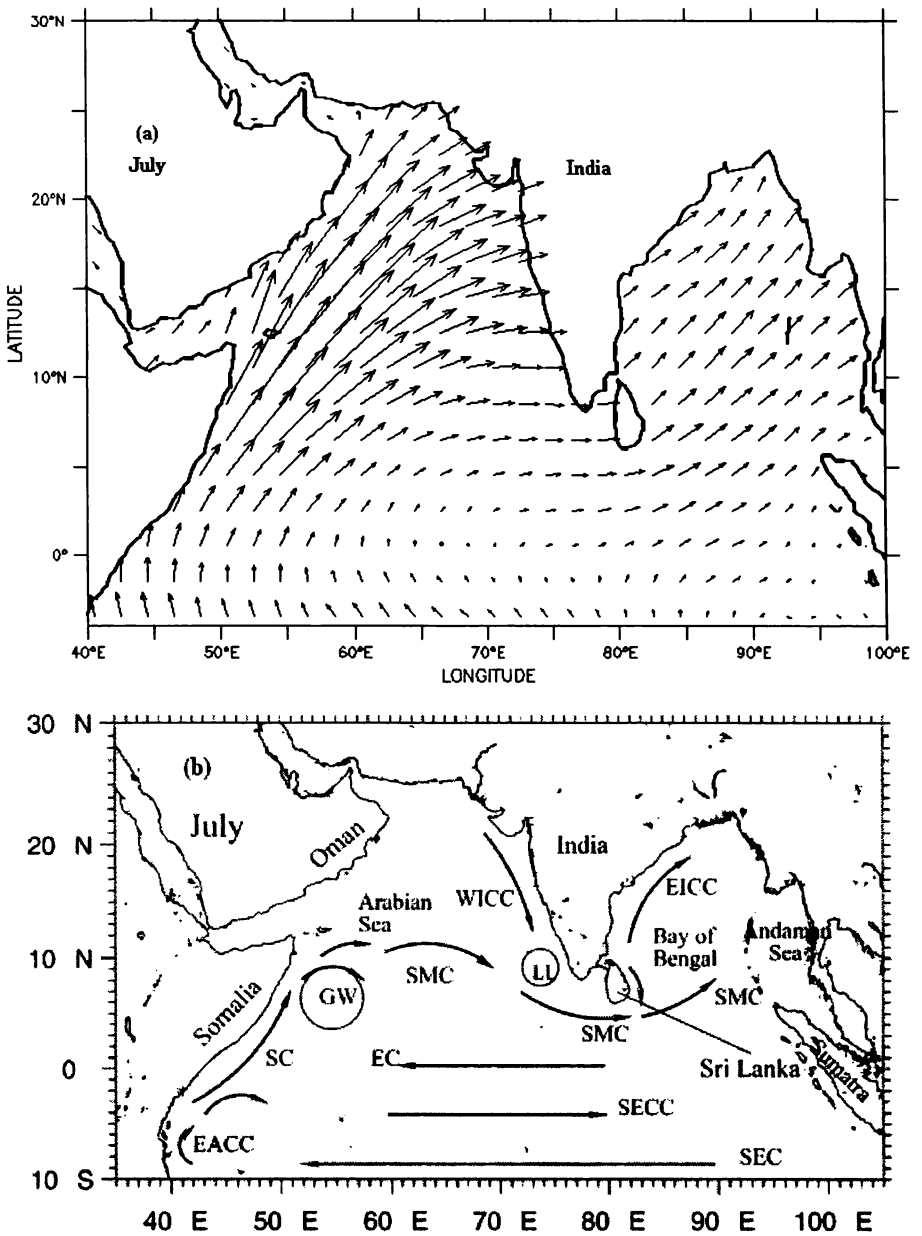

Fig.1.3. Surface wind stress (a & c) and schematic representation of the circulation (b & d) during January (a & b) and July (c & d) in the Northern Indian Ocean. Wind stress is produced form the SOS flux climatology data (Josey et al.,1999), while circulation schematics from Shankar et al.(2002).

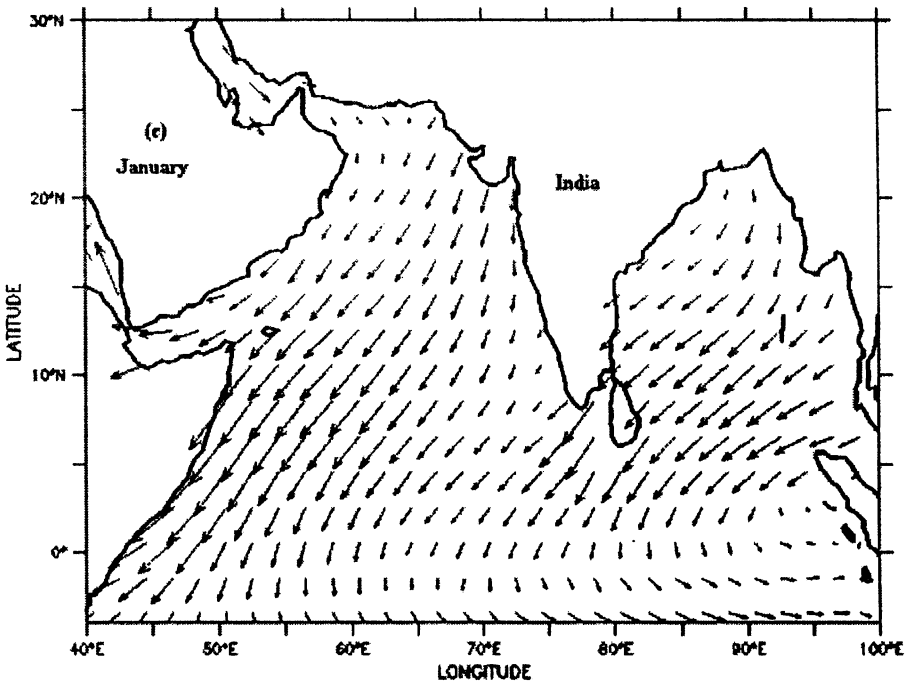

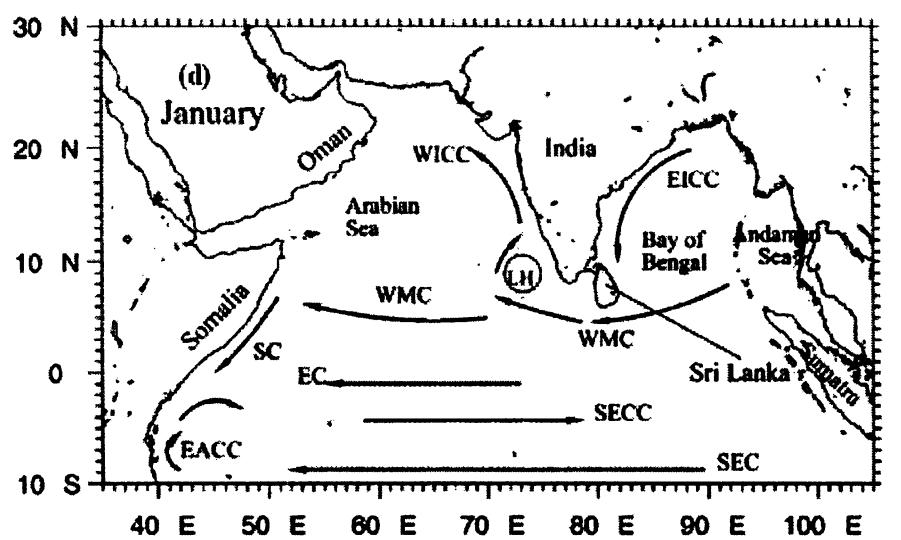

Fig.1.3. (continued)

****

Chapter 2

Materials and Methods

Contents

2.1 Study Area

The Arabian Sea, particularly the west coast of India, has a crucial role on the weather, climate and fisheries of India. The southeastern Arabian Sea (SEAS), in particular has several distinguishing features that makes it a unique and dynamic region in the north Indian Ocean. The Lakshadweep Island chain comes under this region, and the average depth of the area is 3.8 km. The width of the shelf varies considerably with narrow shelf at the south (~ 60 km off Cochin) and wider towards the north. The SEAS exhibits strong seasonal variability in both hydrography and circulation under the influence of seasonally reversing monsoon winds. During the southwest monsoon (SWM) the surface currents flow equatorward and the thermocline shallows near the coast whereas during northeast monsoon (NEM) the surface currents are poleward when the thermocline deepens. During SWM, both remotely and locally forced coastal upwelling in the SEAS brings cooler nutrient rich water into the surface. This strong upwelling makes it a highly productive region and contributes a major share towards the fish catch. Another important aspect

related to SEAS is the formation of warm pool before the onset of the SWM. The SST in the warm pool has been recognized as the important oceanic parameter, which controls the air-sea interaction processes. The evolution of SST in the SEAS during March-May has a critical impact on the onset of the southwest monsoon over the country.

The study area includes the SEAS (region marked by the box) represented by five transects between 8°N and 15°N (Fig.2.1) and the observations were mainly focusing on the dynamics and thermodynamics of the ASWP. Hydrographic stations between 8°- 22°N and 66°-76°E in the AS have also been considered to explain the dynamics of the warm pool. For representing the evolution of atmospheric and oceanographic parameters two boxes are defined, one in northern AS and other in southern AS (Fig.2.2). The oceanographic data for this study were collected under the Ministry of Earth Sciences (MoES) programme "Environment and Productivity Patterns of the Indian EEZ"

2.2 Observational data

The study was conducted as part of the Marine Research on Living Resources Programme (MR-LR) to assess the environmental and productivity patterns in the Indian Exclusive Economic Zone (EEZ), funded by Ministry of Earth Sciences (Government of India). The MR-LR programme was designed to assess and evaluate the marine living resource by systematic collection of physical, chemical and biological data from the seas around India (Arabian Sea, Bay of Bengal and the Andaman Sea). The sampling was done at one degree interval of longitude along nine transects in AS viz, 8, 10, 11.5, 13, 15, 17, 19, 21 and 22 °N. The station having depth 200 m is considered as the coastal

station. The hydrographic surveys carried out on board *FORV Sagar Sampada* during the winter (December, 2000), spring intermonsoon (March-April, 2004) and onset of summer monsoon (May-June, 2005) are used for this study.

2.2.1 Data collection and processing

Surface winds were monitored using the ship-borne automated weather station. Sea surface temperature (SST) was measured using a bucket thermometer. Conductivity-Temperature-depth profiler or CTD (Sea Bird Electronics, Inc., USA, model: SBE-911 plus, Fig.2.3) was used to collect temperature, salinity and density profiles. The accuracy and resolution for each parameter is given in the Table 2.1. Salinity values from CTD were corrected using the values obtained from the Autosal (Guildline, model 8400A) onboard. The data on temperature and salinity measured at 1 m bin at each station were examined and outliers were discarded manually. Only the quality-checked data on temperature and salinity were used for processing. Horizontal advection due to the pressure gradient was estimated using geostrophic method (Pond and Pickard, 1983). For this computation, 1000db was considered as reference level. For stations shallower than the reference level, the geostrophic currents were computed following Howling and McLellan (1967) where the dynamic height of the adjacent deeper station (>1000db) are appended below the depth of observation of coastal station.

2.3 Climatological Data

For describing the evolution of Arabian Sea Warm Pool (ASWP, Chapter 1) and for the comparison of insitu temperature and salinity with climatological data, the World Ocean Atlas 2005 (WOA05) dataset

(Antonov et al., 2006; Locarnini et al., 2006) was used. The computation of temperature anomaly was carried using the high resolution World Ocean Atlas 2001 (WOA01) dataset. For short wave radiation, SOC flux climatology was used.

2.3.1 WOA05 climatology

WOA05 is maintained by NODC (National Oceanographic Data Centre), NOAA (National Oceanic & Atmospheric Administration), USA. This consists of a set of objectively analyzed gridded (1° x 1°) climatological (regardless of year) fields of in situ temperature, salinity and many other oceanographic variables. Historical oceanographic profiles of only selected surface data have been used in the objective analysis. WOA05 fields are available at standard depths for annual, seasonal, and monthly interval for the World Ocean. It also includes associated statistical information on the observed oceanographic data interpolated to standard depths.

2.3.2 WOA01 Climatology

WOA01 data used in the present work is an earlier version of NODC world ocean data, with high horizontal resolution (1/4° x 1/4°). However, this version is available only for temperature and salinity in ASCII format. WOA01 is created in a similar manner as that of WOA05, using optimal interpolation. WOA01 data were used in this study to compute the temperature anomaly (T') of in-situ observation.

2.3.3 SOC flux Climatology

The short wave radiation available from Southampton surface flux climatology (version 1.1) was used for the computation of surface flux in the study area. Data is available for the air-sea fluxes on a global grid

(1°x1°) in NetCDF format produced at the National Oceanographic Centre, Southampton (NOCS).

2.4 Satellite Derived Data

2.4.1 TMI Sea Surface Temperature

Sea surface temperature (SST) from TRMM/TMI (Tropical Rainfall Measuring Mission/TRMM Microwave Imager) is used for describing the evolution and interanual variation of ASWP (Chapter 3). Also, this data is used for the computation of temperature tendency described in section 2.3.1. TMI data are collected by Remote Sensing Systems at NASA (National Aeronautics and Space Administration) under Earth Science REASON DISCOVER Project. This dataset is freely available on a real-time basis (from December/1997 onwards), from SSM/I (Special Sensor Microwave/Imager). The spatial coverage of TMI data is between 40°S and 40°N, with a resolution of 1/4°. Data is available at daily frequency and as mean maps with 3day, weekly and monthly frequencies. The standard data format is binary.

2.4.2 AVISO/MSLA Sea Level Anomalies

For model evaluation (Chapter 4), sea level anomalies (SLA) from a merged satellite product (Maps of Sea Level Anomalies (MSLA) were used. Data is available on a real-time basis from October/1992 onwards, with weekly or near weekly frequency. The horizontal resolution of data is 1/3°. Data is available in NetCDF format in public domain. Data for 1992–2002, obtained from AVISO (Archiving, Validation and Interpretation of Satellite Oceanographic data) is used for computing gesostrophic currents and to understand the variation of SSHA.

2.4.3 QuikSCAT Winds

In order to present the spatial pattern of winds in and around the SEAS during winter (December) spring (March-April) and onset of monsoon (May-June), QuikSCAT (NASA SeaWinds scatterometer, onboard QuikSCAT) winds were used (Chapter 3). This data has a global coverage over oceans, at 1/2° spatial resolution. Data is available at daily, weekly and monthly frequencies. Data is in public domain and is available on a real-time basis from July/1999 onwards. The standard data format is NetCDF.

2.4.4 OAFlux data

Multidecade Global Flux datasets from the objectively analyzed air-sea fluxes (OA flux) project were used to study the air-sea fluxes in the SEAS. The OA flux products were constructed from an optimal blending of satellite retrievals and three atmospheric reanalysis. Daily fluxes were computed from the optimally estimated variables using the COARE bulk flux algorithm. Monthly products were made for the entire 49-year period, where daily products are available from 1985 onward. The data sets are freely available for non-commercial scientific research. The data resolution is 1° x 1° and the available in netcdf format.

2.5 Methods

2.5.1 Mixed Layer Depth (MLD) and Barrier layer thickness (BLT)

The mixed layer plays an important role in the exchange of heat, moisture and momentum between the atmosphere and the ocean. In view of importance of MLD in the ocean, researches have developed different techniques to determine MLD. The most accurate method of obtaining MLD is by plotting profiles of temperature, salinity and density against

depth and thereby determining the depth of isoproperty layer by visual inspection. The distribution of physical properties within the upper layers determines the criteria to define MLD. Visual inspection of temperature, salinity and density profiles indicate that while the isohaline and isopycnal layers are similar, the isothermal layer remains different. The temperature and density at 5m is taken as a reference for determing the MLD. This depth is chosen to eliminate any possible bias in the profile due to skin effects at the ocean surface (Fairall et al., 1996). Majority of the profiles in the present study showed that the properties at 5m are very close to the surface. In this study, MLD is defined as the depth at which, density rises by 0.2 units from the 5m depth value. Shetye et al. (1996) and Madhupratap at al., (2003) used the same density criteria (0.2 kg/m^{-3}) to define the MLD. The isothermal layer depth (ILD), the depth of the top of thermocline, is defined as the depth at which temperature decreases by 1°C (Sprintall and Tomczak, 1992; Kara et al., 2000; Rao and Sivakumar, 2003). In location of thermal inversion, ILD is defined as the depth at which the temperature at the base of the inversion layer is equal to the temperature at the top of the inversion layer (Thadathil et al., 2007). The barrier layer thickness (BLT) is defined as the difference between ILD and MLD.

BLT=ILD-MLD

2.5.2 Heat budget in the MLD

The mixed layer temperature in the upper ocean is controlled by the surface heat fluxes, horizontal advection, eddy diffusion, vertical mixing and entrainment. The evolution of mixed layer temperature (T) can be written as,

$$\partial T/\partial t + [u_T \partial T/\partial x + v_T \partial T/\partial x] + w\partial T/\partial z =$$

$$[Q/h\rho C_p] + \partial/\partial z(K_h.\partial T/\partial z) + A_h(\partial^2 T/\partial x^2 + \partial^2 T/\partial y^2)$$

where $\partial T/\partial t$ is the rate of change in the mixed layer temperature,

$u_T \partial T/\partial x + v_T \partial T/\partial x$ is the horizontal advection,

$A_h(\partial^2 T/\partial x^2 + \partial^2 T/\partial y^2)$ is the eddy diffusion,

$(w\,\partial T/\partial z + \partial/\partial z(K_h\,\partial T/\partial z))$ is the vertical mixing and entrainment term

and $Q/h\rho C_p$ is the surface heat flux.

2.5.2.1 ***Temperature tendency***

The temperature tendency ($\partial T/\partial t$) was computed from the satellite derived SST, because the ship could cover each observational location only once, thus losing a finer temporal resolution of temperature changes at any grid. Although the SST is not the exact representation of mixed layer temperature, it is assumed that the temporal variation in the mixed layer temperature is represented in the SST changes as well. The TRMM Microwave imager (TMI) SST on a 0.25° x 0.25° grid was used to get a time series at any location. The satellite data was derived in the region 7°N-16°N and 69°E- 77°E for the period of observations. Linear interpolation is done to avoid the data gaps at certain locations. Thus, the tendency of the SST at all locations were computed from TMI SST data on a two-day time interval. For example, the tendency of temperature on 23- March- 2004 was taken as,

$$\partial T/\partial t = (TMI_{24-03-4} - TMI_{22-03-04})/2\,days$$

2.5.2.2 *Horizontal advection*

The horizontal velocity components $u_T(u_g + u_e), v_T(v_g + v_e)$ include the geostrophic and Ekman velocity. Computation of geostrophic currents is described in section 2.2.1. The Ekman components are computed from observed winds using the equation,

$$u_e = V_0 \cos(\Pi/4 + ((\Pi/D_E).z)\varepsilon^{(\Pi/DE.z)}$$

and

$$v_e = V_0 \sin(\Pi/4 + ((\Pi/D_E).z)\varepsilon^{(\Pi/DE.z)}$$

where $V_o = 0.79\times10^{-5}(W^2/D_E.f)$, W is the wind speed (ms^{-1}) and D_E ($\Pi\sqrt{2.(A_z/f)}$ is the Ekman depth, f is the Corilois force and A_z is the eddy viscosity.

The advection is calculated by centered finite difference scheme. A boundary value is provided from the observations at the domain edges. It should be noted that since the observations on the individual grid faces are done on separate days, the advection and diffusion component does not represent the value for a particular time.

2.5.2.3 *Surface heat flux*

$Q/h\rho C_p$ is the flux term in the heat budget equation, where Q is the net radiation (short wave and long wave radiations, latent and sensible heat fluxes. ρ is the density of seawater (1025 kgm^{-3}), h is the mixed layer depth and C_p is the specific heat of seawater (4300 j $kg^{-1}k^{-1}$) at constant pressure.

The surface meteorological parameters (wind speed, direction, humidity, dry and wet bulb temperatures and atmospheric pressure) were measured from all stations along the ship track using the shipboard automatic weather station. These data were used for the computation of long wave radiation, latent heat flux (LHF) and sensible heat flux (SHF) using bulk formula for humidity and heat exchange as,

$$LHF = \rho C_d L_v U(q_s - q_a)$$

$$SHF = \rho C_d C_p U(T_s - T_a)$$

where ρ is the density of air, C_d is the drag coefficient, L_v is the latent heat of vaporization, U is the wind speed, q_s is the saturated specific humidity and q_a is the humidity. Q_s is calculated using Clausius-Clapeyron equation. The Cp is the specific heat capacity of air per unit volume, T_s is the sea surface temperature and T_a is the temperature above the sea surface.

2.5.2.4 *Eddy induced diffusion*

The term $A_h(\partial^2 T/\partial x^2 + \partial^2 T/\partial y^2)$ is the eddy-induced diffusion. The K_h and A_h are the vertical and horizontal eddy diffusion coefficients in the mixed layer. The eddy-induced diffusion is due to the turbulent transport of heat which can be written in the turbulent form as $u'\partial T'/\partial x + v'\partial T'/\partial y$. In order to find the turbulent velocity in the surface layer, the satellite altimetry data from the TOPEX/POSEIDON altimetry (Qiu et al, 2004) was used. The SSHA is the deviation from the mean geopotential height (dynamic height) and thus, assumes the removal of the mean flow associated with the mean dynamic topography. Thus,

remaining component is taken as the fluctuation of the mean flow primarily driven by eddies and thus it provides u' and v' through the geostrophic relation as,

$$u' = -f/g\,(\partial SSH/\partial y)$$

$$v' = f/g\,(\partial SSH/\partial x)$$

where □ is the Coriolis parameter and g is the acceleration due to gravity. This assumption is valid only to the near surface, and not at depths where baroclinic currents dominate. The density derived mean geostrophic currents showed no reversal in the mixed layer. Thus the eddy induced surface current is well represented in the mixed layer, which never exceeded 100m. The eddy induced diffusion is computed from u' , v' and T'.

2.5.2.5 *Vertical mixing*

The mixing in the boundary layer near the surface under a variety surface forcing and mixing in the ocean interior due to internal waves, shear stability and double diffusion. Mixing is also enhanced by the contribution from shear instability which is a function of the Richardson number. In this study the K-profile parameterization (KPP-hereafter) given by Large et al. (1994) was used to find the mixing coefficients (K_h) from the observed current and density of the mixed layer with a vertical resolution of 1m from the surface to the bottom of the mixed layer. The KPP was performed within this mixed layer to find the vertical mixing coefficient (K_h) according to the observed currents and density of the mixed layer.

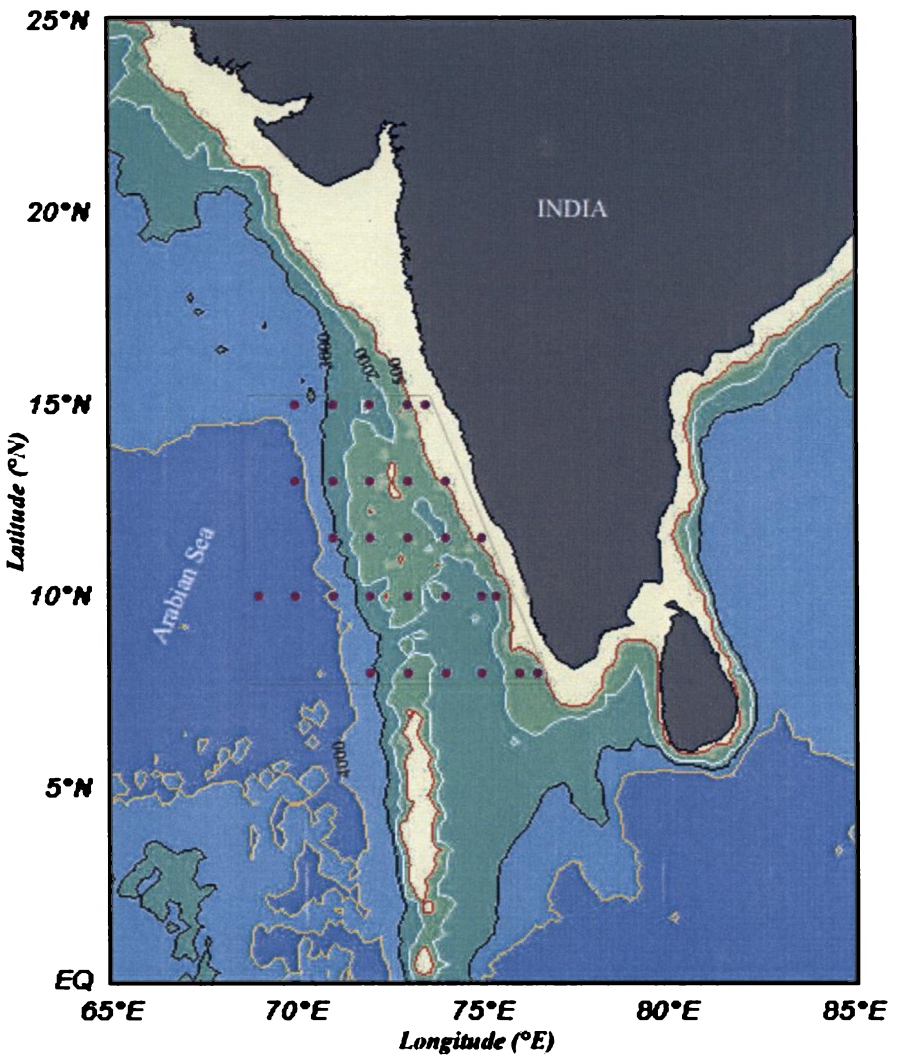

Fig.2.1. Map showing the study region in the AS. The marked box shows the southeastern Arabian Sea (SEAS) and dots represent the hydrographic stations.

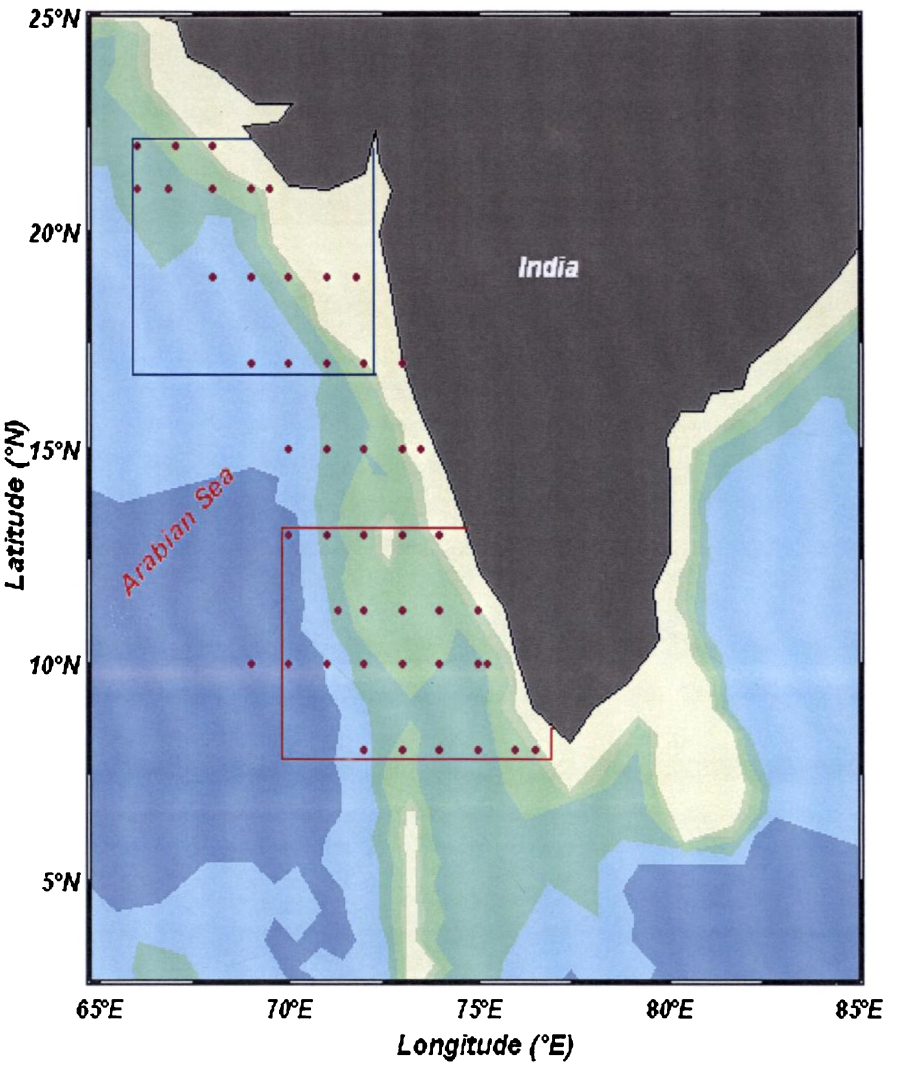

Fig 2.2. Map showing the hydrographic stations in the AS. Region in the boxes are used for a comparative study between northern AS and Southern AS

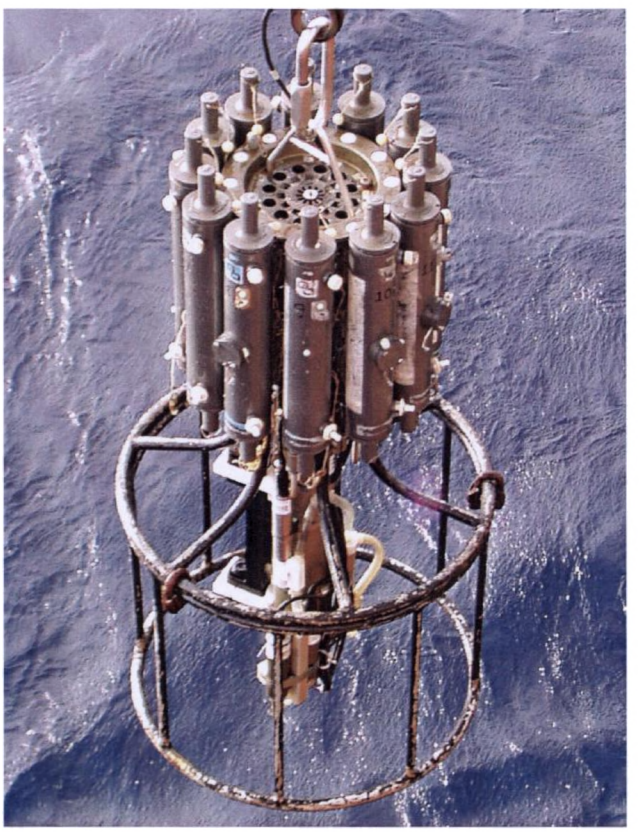

Fig. 2.3. Rosette sampler with CTD sensors and Niskin bottles

Table 2.1. CTD sensors and specifications

Sensor	Range	Accuracy	Resolution
Temperature	-5 to 35°C	± 0.001°C	0.0002°C
Conductivity	0 to 7 S/m (0 to 70 mmho/cm)	± 0.0003 S/m	0.00004 S/m
Pressure	Up to 10500m	0.015% of full scale range	0.001% of full scale range

****

Chapter 3

Hydrography and Circulation of the Southeastern Arabian Sea

Contents

The hydrography and circulation of the SEAS during December, March-April and May-June are described in this chapter. The vertical profiles of temperature and salinity interpolated from the data collected at 1m depth intervals from the hydrographic stations along 8°N, 10°N, 11.30°N, 13°N and 15°N are discussed in this section. The Evolution of Arabian Sea warm pool can be explained based on the observations in the SEAS during December, 2000. Similarly the mature and collapsing stages of the warm pool are discussed in reference to the observations during March-April, 2004 and May-June, 2005 respectively. Monthly averaged satellite data of wind (QuickScat), SSHA (Topex/Poseidon), SST (TMI-SST) and climatology data of temperature and salinity (WOA05) for the months of March, April, May, June and December, are also presented.

3.1 Evolution of ASWP

3.1.1 Hydrography and Circulation

The northeasterly winds that prevailed over the AS was stronger (~7m/s) over western side and southern tip of India (Fig.3.2d) whereas

SEAS generally experienced weak winds (~3m/s). The SST varied between 28.2°C and 29.2°C, with meridionally aligned isotherms representing the colder water along the northwestern region and warmer water along the southeastern region. Maximum SST (SST>28.8°C) was centered on the LS region with an entire mixed layer warming (Fig.3.1a). During this time, the coastal and open ocean variability of SST was minimum. Satellite (>28.6°C) and climatological (>28.4°C) observations of SST during this period showed patches of warm waters in the LS region (Fig.3.2 a & b).The vertical structure of temperature along 8°N and 10°N showed warm (>29°C) and relatively deeper (>60 m) isothermal layer (Fig. 3.3 a & b). The 20°C isotherm was found at 110-120 m depth at 8° and 10°N transects while it was deeper towards the coastal stations of 13° and 15°N transects. A strong downsloping of isolines towards the coast along these transects (13° and 15°N) indicated an active downwelling processes occurring in the upper 200 m (Fig.3.3 c & d).

The conspicuous feature in the SSS distribution was the occurrence of low saline waters (<34) along the southwest coast of India (Fig.3.1a) dissipating (>36.4) towards offshore. This is in agreement with the climatological SSS (<34.4 in the coastal region and >36.4 in the offshore region, Fig.3.3c). However, the observed salinity was fresher and widely spread in the SEAS than indicated by the climatology. The spreading of low saline waters towards the coast (8°N and 10°N) in the upper 30 m was evident from the strong vertical gradient (0.15/ m) (Fig.3.3 a & b). The thickness of low saline water was maximum (30m) at 8°N and 74°E indicating freshwater influx in to this region. Below 100 m depth, the gradient was absent and the water column remained almost homogeneous. Along 8°N, the offshore spreading of this low saline waters was seen up

to 500 km from the shore, whereas along 10°N, it was narrow and limited to 120 km. The waters near the coast showed considerable increase in salinity (35.2) from that of 8°N. Along 15°N, waters with salinity > 35.8 was observed near the coast (Fig.3.3 c &d). Also the horizontal and vertical gradients in the upper 50 m of the 13° and 15°N transects appeared to be minimum. The density distribution showed the occurrence of lighter waters along the shelf and denser waters offshore (Fig 3.1c). The density stratification was in accordance with the salinity distribution in the surface layer. The high salinity (> 36.4) tongue from the open ocean towards the coast suggested the intrusion of Arabian Sea High Saline Water Mass (ASHSW). The salinity of ASHSW (20-60m) was found to be modified by the effect of low saline waters in the coastal region.

Shallow MLD was the feature in the low saline region (minimum of 15 m) at 8°N & 75°E which increased progressively to >50 m in the open ocean (Fig.3.4a). The barrier layer (BL) was thick (~ 40m) in the regions of low saline water, while north of 13°N, it was thin (Fig.3.4b). The barrier layer was completely absent in the open ocean region of the SEAS. The spatial variation of temperature inversions (Stations with inversion represented by red dots and profiles having subsurface temperature higher by 0.2°C than the SST is considered for inversion study) in the SEAS is shown in Fig 3.4.a. Inversions are observed in the shelf region between 8° and 10°N in the depth range of 20 to 40 m.

The geostrophic currents derived from monthly mean of sea surface height was used to understand the surface circulation in the SEAS (Fig.3.5). In November, a narrow equatorward surface current is observed along the entire east coast of India which bifurcates to an offshore and alongshore component. The alongshore current flows along the west coast

of India in the poleward direction (Fig.3.5). A high in sea level (5 to 10 cm) and the presence of an anticyclonic eddy is evidenced in the circulation pattern in the south of the SEAS. The vertical section of temperature and salinity along 8°N also supports the presence of the anticyclonic eddy. The core of the eddy characterized by low saline waters was located near 8° N & 74° E. The high in sea level (15-20cm) during December (Fig.3.5) is probably the manifestation of anti-cyclonic circulation between 7°N and 10°N.

3.1.2 Discussion

During December, the SST in the SEAS and especially in the LS region is higher than surrounding waters. The satellite and climatological data show patches of high SST, in the LS region. Cooling of northern and southern AS, due to the cool dry northeasterly winds during December was reported earlier by Luis and Kawamura, (2000) and Prasanna Kumar et al., (2004). During the present study, the southern tip of India was cooled by more than 1°C (SST<27 °C), while the cooling was less in the SEAS. (Darbyshire, 1967; Banse, 1968; Shetye, 1984; Thadathil and Ghosh, 1992; Antony et al., 2002; Prasanna Kumar et al., 2004; Sanilkumar et al., 2004).

The winds over the SEAS are weak (~3m/s) in December. Thus the isothermal layer (IL) and thermocline were mainly determined by downwelling associated with the coastal currents and eddy. Banse (1968) pointed out that the mean sea level along the coast rises sharply from October to November due to the northerly flow. The vertical temperature and salinity during the observation showed downsloping of isotherms towards the coast indicating downwelling. This can be

attributed to the anticyclonic circulation associated with Lakshadweep High (LH). The LH is a large anticyclonic eddy that regularly appears near the southwestern tip of India during NE monsoon (Bruce et al., 1994). Development of LH associated with the anticyclonic circulation is evidenced in the distribution of SSHA. The anticyclonic circulation spreads the low saline waters up to the east of 72°E. Shankar et al., 2002 showed that the anticyclonic circulation associated with LH cause downwelling and modifies the vertical distribution of temperature and salinity at 8° N

The presence of low saline water in the SEAS is attributed due to the intrusion the Bay of Bengal water, as evidenced from the circulation pattern along the western Bay of Bengal and eastern Arabian Sea (Fig.3.5). The geostrophic currents show a well organized EICC along the western Bay of Bengal during November-December in a narrow (100 km width), stretch confined to the coast flowing along the east coast of India (Shetye et al., 1993, 1996). The EICC is driven by the alongshore pressure gradient, which overwhelms the winds during the northeast monsoon (Shetye et al., 1991). But, the role of remote forcings (Kelvin and Rossby waves) has been the new theories on the dynamic processes in the region (McCreary et al., 1993, Bruce et al., 1994, Shankar and Shetye, 1997). The EICC turns around Sri Lanka and feeds into the WICC, along the west coast of India (Shetye *et al.*, 1991a). This is further evident from the geostrophic currents derived from altimetry. The EICC transports large amount of low-saline waters from BoB into the SEAS. The inflow of BoB starts in early December (Shetye *et.al*, 1991; Shanker *et al* 2003), when the westward Winter Monsoon Current (WMC) feeds into the poleward WICC (Shanker.*et.al*, 2002).

It is observed that the low saline waters were not present in the SEAS north of 10°N. According to Kumar and Mathew (1997), the maximum extension of the low saline waters was 12° N in January. In the present observations also, the presence of low saline waters were well discernible upto 10° N and induced stratification near the coast, overwhelming the deep MLD caused by the downwelling processes. The presence of low saline water ultimately leads to the formation of BL. Climatological datasets show a 25m thick BL in the SEAS during November–January (Sprintall and Tomczak, 1992). In general, the thickness of the BL varied from 10 to 40 m during December to March (Rao and Sivakumar, 1999).

TI was observed with the BL in the eastern side of the SEAS influenced by the cold, low-saline waters, with in the BL. During the present observation, only a few (four) exhibited TI. The magnitude of inversion was about 0.5°C and the thickness varied from 20 to 40 m. The SEAS is known to host thermal inversions during October-April, with considerable variation in frequency, intensity depth and duration. Observations show that TI was a stable seasonal feature and frequent in the coastal waters (Thadathil and Ghosh, 1992).

3.2 Establishment of ASWP (March-April)

3.2.1 Hydrography and Circulation

The meteorological conditions (clear sky, high solar isolation and weak winds) that prevailed in the SEAS during the observational period represented the characteristic features of the spring inter-monsoon (SIM). In March, the winds were northwesterly over AS (3m/s) and of weak (2m/s) over the southern tip of India (Fig.3.8a), which strengthened (4m/s) in April (Fig 3.8b).

Fig 3.6. shows the distribution of sea surface temperature (SST) where warm water (30.2°C) was hugging the coast. The satellite and climatological data on SST during March and April also shows a similar feature in the coastal region (3.7.a). Satellite SST during March and April was higher than the observed and climatological data (3.7 .b & d). The satellite SST shows an increase of 1°C from March to April. A zone of warm waters (>30°C) was noticed in the upper layers (<50 m) of the SEAS near the shelf region (Fig .3.6a). The zone was approximately 50 km wide off Goa, 150 km off Mangalore, 320 km off Calicut and 220 km off Kochi. The core of this warm water was centered on 10°N, 74° E (near LS) with a maximum thickness (>30 m) along 11.5°N. The interesting feature was that the extension and thickness of the warm water coincided with the low saline water. Another feature of the region was the shallow ILD (30 m) and deeper thermocline (125 m) in all the transects, indicating that the SEAS is still experiencing downwelling (Fig 3.9 a & 3.10).

The low saline waters (<34.2) in the upper few meters of SEAS became shallower towards the north (Fig.3.6b). The isohalines were more or less similar to isotherms and the thickness and extent were maximum in south (8°N & 10°N) and gradually decreased towards north (Fig.3.6 b & 3.10). The climatological SSS also showed the presence of low saline water (<34.2) was confined to the shelf region (Fig.3.6.b). The offshore spreading of low saline waters (<34.4) can be seen upto 500 km at 8°N, 700 km at 10°N, 270 km at 11.5°N, 250 km at 13 °N but only to 100km at 15°N. The core of this low saline water was centered at 10°N and 74° E coinciding with warm water. A tongue like distribution of high saline water towards shelf (60 and 120) was noticed along 11.5° N, 13°N and 15°N. The high saline layer below the surface was found to be thicker in

the north SEAS than that of south. The density distribution identified lighter waters along the coastal region and denser waters offshore (Fig.3.6c). The isopycnals are exactly similar to isohalines indicating that density of the sea water is controlled by temperature and salinity.

The isotherms, isohalines and isopycnals along 8°N showed a downward shift (Fig 3.10 a, b & c) between longitudes 72-74°E and slightly westward (69°E) along 10°N, which can be attributed to the presence of eddy at these regions. Also the SSHA distribution confirms the presence of eddy at this region (Fig. 3.13.c).

Depth of mixed layer varied considerably during the period, with deeper MLD in the south (~30m) and shallow in the north (~20m) (Fig.3.9a). MLD was deepened due to the anticyclonic eddy. Even though the TI was absent during this period a thick barrier layer (25m) was noticed in the low saline waters, which gradually decreased towards north and south (Fig.3.9b).

The geostrophic currents derived from the monthly SSHA showed a westward flow along the Sri Lankan coast (Fig.3.8 c & d). This was not evident in SEAS, but the poleward surface current was intruding to the SEAS. The SSHA showed positive anomalies in the SEAS during March and April when the circulation was characterized by anticyclonic circulation centered at 8°N and 72°E.

3.2.2 Discussion

The SEAS gets warmed up during March-April especially close to the coast (30.2°C). The warm water (>30°C) was extended between 8° and 15°N along the coast with great variation in thickness and spatial extension. SST in the range of 29 - 30°C has been observed earlier in the

SEAS (Ramesh Babu et al., 1980; Luis and Kawamura, 2003; Jossia Joseph et al., 2005). The SST was higher than 30°C in the eastern and southern part of the SEAS in March (Shenoi et al., 2005b). SST in the range of 30.5°-31°C has also been reported during April, 2006 (Srinivas and Dinesh Kumar, 2006).

During the present observation, the isothermal layer was confined to shallow depth (30 m) and the thermocline was deeper (125m), which can be attributed due to the active downwelling (November-February) associated with the anticyclonic circulation around Lakshadweep High. This deep thermocline (100m) during February was reported earlier by Darbyshire, 1967. By March, the isothermal layer shawls (Ramesh Babu et al., 1980) and reaches 50 m during April (Darbyshire, 1967).

TI was absent during March-April but a very shallow TI was observed near the surface. The TI in the SEAS intensifies during January–February, declines in March (Thadathil and Ghosh, 1992; Shankar et al., 2004; Durand et al., 2004; Gopalakrishna et al., 2005; Rao and Sikka, 2005; Thompson et al., 2006) and disappears subsequently. The shallow TI, developed near the surface during March-April, collapses with the onset of summer monsoon (Shankar et al., 2004).

The interesting feature is that warmer waters are co-existent with the low saline waters (<34.2). During December-January, low-salinity water (30-34) intrudes from the BoB and splits into two branches in the SEAS. One branch flows to the north along with WICC hugging the coast (Shetye et al., 1991a) and the other extends in a northwest direction (Shetye et al., 1991a; Shankar et al., 2004; Gopalakrishna et al., 2005). As a result, the low-salinity water is a character of SEAS (Darbyshire, 1967;

Banse, 1968; Pankajakshan and Rama Raju, 1987). During February, the low salinity water gets redistributed within the SEAS. The lowest salinity observed during March is about 34 (Ramesh Babu et al., 1980; Shenoi et al., 1999b, 2004; Gopalakrishna et al., 2005; Shenoi et al., 2005b). The low saline water shows large variation in its thickness and spatial extension. The maximum extension of low saline water was observed along 8° and 10 °N. This is due to combined effect of northwestward WMC and westward propagating LH, which is clearly evident from the geostrophic currents. Below 60-100 m, a layer of increased salinity was due to ASHSW. The ASHSW separates the low saline surface waters from deeper waters. During February-March, ASHSW core was found to be situated around 50 m depth (Kumar and Prasad, 1994).

The seasonal cycle of SSS in the SEAS shows large influx of low-salinity water from the BoB during November-January (Darbyshire, 1967; Rao and Sivakumar, 2003; Gopalakrishna et al., 2005; Durand et al., 2007b). The variations in the surface currents and eddies make the spatial distribution of salinity rich with fine structures (Shetye et al., 1991a). During the observation, the low-salinity water was confined to the east of 69°E and to the south of 15°N. Kumar and Mathew (1997) showed the maximum extension of the BoB low saline waters up to 12° N in January. Our observation shows the intrusion of low saline water was further upto the 15°N and could be due to the massive influx from BoB during winter 2003-04. The surplus rainfall during an active monsoon could have lowered the surface salinity in the LS during the following winter. The drop in SSS can be as high as 3.4 following a good monsoon as compared to a drop of 1.7 observed after a weak monsoon (Gopalakrishna et al.,

2005). Also, there is considerable variation in salinity both in space and time (Darbyshire, 1967; Shankar et al., 2004; Gopalakrishna et al., 2005).

3.3 Collapse of ASWP (May-June)

3.3.1 Hydrography and Circulation

During May, the winds were southwesterly in the open ocean region (2 m/s) but became strong in the coastal region of AS in northwest direction. During June, strong southwesterly winds (>10 m/s) were observed in the open ocean region and northwesterly winds in the coastal region. The winds show a rapid increase in magnitude from May to June.

The SST varied from 30.2° C to 30.6° C, with meridionally aligned isotherms having higher temperatures in the northwest (Fig.3.11a). The surface isothermal layer was towards north region than the south. Satellite and climatology SSTs showed a warm water region in the entire SEAS which rapidly decreased (~ 2°C) in June along the coastal waters of the SEAS. The thermal structure north of 10°N was vertically homogenous (>30 °C) in the top 25m. In the regions south of 10°S, a temperature <30 °C was observed during this time.

The surface salinity was low in the south and relatively high (>35.8) in the north (Fig. 3.11). Along 8° and 10° N, low saline water (<34.6) was present between 72° and 75° E. The climatological salinity also showed this low saline water (<34.8) in the south between 70-75° E. A strip of high salinity water was observed between 50-100 m along 13° and 15° N, whereas south of 13°N, the high salinity water was found.

The isothermal layer and thermocline along 8° and 10° N transects were shifted upward towards the coast where the ILD was 30 m. The 20°

C isotherm was also shifted to comparatively shallower depth along 8°, 10° and 11.5°N but was observed in deeper depths along 13° and 15°N (Fig.3.15). During this time, MLD was greater than 30m in the north and comparatively shallow (25m) in the southern SEAS.

The vertical distribution of temperature along 8°N exhibited a gentle upsloping of isotherms towards the coast bringing up cold subsurface waters to the surface (Fig. 3.11). The 25°C isotherm shifted from 75m and reached the shallowest depth of about 30m. However, downsloping of isotherms towards the coast was observed below 100 m, which are typical signatures of undercurrent. The presence of low saline waters (<35.2) in the continental slope further supported the undercurrent in this region, which was absent north of 10°N. The distribution of salinity along 8 and 10° N showed spreading of high saline waters towards the coast. The high saline water present at the deeper depths during the months of March-April was seen to be brought up by a depth of 20m due the upward movement of subsurface water. The vertical temperature along 10°N also indicated strong upwelling. The 25°C isotherm was shifted from much deeper depth (115 m) to 40m. At 11.5°N (Fig. 4), up sloping of isotherms was found below the subsurface depth, but to the north of 11.5°N, upwelling was absent.

Geotropic currents during May was weakly organized equatorward flow along the coast. The sea level also showed negative anomalies in the coastal side in association with the upwelling in the coastal stations. The equator wards coastal current intensified during June (30cm/s). A low in sea level (-20 cm) with cyclonic circulation was observed during the month of June in the LS region (Fig.3.13)

3.3.2 Discussion

Very high SSTs (30.2 to 30.6 °C) were observed in the SEAS during May-June. The SST was found to be maximum in the offshore regions (30.6°C) and decreased towards coast (29.9°C). Many studies were reported that, during late May and early June, the SST >30°C in the offshore areas and tends to decrease towards the coast (Ramesh Babu et al., 1991; Sanilkumar et al., 2004; Singh and Hatwar, 2005; Hareesh Kumar et al., 2005), reaching values less than 29°C (Ramesh Babu et al., 1991; Singh and Hatwar, 2005). The cooler SST near the shelf region was mainly due to upwelling. The peak in SST in the SEAS was observed well before the onset of the southwest monsoon, which as 30.8°C (Seetaramayya and Master, 1984).

During May, the low-salinity waters retreat back to Bob, as salinity water flows into the SEAS (Shenoi et al., 2004). The SSS increases from southeast to northwest in the eastern Arabian Sea (Ramesh Babu et al., 1991). The subsurface salinity maximum is weaker during May (Darbyshire, 1967; Kumar and Kumar, 1996) and shallow (30-40 m; Kumar and Kumar, 1996; Shenoi et al., 2005b), due to upwelling. In northern part of the SEAS, the high-saline core was around 75 m during May–June (Ramesh Babu et al., 1991).

With the onset of the SW, steady winds begin prevail over the north Indian Ocean. The wind blowing parallel to the coast generates an offshore transport and causes coastal upwelling between May to September. Sub-surface isotherms and isohalines across the shelf evidence the marked upwards deflection in concurrence with upwelling, which is initiated even before the onset of southwest monsoon

(Darbyshire, 1967; Banse, 1968; Ramesh Babu et al., 1991; Kumar and Kumar, 1996; Luis and Kawamura, 2002b, 2003; Shenoi et al., 2005b) and annihilates warmer waters near the coast. The upwelled water reaches the surface in late May and persists up to July/August.

The alongshore wind stress and wind stress curl have been identified as the most important local forcings responsible for the occurrence of upwelling through Ekman dynamics (Shetye et al., 1985; Shetye and Shenoi, 1988). The upwelling appears along the southwest coast of India and propagate poleward in association with the coastal Kelvin waves resulting in maximum upwelling off Kochi (McCreary et al., 1993; Shankar and Shetye, 1997).

3.4 Interannual Variability of the ASWP

The evolution of warm pool in the SEAS is a continuous process, which begins in December and slowly develops into a mature system. The present study represents the different stages of the warm pool in the SEAS. The thermal evolution from November to July is presented using TMI-SST. The data of TMI SST against the observed SST from CTD during December showed a good correlation (value) indicating strong positive relation between the two. The monthly mean SST computed from the daily TMI-SST data has been analyzed to delineate the spatio-temporal variability of the ASWP. The evolution of SST during November to July along 10°N is shown for the years 2000-2001, 2003-2004 and 2004-2005 (Fig.3.16). The ASWP exhibits large interanuual variability among these years. The Hovmuller field of SST evolution along 10°N also shows wide variations in the amplitude and extension of the ASWP. The SST evolution in the SEAS is characterized by a mild cooling (but temperature greater than 28.4°C) in January and a strong

heating from February to May. During 2001, the warming in the SEAS started from early February to mid May, after which SST gradualy decreased. In mid May, SST >30.4°C is observed along 10°N. During 2004, SST reached its peak in mid April (>30.6°C). During 2005, the warming event continued upto the last week of May and which was stronger compared to the other years suggesting that warming was intense during 2005. The warmer water during 2004 was for shorter time than 2001 and 2005. The early dissipation may be due to the commencement of strong winds associated with the onset of SWM. This analysis clearly shows that the warm pool forms in every year in the SEAS with varying intensities. With the onset and progress of SWM, the warm pool collapses but is highly related to the onset date and intensity of monsoon. The XBT data in the LS over a period of five years from 2002 to 2006, showed the occurrence of warm pool during March-May with minor differences in the intensity (Gopalakrishna et al., 2008). Deepa et al., (2008) examined the plausible reasons for the formation of onset vortex in the presence of ASWP based on the data for the period 2000-05 and concluded that warm pool was present during 2001,02,03 & 2005 and absent during 2000 & 04. This is contradicted by Sanilkumar et al, 2008, stating that, this might be due to the early disappearance of the warm pool during the years.

3.5 Conclusion

This chapter presents a detailed description of the hydrography and circulation of the SEAS during different stages of the ASWP. Most of the features and structure of the temperature and salinity in the SEAS evidenced in an *in-situ* observation similar to that from the climatology. The salient features in the hydrography of the SEAS include the presence of warm pool during March-May, intrusion of low-salinity and high-

salinity waters, presence of thick barrier layer and the thermal inversion during December. The SEAS has a seasonal cycle in salinity, with high-salinity water in the subsurface depth and low saline water in the surface during December to April. Upwelling starts in May-June and downwelling during December-March, in accordance with the eddies and circulation. The upwelling promotes the annihilation of warm pool in the SEAS. The circulation in the SEAS is characterized by the presence of seasonally reversing coastal current and westward propagation of anticyclonic eddies, which are driven by local and remote forcings. Present study explains the mechanism by which the low salinity water enters into the SEAS during December and March-April.

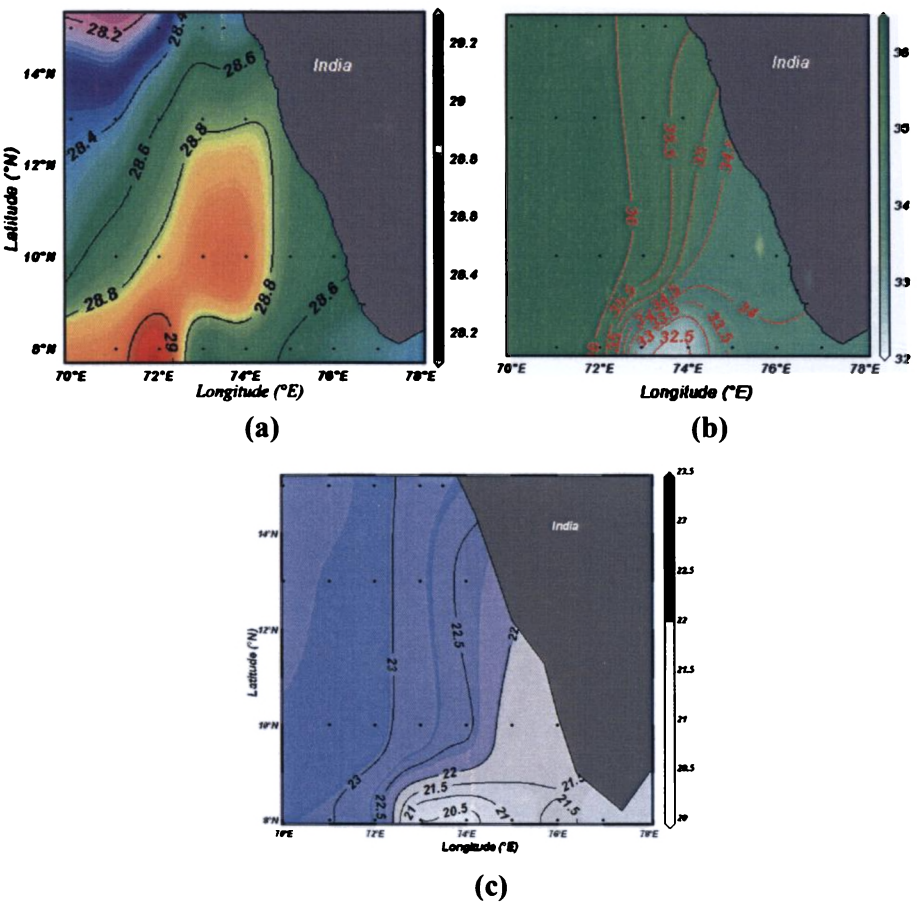

Fig.3.1. Surface distribution of (a) Temperature (b) Salinity (c) Density along the SEAS during winter.

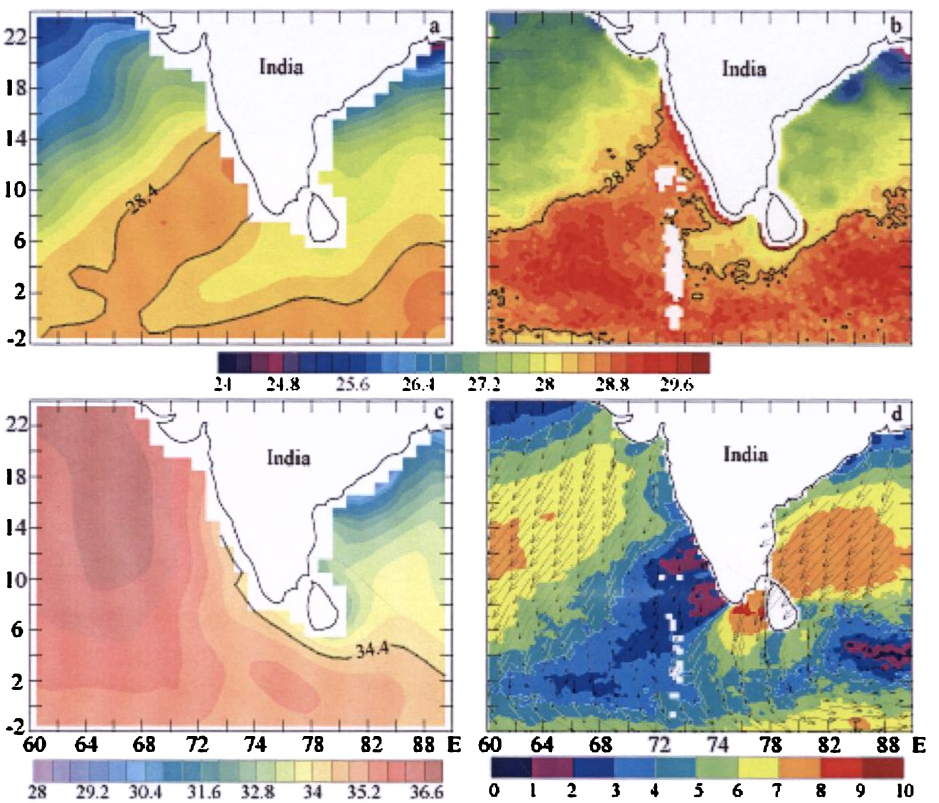

Fig. 3.2. Surface distribution of (a) & (c) monthly mean SST (°C) and SSS from WOA05 climatology. (b) TMI monthly mean SST (°C) (d) Quickscat monthly mean winds (m/s) during December in the SEAS.

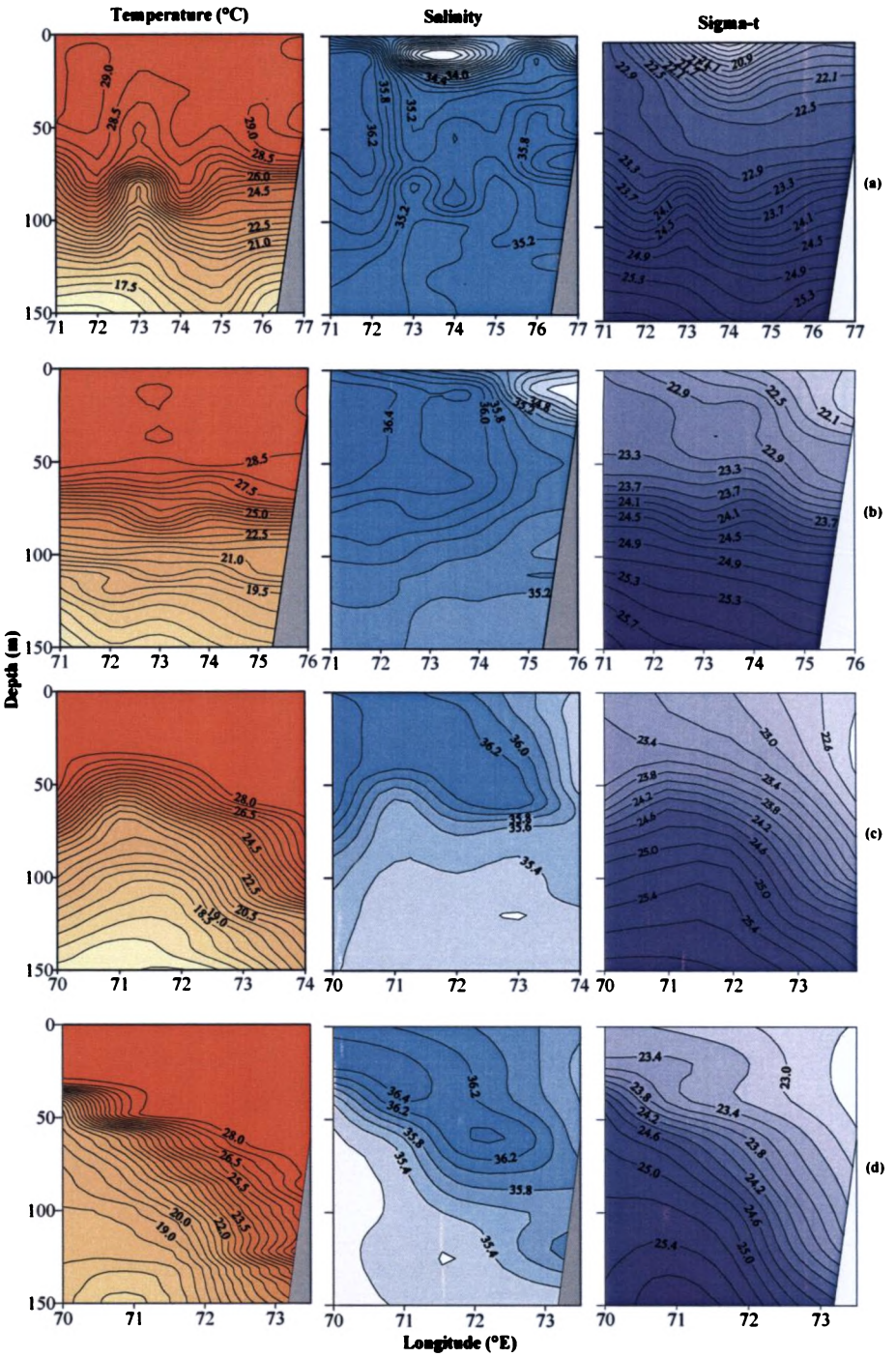

Fig. 3.3. Vertical distribution of Temperature, Salinity and Sigma-t along (a) 8°N (b) 10°N (c) 13°N (d) 15°N

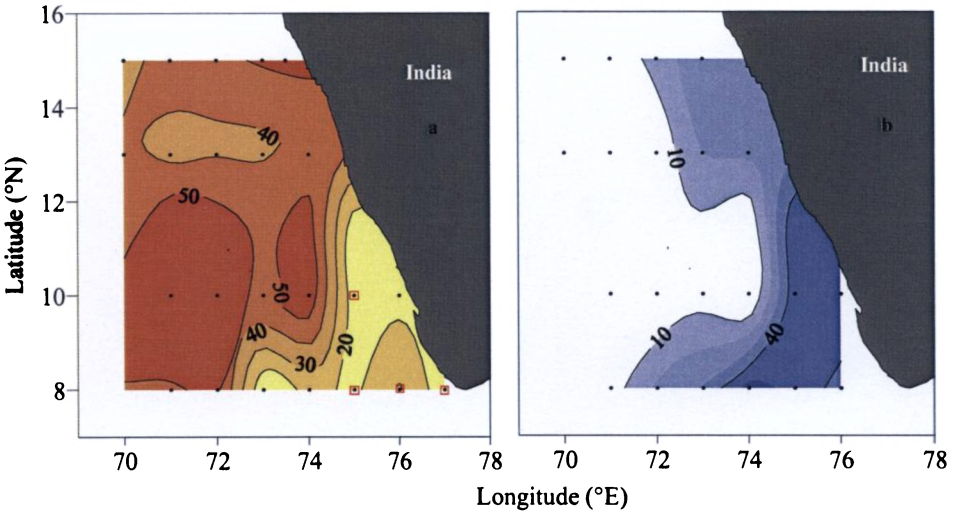

Fig.3.4. Spatial distribution of (a) Mixed Layer and (b) Barrier Layer. The red dots represent stations where thermal inversions are observed

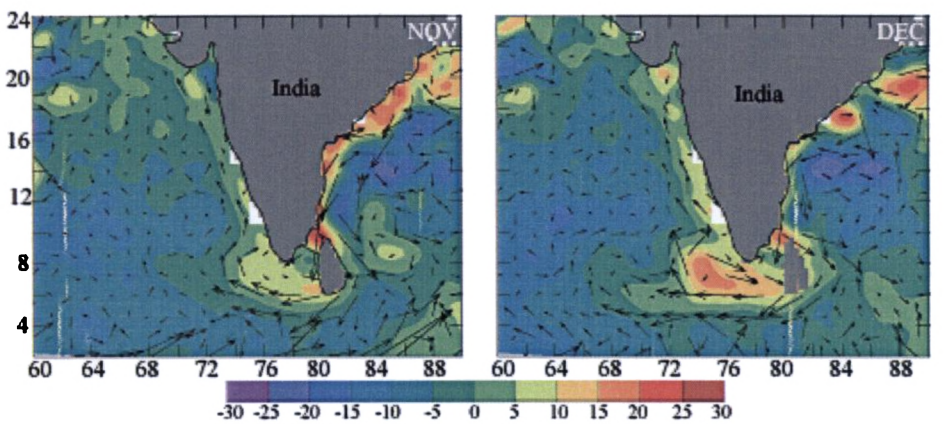

Fig.3.5. Distribution of monthly mean sea surface height anomaly for the month November and December, 2000 derived from TOPEX/POSEIDON. The vector represent the geostrophic currents derived from the SSHA.

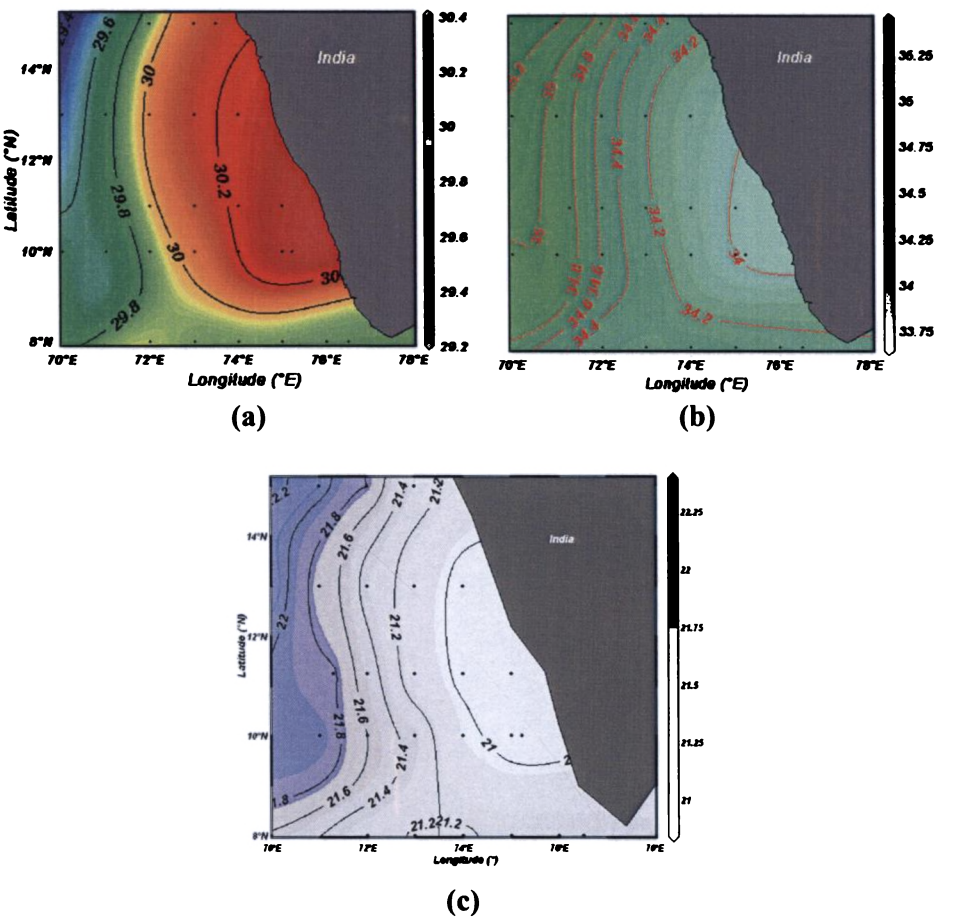

Fig.3.6. Surface distribution of (a) Temperature (b) Salinity (c) Density along the SEAS during March-April

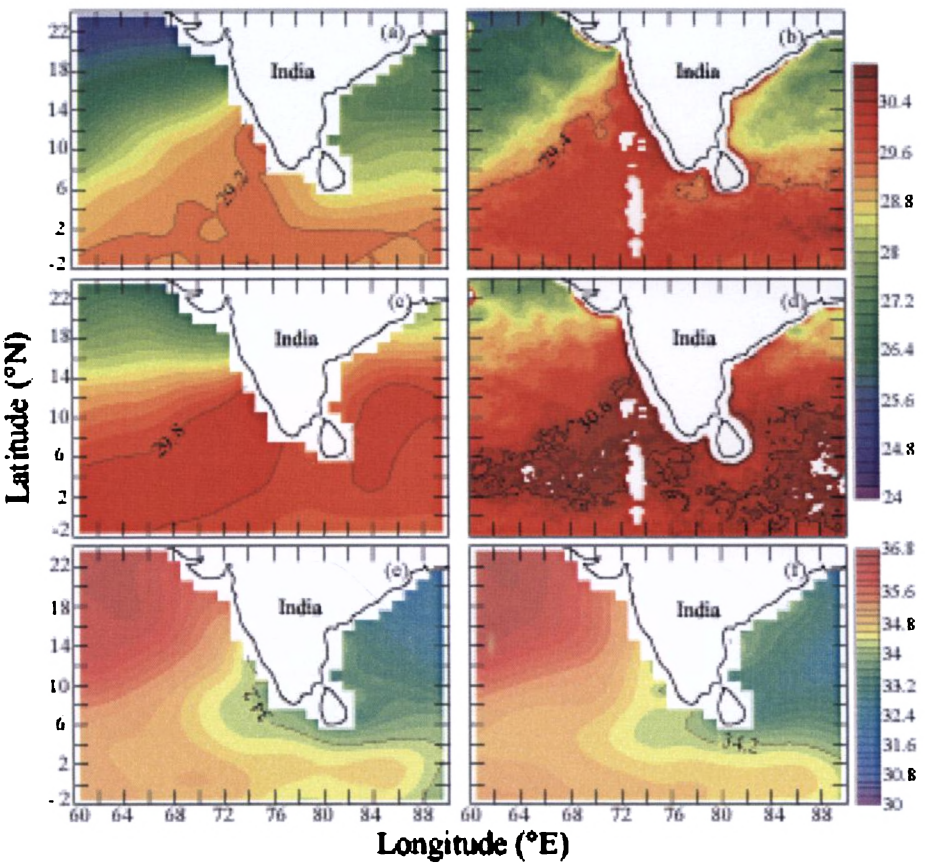

Fig.3.7. Surface distribution of SST (°C) (a), WOA05 climatology (c) and (b) & (d) TMI SST (°C) during March and April. Distribution of WOA05 salinity during (e) March (f) April.

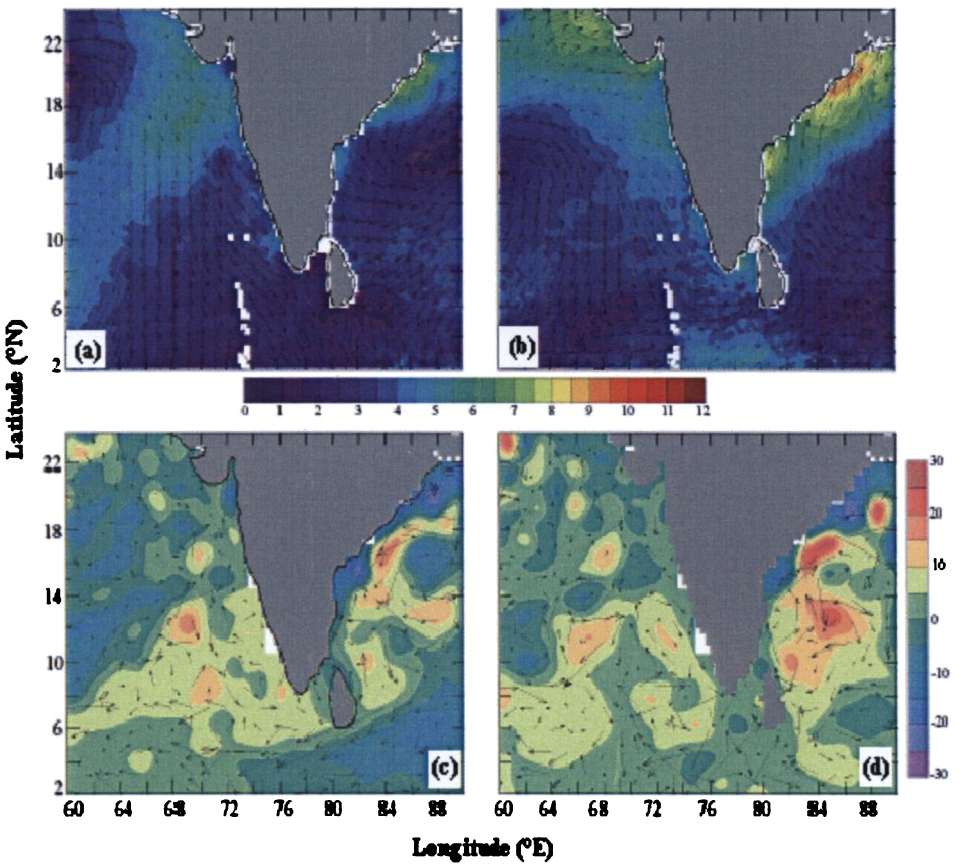

Fig.3.8. Spatial distribution of QuickScat winds (monthly mean) during (a) March (b) April. Fig. (c) & (d) shows monthly mean sea surface height anomaly for the month March and April, 2004 derived from TOPEX/POSEIDON. The vector represents the geostrophic currents derived from the SSHA.

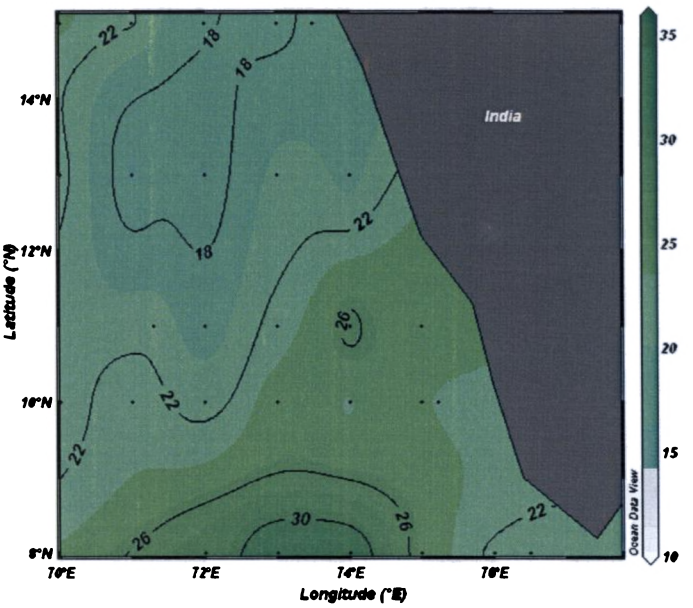

(a)

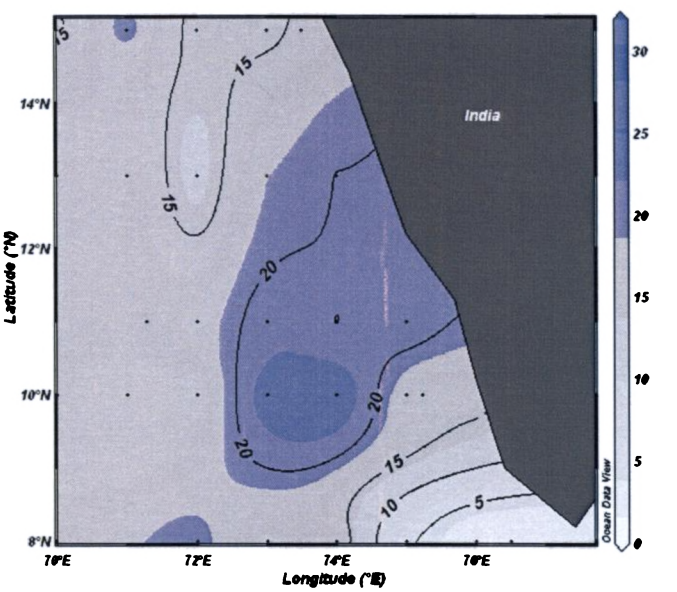

(b)

Fig.3.9. Spatial distribution of (a) Mixed Layer Depth (b) Barrier Layer thickness during March-April.

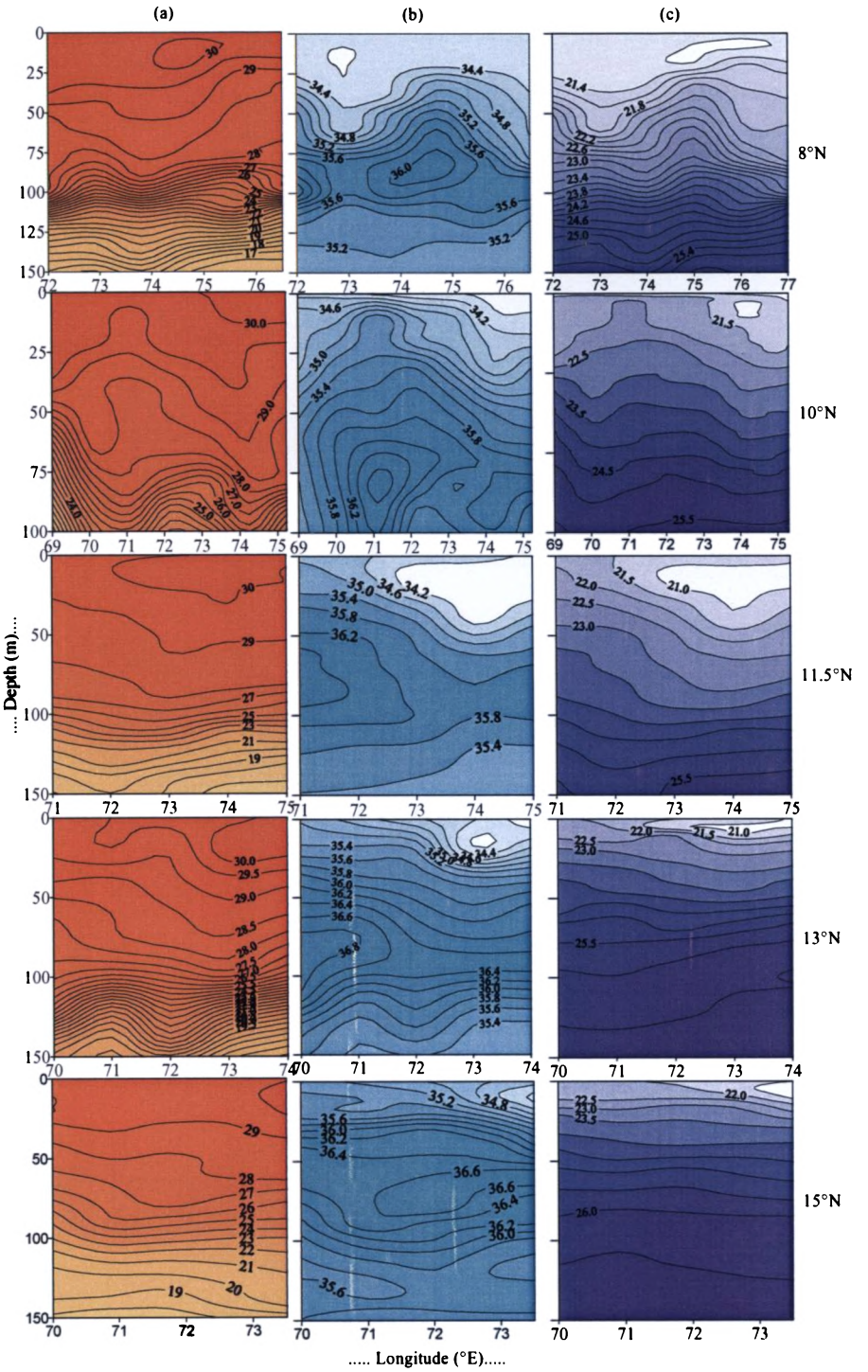

Fig.3.10. Vertical distribution (a) Temperture (b) Salinity and (d) Density during March-April

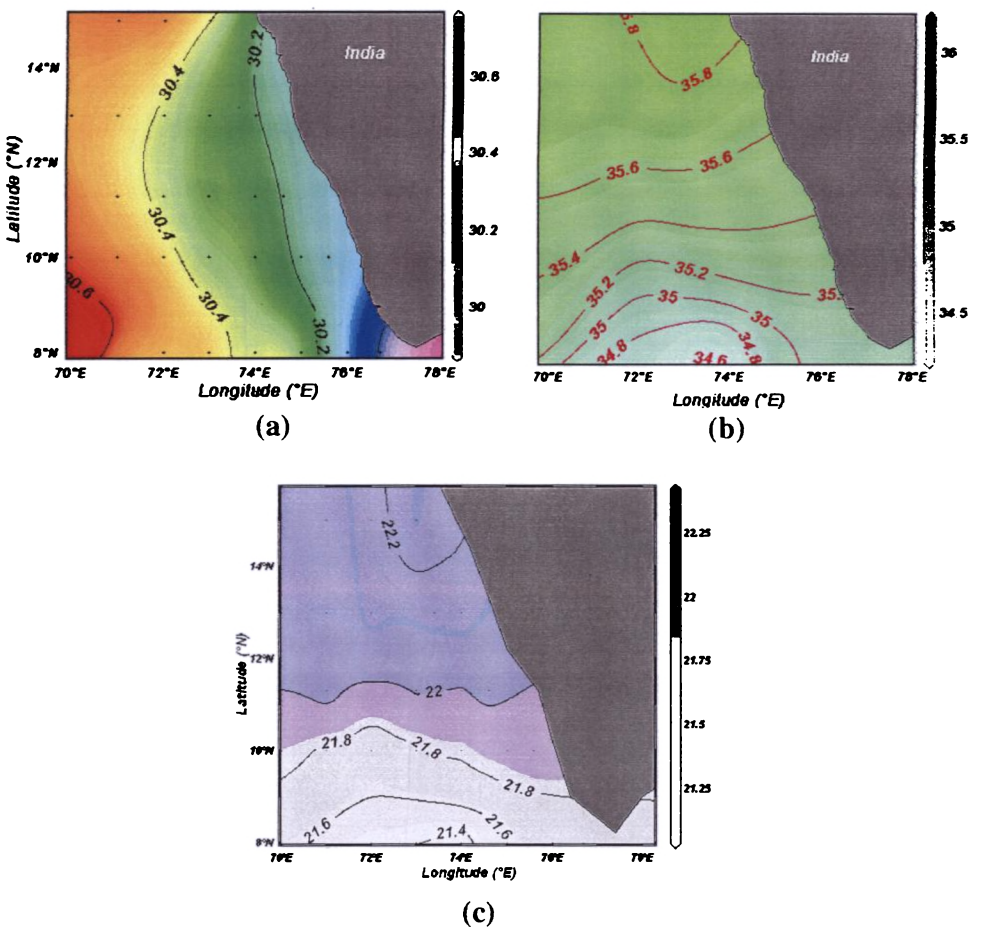

Fig. 3.11. Surface distribution of (a) Temperature (b) Salinity (c) Density along the SEAS during May-June

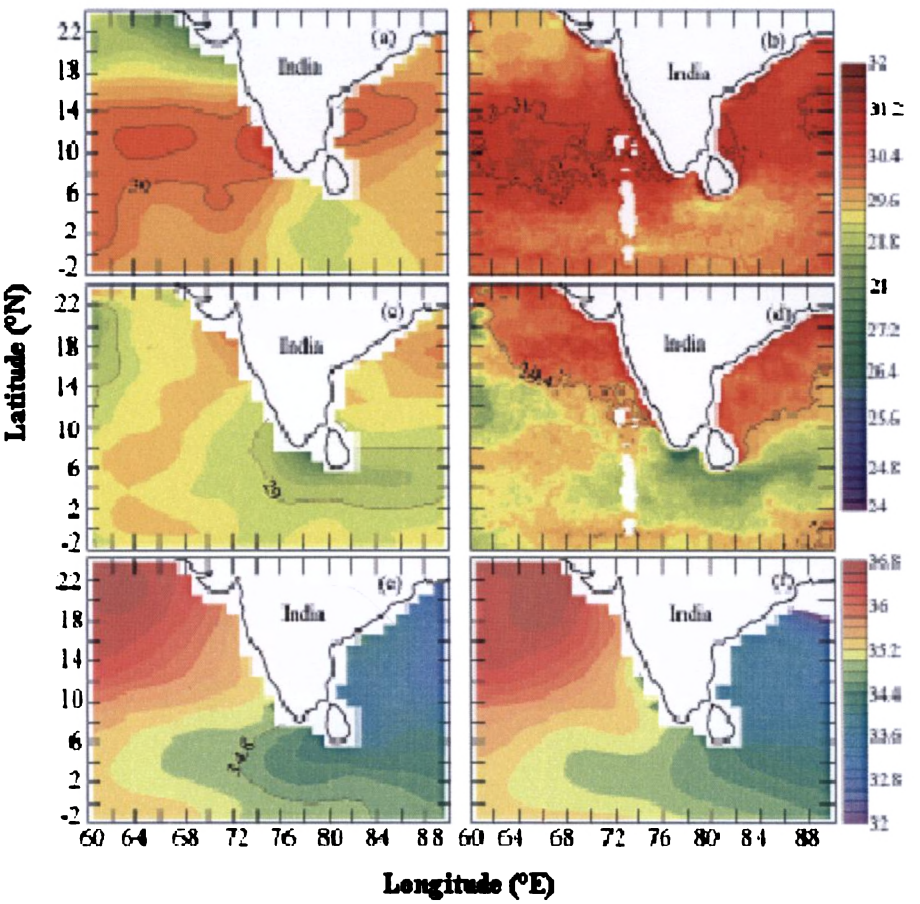

Fig. 3.12. Distribution of SST (°C) (a) & (c) WOA05 climatology and (b) & (d) TMI SST (°C) during May and June. Distribution of WOA05 salinity during (e) March (f) April.

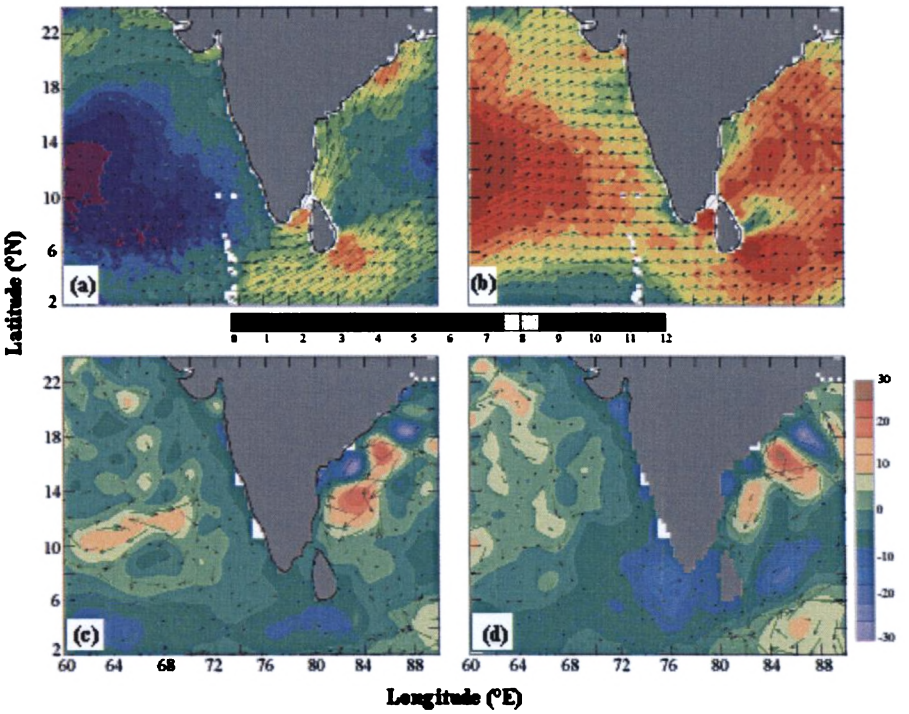

Fig.3.13. Spatial distribution of QuickScat winds (monthly mean) during (a) May (b) June. Fig. (c) & (d) shows monthly mean sea surface height anomaly for the month May and June, 2004 derived from TOPEX/POSEIDON. The vector represents the geostrophic currents derived from the SSHA.

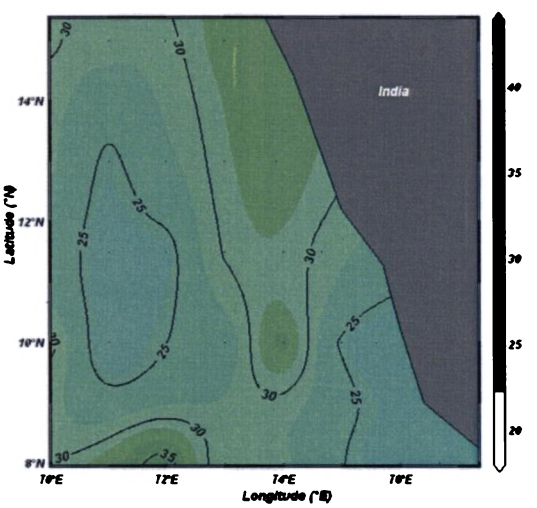

Fig..3.14. Spatial distribution of Mixed Layer depth (m)

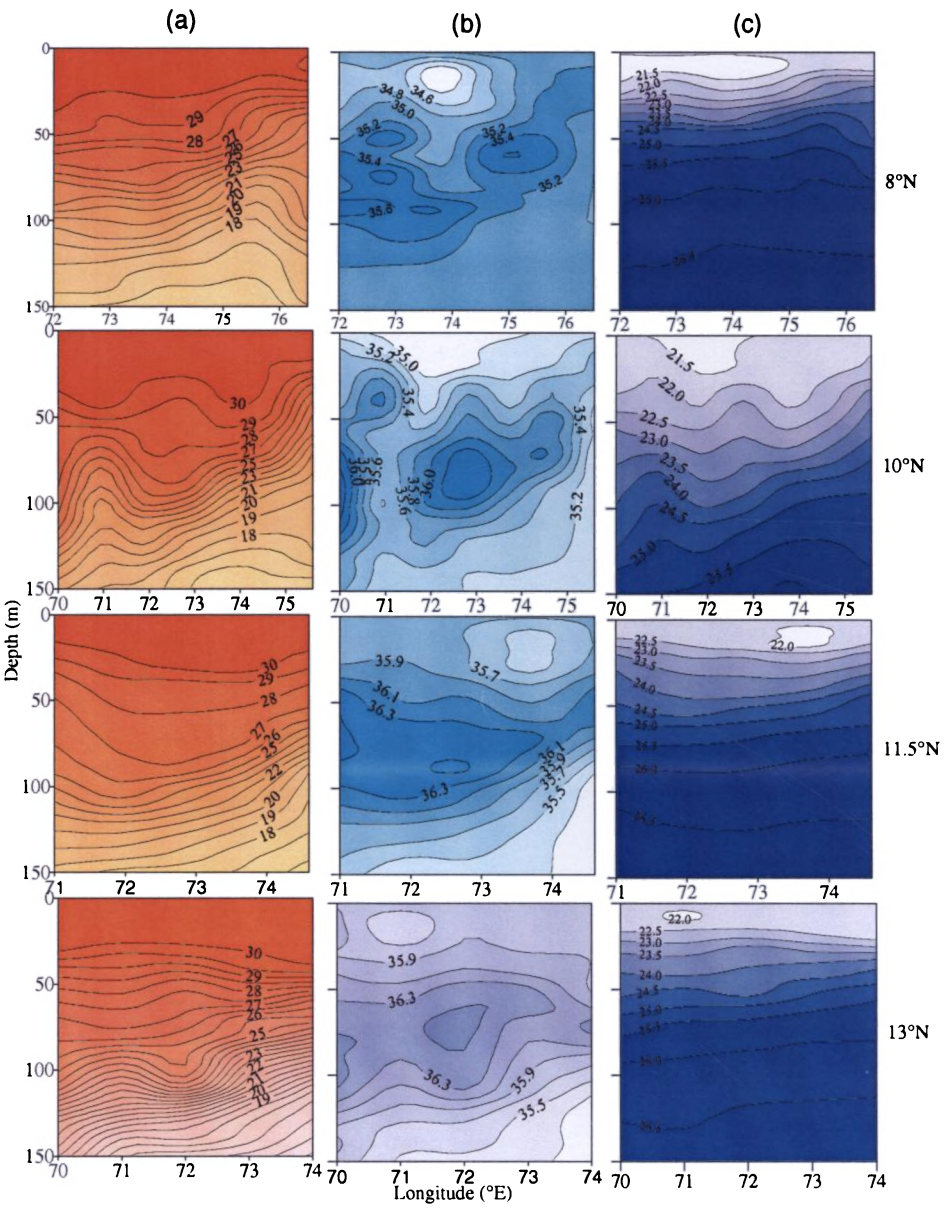

Fig.3.15. Vertical distribution (a) Temperature (b) Salinity and (d) Density during May-June

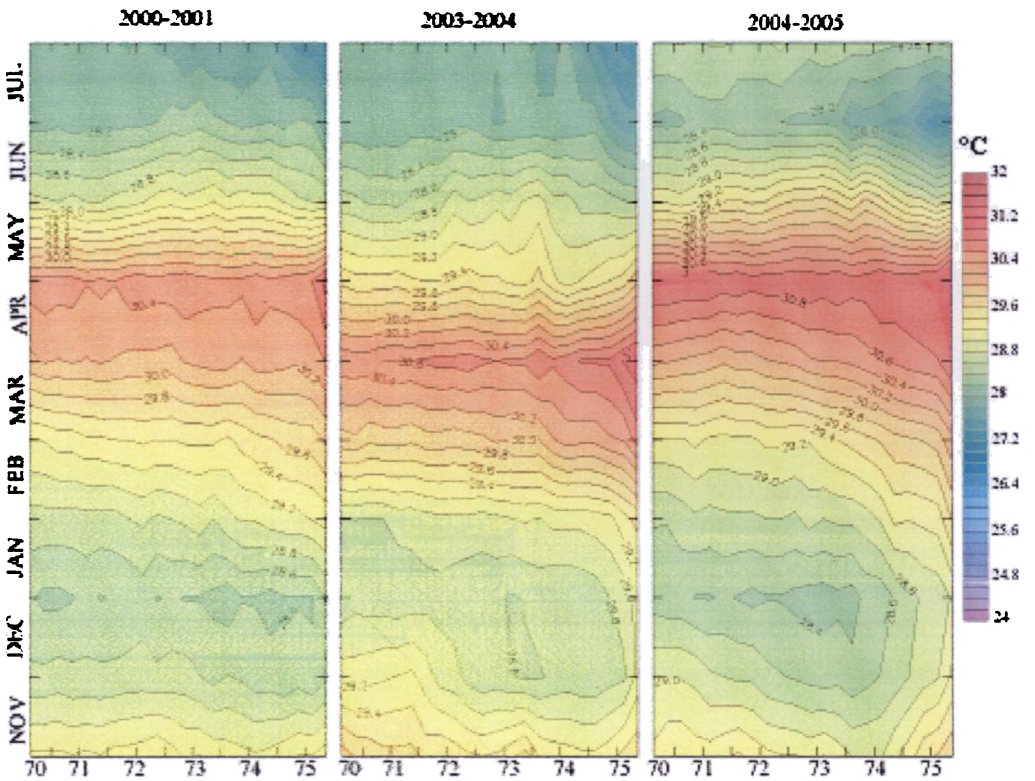

Fig.3.16. Evolution of SST along 10°N

****

Chapter 4

Role of Salinity on the Evolution of Arabian Sea Warm Pool

Contents

The AS exhibits distinct horizontal salinity gradients in the upper layers during winter. The net loss of fresh water in the northeastern AS (NEAS), due to excesses evaporation, and net fresh water gain in the southeastern AS (SEAS) due to the influx of Bay of Bengal water determines the salinity pattern of the SEAS. Thus the NEAS and SEAS have contrasting salinity characteristics during the period. Many previous studies showed that one of the mechanisms for the formation of the ASWP is the occurrence of low salinity waters in the surface layers of the SEAS. To understand the relative importance of low saline waters and local air-sea fluxes on the formation of ASWP, a comparative study has been conducted between NEAS and SEAS considering the hydrographic stations along 17°, 19°, 21° and 22°N (Fig.x). Role of different atmospheric and oceanographic parameters in the evolution of ASWP is explored, defining the entire EAS in two boxes as NEAS (NBox) and SEAS (SBox) the evolution of atmospheric and oceanographic parameters two boxes are defined, one in the NEAS (NBox) and the other in the SEAS (SBox, Fig.2.2). Monthly average data of SST (TMI-SST), wind (QuickScat), flux data (OA and SOC flux) fluxes are used in this study.

4.1 Evolution of ASWP

4.1.1 Results

The SST varied between 25.5° and 29.2°C, having colder water in the NEAS and warmer water in the SEAS (Fig 4.1). SST in the SEAS was greater than 28.6°C with maximum 29.2°C at 8°N, 72°E and showed a steady decrease northwards to a value of 25.2°C at 21°N. Average SST in the SEAS was greater than 28.7°C which, over the NEAS was 26.5°C. The SSS pattern showed the occurrence of low saline waters in the shelf region of the SEAS (average 35.13), while NEAS occupies relatively high salinity waters. The core of this low saline water (30m) from the BoB (detailed description in Chapter 3) is situated at 8°N and 74°E and towards north (upto 10N) it is confined to the shelf region. North of 10°N the presence of this low saline water is hardly visible. The intrusion of low saline waters to the SEAS is clearly observed in the horizontal distribution at different depths (Fig.4.1). MLD varied from 15m at 8°N to 75m at 21°N and shallow MLD were recorded in the low saline region. A thick barrier layer (40 m) was observed in the low saline water region and thickness decreases towards north. During this time, the low saline waters were confined to the shelf region and the warmer waters are situated at the central SEAS. The high SST in the SEAS during December-January was not due to the presence of low salinity water (Fig.4.1).

The SEAS is warmer than NEAS during December-January. The NEAS was under extensive winter cooling during the period while the intensity of cooling was less along SEAS. During late intermonsoon fall (Early November), the two regions show almost similar SSTs in the range 29°-29.2°C (Fig.4.2). The cooling (difference between the blue and red color in Fig. 4.2) during December over the SEAS was 0.4°C while that

over the Nbox are significantly higher (1.8°C). During the intensive cooling over the NEAS, in January, SEAS remain warmer by 2.2°C indicating that SEAS starts warming from higher SST (Fig.4.2).

During November-January, the SBox and NBox receives almost equal amount of short wave radiation of nearly 200-210 W/m2. The average wind speed over the Nbox was 6.2 m/s and in SBox it was 4.2 m/s. As a result, the net heat loss over the SBox was less (130 W/m^2) compared to the NBox (180W/m^2). Thus, the SBox loses less latent heat flux (50W/m^2) compared to the NBox, that is the SEAS gains about 50W/m^2 more heat than SEAS.

4.1.2 Discussion

SST in the SEAS is warmer (~ 2°C) than NEAS due to the net heat gain during December-January. Using the data from Hastenrath and Lamb, Thadathil and Ghosh (1992), showed that the SEAS remain as a region of net heat gain during November-January. Shenoi et al.1999b observed a localized patch of low heat flux over the SEAS during the period. The cold, dry northeasterly winds, which cause extensive cooling over NEAS, remain very week over the SEAS during the entire winter. The low winds over the SEAS are caused by the orographic effects of Western Ghats. The Western Ghats, spread over the east of the SEAS, effectively block the northeasterly winds and resulting less intensity over the SEAS (Kurian and Vinayachandran 2007). The modeling study by Kitoh (2002) agrees with the argument that, the weak winds over the SEAS is caused by Western Ghats. The low winds considerably decrease the loss of heat from the SEAS and keep it warmer. Thus the initial warming in the SEAS is due to the weak winter cooling and direct

influence of salinity is not evidenced in the observation. But the low saline waters from the BoB may provide favorable condition for the intensification of SST.

4.2 Establishmnet of ASWP

4.2.1 Results

SST varied between 28.2°-30.2°C, with colder water in the NEAS and warmer water in the SEAS. A zone of warm waters (>30°C) was noticed in the upper layers of the continental shelf of the SEAS (<50m). The width of the warm water showed large spatial variation with maximum extension along 11.5°N. The core of this water is centered at 10°N and 74 °E (near LS region) with a temperature greater than 29.4°C and it was clearly evident from the spatial of distribution of temperature at different depths (Fig.4.3). The observed average in SST in the SEAS was 29.9°C and that over NEAS was 28.8°C. Interesting feature is that the extension and thickness of the warm water coincides with the low saline water. The vertical extent of low saline waters (<34.2) in the upper few meters (~40m) became thinner (15) towards north. Interesting feature is that this low saline core centered at 10°N and 74°E coincides with warm water pool (Fig.4.3 & 4.6). The horizontal distribution of temperature and salinity along different depths shows the strong correlation between the warm water and salinity. Also, the horizontal and vertical extension of the warm water was found to be controlled by the low saline waters. Thick barrier layer of 25m observed due to the presence of low saline waters.

The SEAS is warmer than NEAS during March-April by 1.2°C (Fig.4.5). The NBox receives 20 W/m^2 more short wave radiation than SBox and the wind speed over the SBox (4.2 m/s) was weaker than the NBox (5.3m/s). The latent heat loss from the SBox was slightly higher

than (20 W/m^2) the NBox. Thus during March-April, NBox receives large amount of heat flux (80W/m^2) compared to the SBox (45W/m^2).

4.2.2 Discussion

During March-April, the NEAS receives large amount of heat than the SEAS. But the progressive warming in the SEAS was higher than NEAS. During the northeast monsoon, the latent heat flux over the SEAS is low but it starts disintegrating in March. By April, the SEAS experiences higher latent heat flux (Shenoi et al., 1999). They also showed that during March-April, there is no localized high in the net short wave radiation in the SEAS. Hence it appears that the air-sea fluxes are not the primary reason for the high SST in the SEAS.

The observations show that there is a significant relation between the low salinity water and warm pool. The presence of low saline water and resultant salinity stratification is an important factor in the buildup of heat in the ASWP (Rao and Sivakumar, 1999, Sanilkumar et al., 2004). The strong near surface stratification leads to a shallow mixed layer and consequently the net heat flux is distributed over a thinner mixed layer, resulting the warming in the SEAS. The width and thickness of the warm pool is exactly coincided with the low saline water. Recently Hareesh Kumar et al., 2008 showed that salinity stratification in the SEAS is found a favorable factor for the realistic simulation of the warm pool, especially in its horizontal extent and degree of warming. A 25m thick BL is observed in the low saline water region. The presence of BL favors the spring warming in the SEAS and the maximum effect BL on the SEAS SST (0.5°C) during in April (Masson et al., 2005). Thus the presence of

low saline water and BL are important in the evolution of warm pool and its spatial extension.

4..3 Conclusion

Cold dry northeasterly winds, which cause extensive cooling over NEAS, remain very week over the SEAS during the entire winter. Weak winds caused due to the orographic effects of Western Ghats considerably decrease the loss of heat from the SEAS and keep it warmer. As a result SST in the SEAS was warmer (~ 2°C) than NEAS due to the net heat gain during December-January. Thus the initial warming in the SEAS is due to the weak winter cooling and no direct influence of salinity is evidenced in the observation.

During March-April, NEAS receives comparatively large amount of heat than the SEAS, but the progressive warming is higher in the SEAS. The presence of low saline water and the thick BL (25m) in the SEAS has a major role in the warming. The spatial extension and thickness of the warm water exactly coincides with the low saline patch, again pointing to the significance of low saline water in the formation of warm pool.

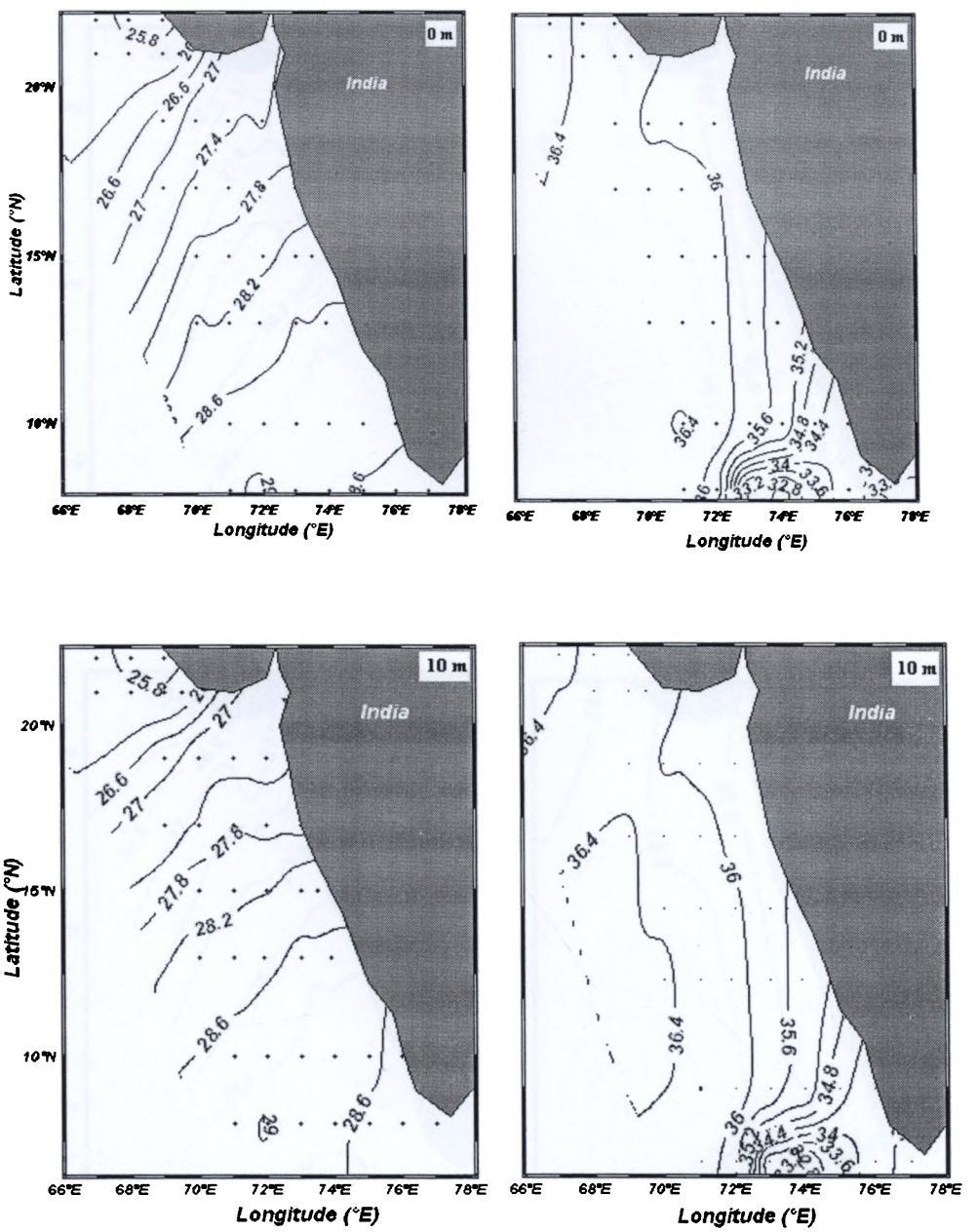

Fig.4.1. Distribution of (a) Temperture (b) Salinity

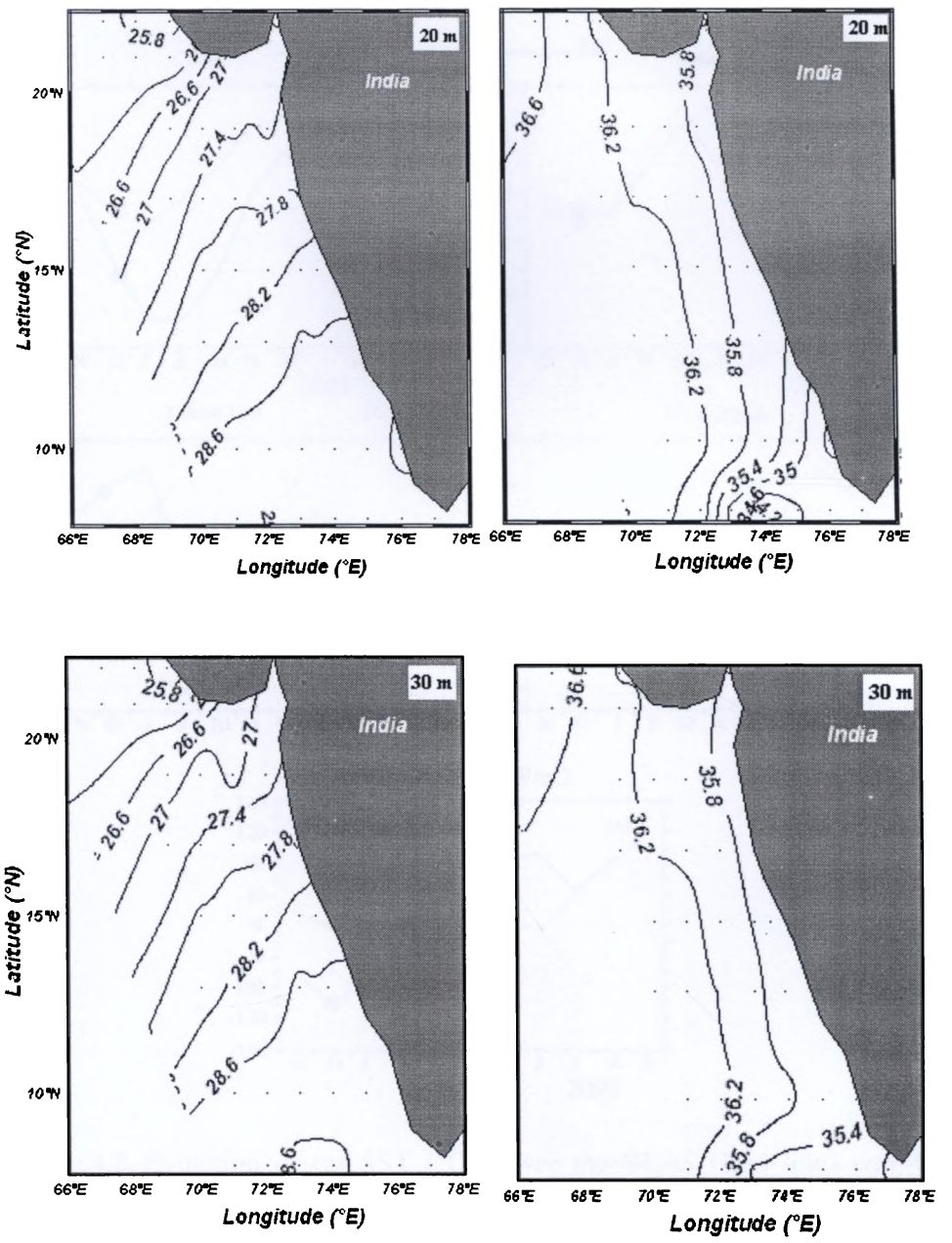

Fig.4.1. Continued

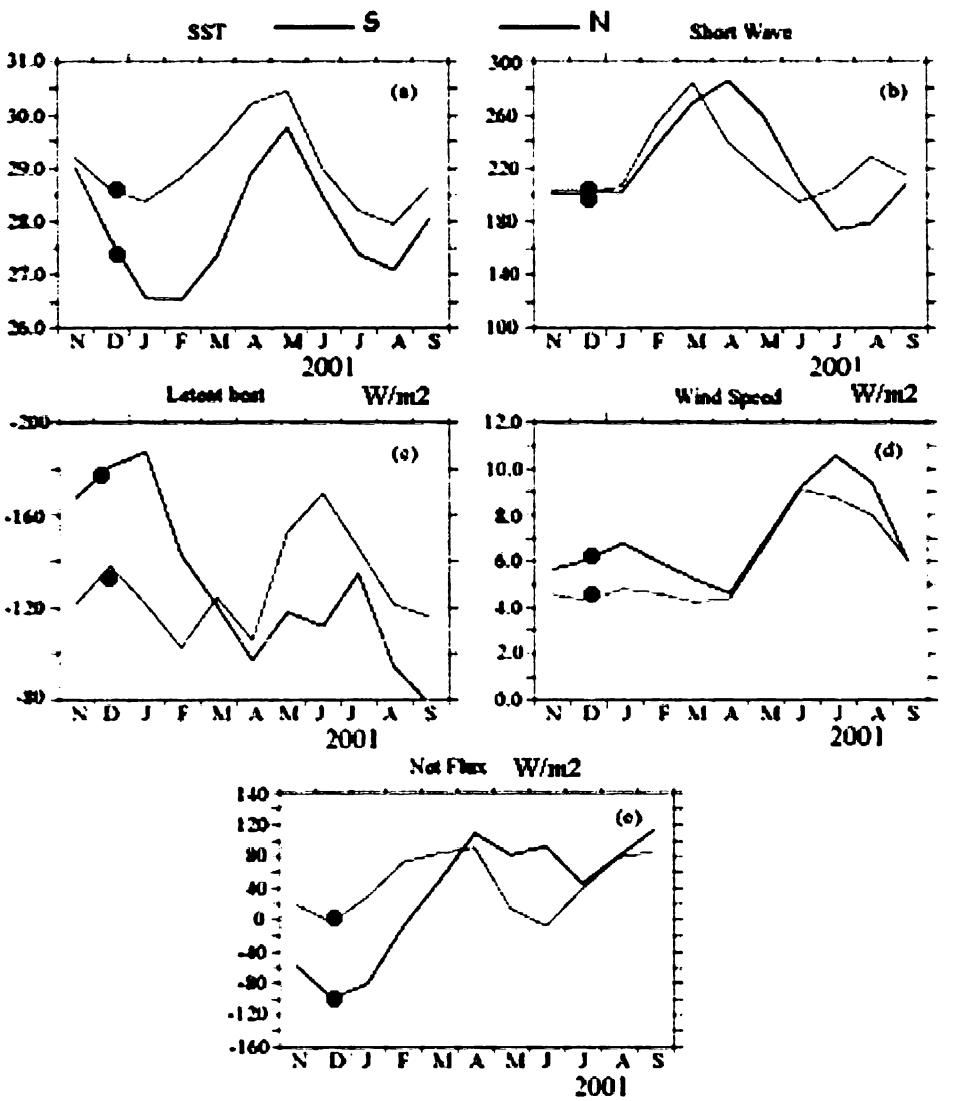

Fig.4.2. Evolution of (a) SST (°C) over the SEAS (Red line) and NEAS (Blue line) from (b) Short wave radition (W/m2) (c) Latent heat flux (d) Wind Speed (e) Net heat flux during the period November-2000 to September-2001

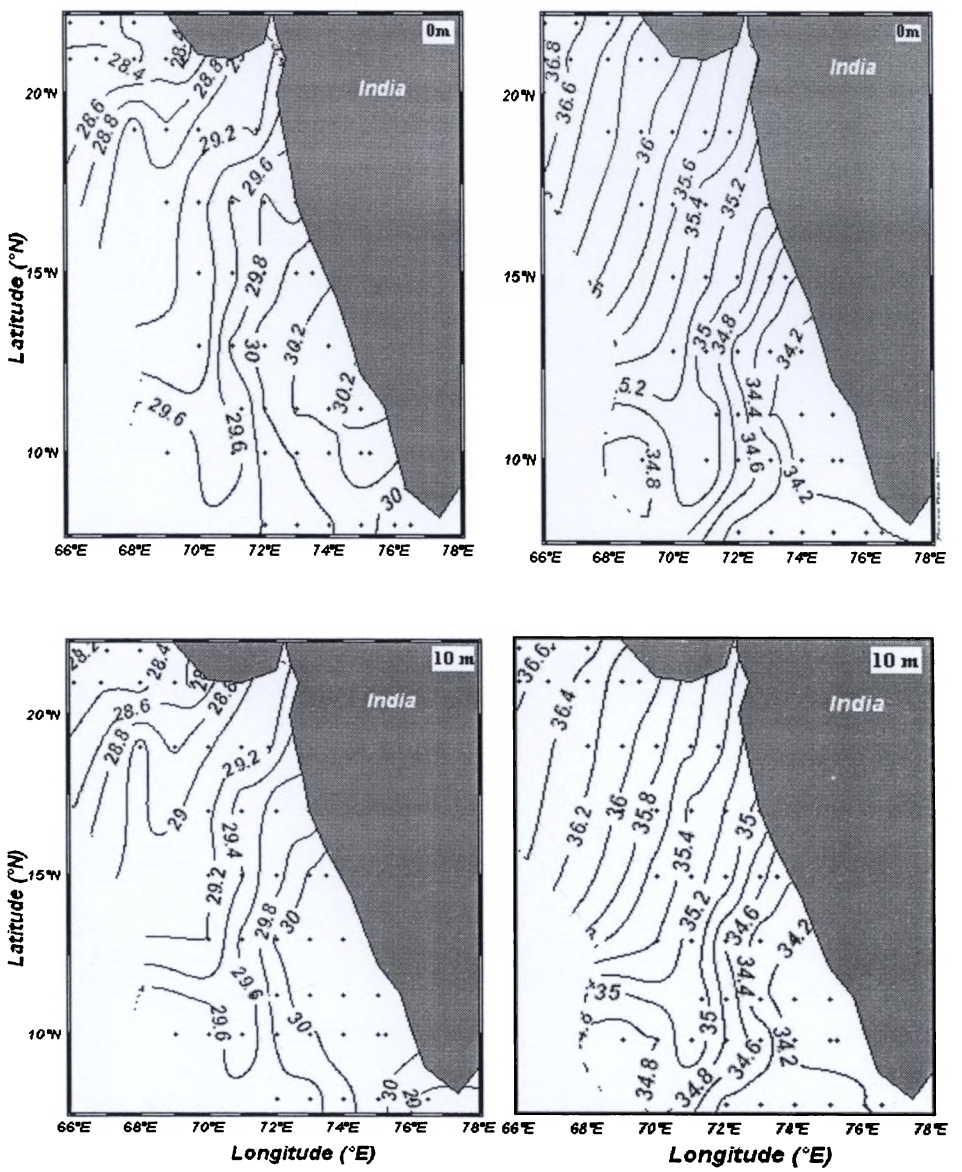

(a) (b)

Fig.4.3. Distribution of (a) Temperture (b) Salinity

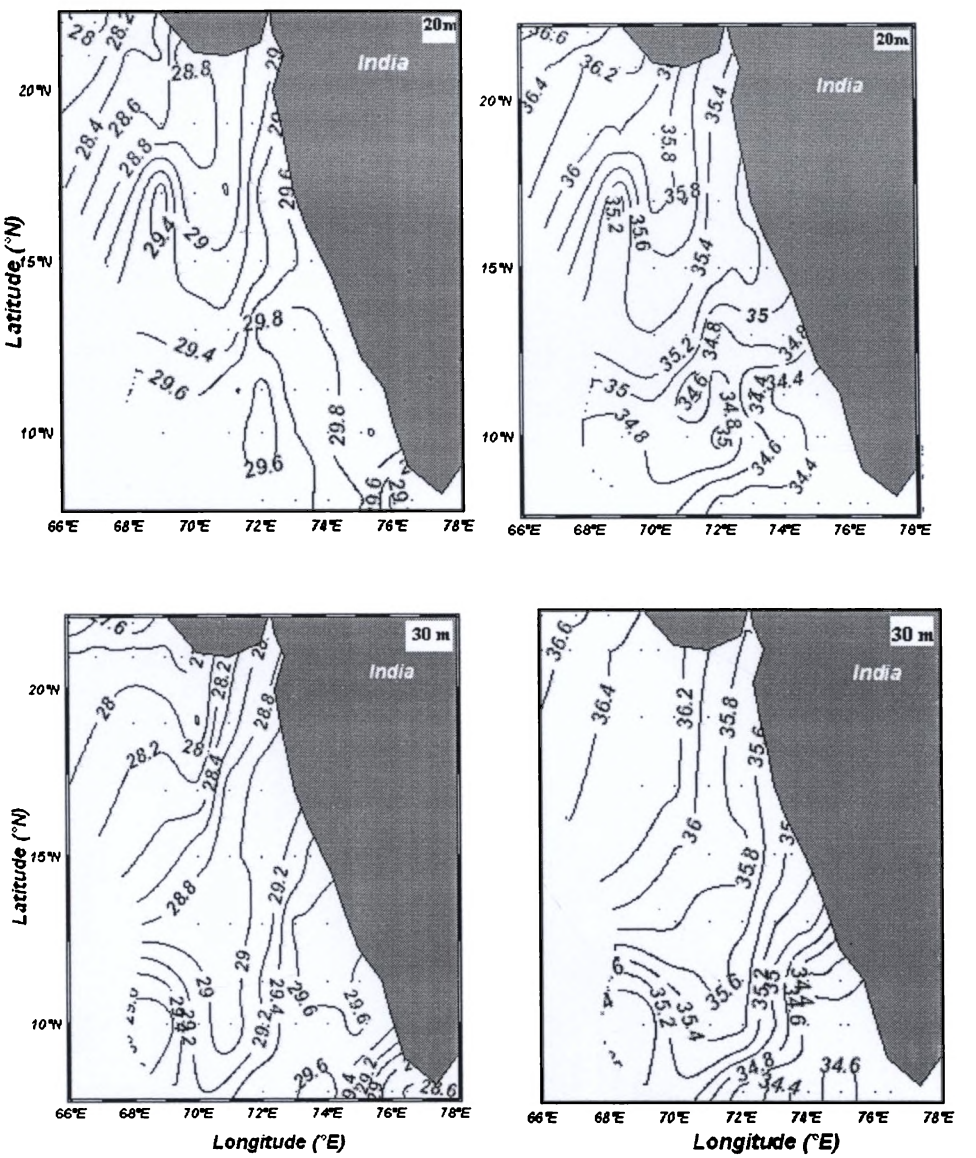

Fig.4.3. Continued.

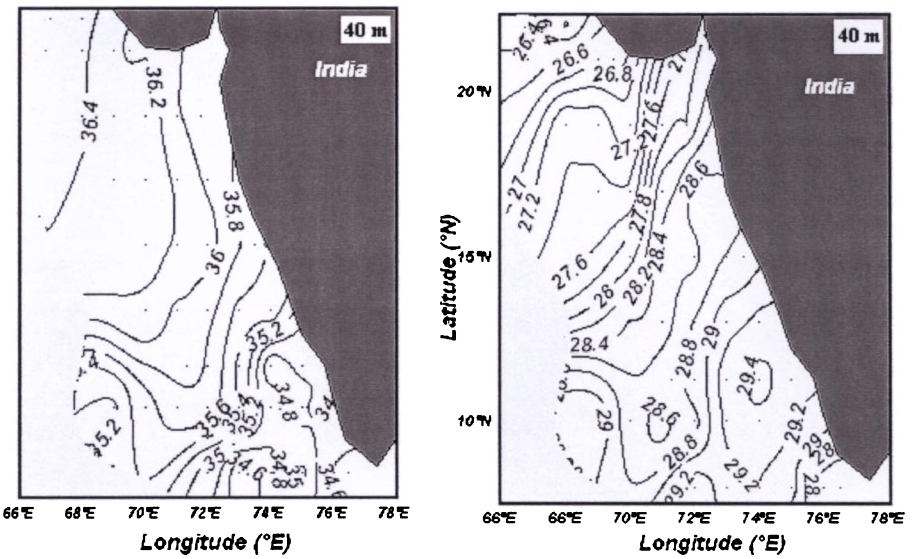

(a) (b)

Fig.4.3. Continued

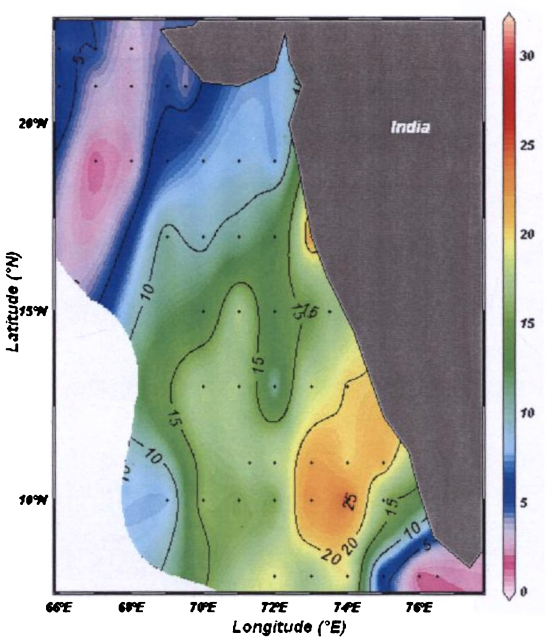

Fig.4.4. Barrier Layer thickness during March-April

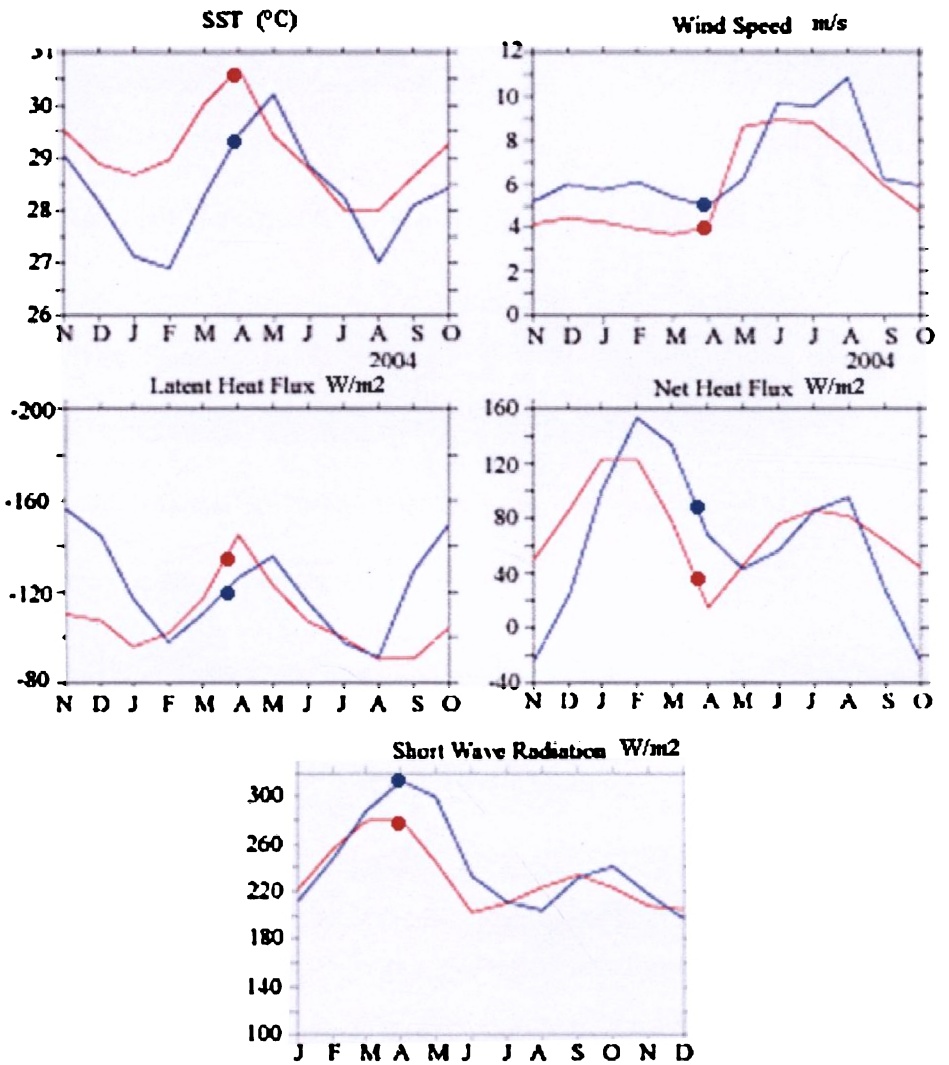

Fig.4.5. Evolution of (a) SST (°C) over the SEAS (Red line) and NEAS (Blue line) from (b) Short wave radition (W/m2) (c) Latent heat flux (d) Wind Speed (e) Net heat flux during the period November-2000 to September-2001.

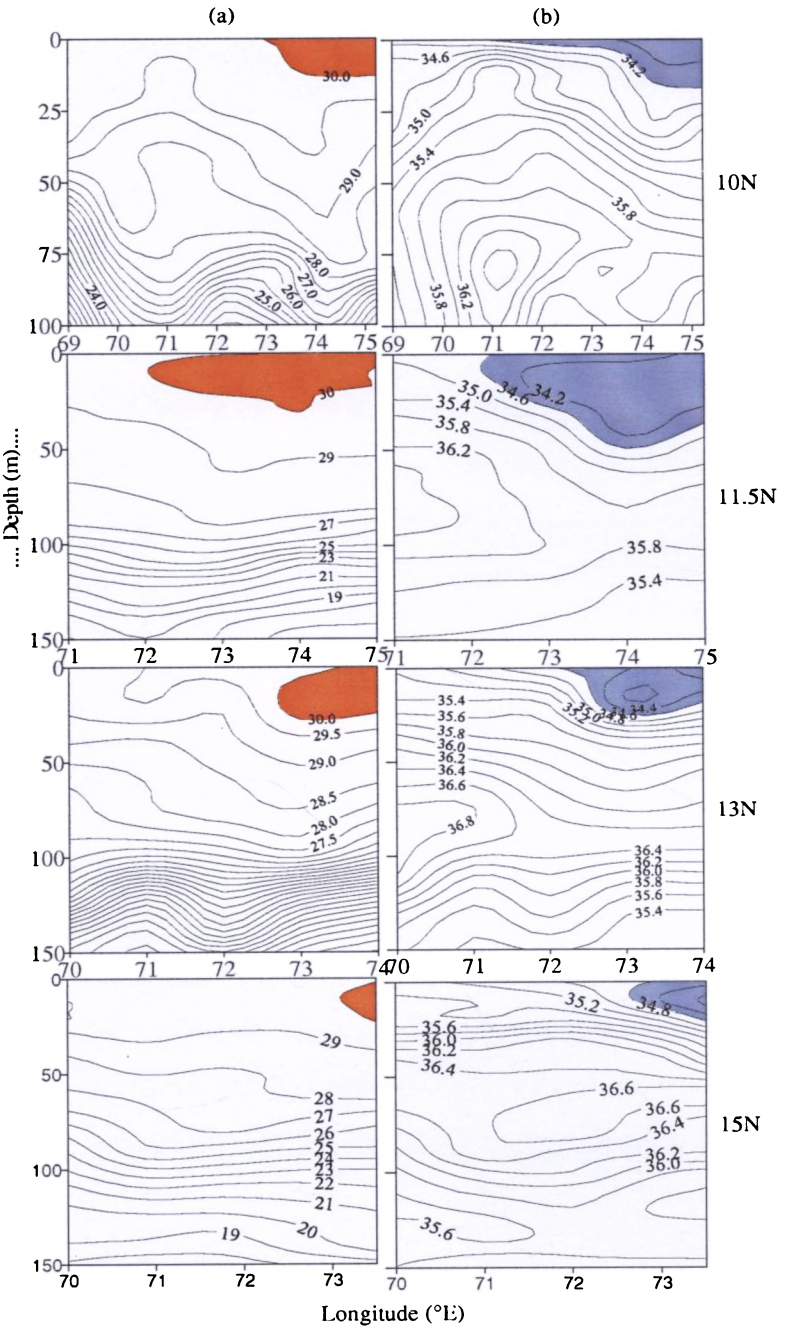

Fig.4.6. Vertical distribution of (a) Temperature and (b) Salinity. Red colored region represents the warm water and blue colored region represents the low saline water region

****

Chapter 5

Role of Mesoscale features on the Evolution of Arabian Sea Warm Pool

Contents

5.1 Introduction

The heat budget of the mixed layer is an important factor to investigate in order to understand the air-sea interaction of the SEAS region. It has profound influence on the Indian summer monsoon. Based on the global and regional climatologies, Rao and SivaKumar (1999) opined that the heat build-up in the mixed layer during the pre-monsoon (March-April) is primarily driven by the surface heat flux through the ocean-atmosphere interface. Weller et al. (2002) also suggest that, the upper ocean processes in the spring season are primarily one-dimensional (i.e., vertical), with the warming being a resultant of the surface heat fluxes and the penetrative radiation. However, recent studies have shown that the horizontal processes of the oceans also play an important role in forming the SST anomalies on seasonal to interannual time scale (Grotnzer et al., 1998). Halliwell et al. (1998) have mentioned that the SST changes in the Gulf-stream region are primarily driven by the changes in oceanic horizontal heat

advection and entrainment heat flux from below the mixed layer. Modeling studies in the North Atlantic Ocean also have shown that the ocean heat transport is as important as surface heat fluxes in determining the SST variability (Seager et al., 2000). Earlier studies in the SEAS during pre monsoon period suggested that the heat budget of the upper ocean is mainly a balance between the vertical mixing and the surface heat flux. However, the role of advection in the ASWP has not yet received considerable attention.

The one-dimensional models are seldom a complete description of the mixed layer processes where variability may still be brought by the oceanic advection and sub grid scale processes (Qiu et al., 2002). The southern part of the SEAS is an eddy prominent region with a horizontal dimension of 100 to 500 km and vertical extent of some hundreds of meters. These eddies play an important role in the ocean dynamics as well as transport of heat, salt and other oceanic properties. In an eddy prominent region, the large-scale mass divergence by the mean flow is balanced by the eddy induced divergence, which becomes an essential part of the turbulent cascading (downscaling) of momentum and heat in the upper ocean into sub grid scales (Gent and Mc Williams, 1990). The eddy presents in the SEAS thus may have an important role on the evolution of ASWP which is, however, not been explored in any detail. Together with this advection, the aforementioned eddies may play a significant role on the evolution of ASWP.

This chapter describes the relative importance of surface heat flux, advection, eddy diffusion, vertical mixing and entrainment on the evolution of ASWP.

5.2 Theory

The mixed layer temperature tendency of the upper ocean is controlled by the surface heat fluxes, horizontal advection, eddy diffusion, vertical mixing and entrainment. The evolution of mixed layer temperature (T) can be written as,

$$\partial T/\partial t + [u_T \partial T/\partial x + v_T \partial T/\partial x] + w\partial T/\partial z =$$

$$[Q/h\rho C_p] + \partial/\partial z(K_h.\partial T/\partial z) + A_h(\partial^2 T/\partial x^2 + \partial^2 T/\partial y^2)$$

where, $\partial T/\partial t$ is the mixed layer temperature tendency,

$u_T \partial T/\partial x + v_T \partial T/\partial x$ is the horizontal advection,

$A_h(\partial^2 T/\partial x^2 + \partial^2 T/\partial y^2)$ is the eddy diffusion,

$(w\partial T/\partial z + \partial/\partial z(K_h \partial T/\partial z))$ is the vertical mixing and entrainment term and $Q/h\rho C_P$ is the surface flux (Schematic representation as shown in the Fig.5.1). The computation methods of each term are described in section 2.3.1 to 2.3.5. Accepting the fact that the effects of tidal processes on the heat budget terms can not be explicitly resolved in the given set of data. However, considering the objectives of the present work to look at the spatial pattern of heat budget terms on the evolution of the ASWP, the effects of tides can safely be disregarded.

5.3 Results and Discussion

Spring inter monsoon (SIM) periods in the Arabian Sea normally experienced by light winds, clear skies and strong solar radiation yielding an average heat gain of 101.1 W/m2 (Wiggert et al, 2005). The high solar insolation and relatively weaker winds during this time enhances the surface temperature of Arabian Sea warm pool. Fig.5.2. shows the

distribution of sea surface temperature (SST) from our ship observations. The warmer regions are close to the coast with maximum value of 30.2 °C and the isotherms are running almost parallel to the coast.

Salinity structure showed that a low saline water (<34.2) occupied between 8°N and 13°N in the upper few meters and tapered towards the north. This low saline plume was confined to the shelf region with minimum value of 33.9 at 10°N (Fig.3.6.b). The isohalines are almost aligned in a similar pattern of isotherms. The vertical structure of isotherms and isohalines along 8 and 10° N showed a downward shift between 73° - 74°E (Fig.5.3). This downward shift in isotherms and isohalines was due to the presence of eddies that as evident in the SSHA pattern (Fig.3.8c). The low saline water mass in the SEAS was due to the intrusion from the Bay of Bengal. In the subsurface, the presence of high saline core (>35.6) was observed. This was due to the presence of Arabian Sea High Salinity Water (ASHSW) subducted from northern part of the Arabian Sea and advected towards the south along the main thermocline (Prasad and Ikeda 2004) (detailed description of the circulation in section 3.1.2).

In this study each term of the temperature evolution is analyzed for the entire mixed layer depth (MLD). A deeper MLD (>30 m) is observed in the southern part of the study region with a relatively shallow MLD (18 m) in the north (Fig.5.4). A shallow MLD of (<20m) is found in the southern tip of the peninsula.

5.4 Heat budget in the mixed layer

In this section the heat budget of the mixed layer are described as resolved from the analysis. All terms are expressed as depth integral over the mixed layer depth, unless specified otherwise.

5.4.1 Temperature tendency

Tendency of temperature is an order of magnitude weaker compared to the other heat budget terms and it represents the net effect that brings by a combination of other mixed layer processes such as advection, vertical mixing, horizontal diffusion and surface heat fluxes. The temperature tendencies of the ASWP are found as positive (i.e. warming) in the northeastern side of the pool with a maximum approaching $1.5x10^{-6}$ $°Cs^{-1}$at the coast (Fig 5.5). The northwest warming in the study area is due to the net surface flux (positive toward the ocean) into the ocean (Fig.5.6). The tendency of mixed layer temperature shows that the mixed layer warming in the northern part of the warm pool mainly follows the surface heat flux. It gives an indication that the northern part of the ASWP surface heat flux has a larger control on the mixed layer warming.

In the southeastern part of the warm pool (south of 11°N), the tendency of temperature has some features with a horizontal size of 100km. Positive and negative temperature tendencies with size of eddies are the prominent feature in this region (Fig.5.5). The surface heat flux has no resemblance to this shape of tendency. This is the region where mesoscale features were prominent during the study period as evident in the altimetry data. The magnitude of this warming is only 10% of that of the warming in the north (Fig.5.8).

5.4.2 Advection

Advection is the processes by which a local gradient of material property (here it is the temperature) is being transported according to the currents. The advection of the northeastern part of the warm pool shows a strong positive value (Fig.5.7). The positive value of advection shows the

advective warming. The advection patterns in warm pool area shows coastally oriented strong positive contours upto the central region of the warm pool. The background mixed layer temperature was warmer in the costal side and relatively colder farther west (Fig.5.2). Thus the effect of advection reduces this gradient by transferring more warm water to the western side of the warm pool and causing an advective warming. The magnitude of advection in the northwestern part of the warm pool region is $0.5x10^{-5}$ °C m s^{-1} which is only 10% of the net surface heat flux. The magnitude of the diffusion cannot balance the rest of the surface heat flux, which might be the residue due to vertical advection and entrainment.

In the northern part of the warm pool the surface heat flux shows the highest value in the study region. The advection delineates a zero contour running northwest and passing through the center of the study region. To the east of the zero contours the advection warms the region. Thus the highest surface heat flux into the ocean in the northern part is exported to the west to further warming the western side of the warm pool. Thus advection exports the heat from the warm pool, which mostly comes as the surface heat flux in the northern side. This export causes the mixed layer depth to an average value of 40m in the northwest. In the extreme southeast the tendency term (Fig. 5.5) show a strong cooling and it is well explained by the negative advection there.

The effect of local wind and subsequent Ekman transport has been computed and compared with the geostrophic currents in odder to find the impact of Ekman transport on the total advection of heat in the mixed layer. It has been found that the Ekman velocity is much smaller (average 4 cm/s) than the near surface gostrophic currents. The analysis period represents the transition period of monsoon (from northeast to southwest

monsoon), and thus the winds are generally weaker and resulting in a smaller Ekman drift than the background geostrophy. The computed advection term with a total current of geostrophy and Ekman drift and the results show that no appreciable differences in the advection term compared to the non Ekman drift case, except small changes found in the southern part. Thus, the advection due to the Ekman component is eliminated.

5.4.3 Diffusion

Unlike the advection, the effect of horizontal diffusion is not so significant in the northeastern part of the domain (Fig.5.8). The average value of diffusion is nearly zero in the northeastern part of the domain where advection showed a warming effect. The effect of eddy diffusion becomes significant on the southern part of the domain where eddy features where prominent during the observation period. The maximum diffusion in the southern part of the domain is found to be 2.5×10^{-5}°cm s^{-1} which is greater than the amount of advection there (Fig.5.7). The effect of eddy induced diffusion is to smooth the temperature gradient. The prominent pattern of eddy-induced diffusion has size of mesoscale close to the southern part of the domain. It is interesting to note that the mixed layer temperature tendency in the southern part of the domain also have features similar to the size of mesoscale as shown in the diffusion term. Thus the effect of eddy induced smoothing of temperature in the mixed layer is prominent in the southern part of the warm pool region. The surface heat flux didn't have such fine scale structures to reflect in the temperature tendency.

The magnitude of diffusion in the southern part of the warm pool region suggests an eddy diffusion coefficient as large as $A_h=3x10^4$ m^2/sec. This high value resolved in the analysis was of course partially related to the course resolution of the data (1 degree) used in the present study. The demand of a high eddy diffusion coefficient shown in the present data analysis implies that a coarse resolution model should include this large value of eddy diffusion coefficient, in order to have reasonable account of eddy induced lateral mixing. However such large value of eddy diffusion smoothes out the variability of the order of mesoscale in a numerical model. This eventually points to the necessity of resolving eddy induced diffusion as an indirect estimate of eddy induced transport as used Gent and McWilliams parameterization (Gent and McWilliams, 1990). The present analysis showed that the models have a reasonable simulation of diffusive processes in the ASWP, especially in the southern part of the domain, either a fine resolution is necessary to resolve mesoscale induced mixing reasonably or an indirect parameterization of eddy induced transports should be included in the coarse model.

5.4.4 Vertical mixing

Although the horizontal advection, diffusion and surface heat fluxes can account the major features of the temperature tendency qualitatively, it is necessary to consider the effect of vertical mixing in the detailed account of surface heat budget. The Fig. 5.9 shows the vertical mixing term integrated over the mixed layer. The negative values showed the cooling by deepening of mixed layer and positive value show the warming by shoaling of mixed layer. Unlike the other terms presented above, the vertical mixing does not show much similarity with the temperature tendency except in the southern domain. In the southern part

of the domain the vertical mixing also shows features of size 100km in horizontal as similar to the eddy induced heat flux and temperature tendency. However the magnitude of the vertical mixing brought by the eddy induced currents are stronger than the eddy induced lateral heat flux.

The study area is divided into two regions (a) North box (B_N) (region between 11°-15°N) and (b) South box (B_S) (between 8° -11°N). The vertically integrated mixed layer heat budget terms were spatially averaged for each box (Fig. 5.10). The surface heat flux is stronger in the north than in the south. The vertical mixing dominates the advection in the southern part. This is clearly evident in the deeper mixed layer depth as seen in the southern part of the SEAS (Fig.5.3). The input surface heat is thus balanced between vertical mixing and horizontal advection in the southern part of the domain. The eddy diffusion shows a slight warming although the magnitude is relatively lower than the advection or vertical mixing. In the northern part (B_N), the surface heat flux is balanced between advection and diffusion while the southern domain (B_S), the advection is dominated over vertical mixing and the horizontal diffusion is negligible.

5.5 Conclusion

The study estimated the importance of various mixed layer processes such as horizontal advection, horizontal eddy induced diffusion and surface heat fluxes on the formation of ASWP during the SIM. The study showed the warmpool have a scale selection over various mixed layer processes according to the region. The largest variability in the heat content of the surface ocean of ASWP is mainly influenced by the surface heat fluxes in the northern part of the domain while the advection have

only a subsidiary role to spread the warmpool from coast to far west. In the far south of the domain, the effect of eddy-induced transport is seen as large as the advection. This is mainly associated with the eddy prominence in that region during the transition of monsoon.

It is to be noted that the present study is not a climatological representation of the warmpool mixed layer processes. More over the coarse resolution of the *in situ* data limits to get closer look into more detailed processes of mixed layer heat budget evolution of ASWP. However, with the available data the study categorized the significance of various mixed layer processes and its regional dominance through out the evolution of ASWP. The study also dictates those processes/parameters which are necessary for the regional modeling of the ASWP to have a reasonable simulation.

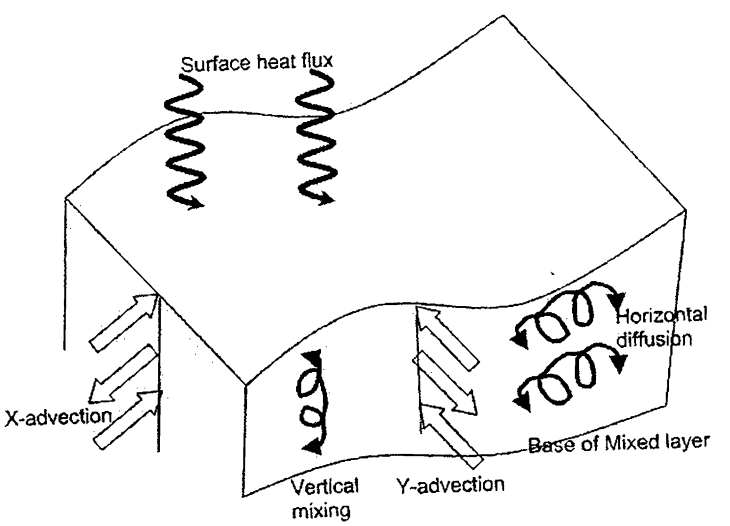

Fig.5.1. Schematic representation of the mixed layer processes

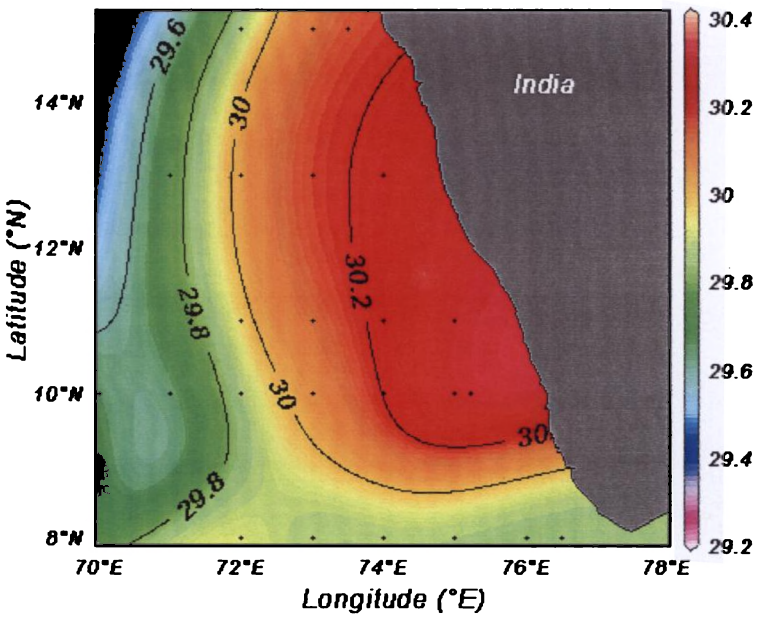

Fig.5.2. Spatial pattern of SST during the observation time

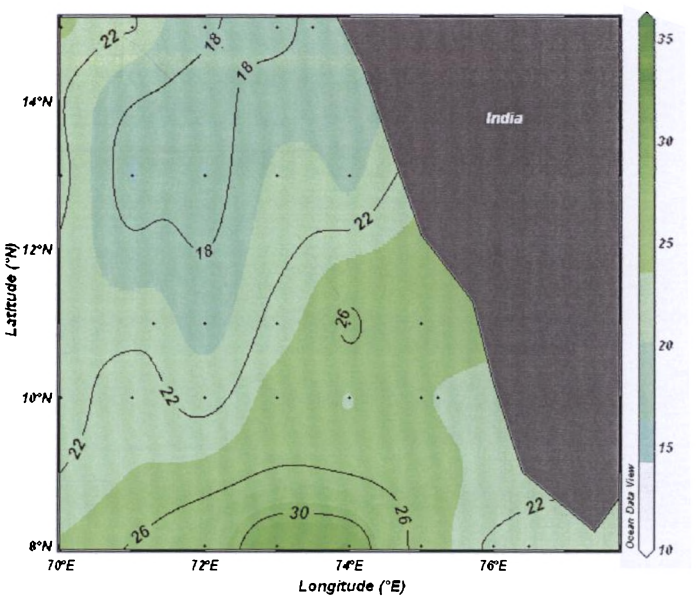

Fig.5.2. Distribution of mixed layer depth (m) during March April

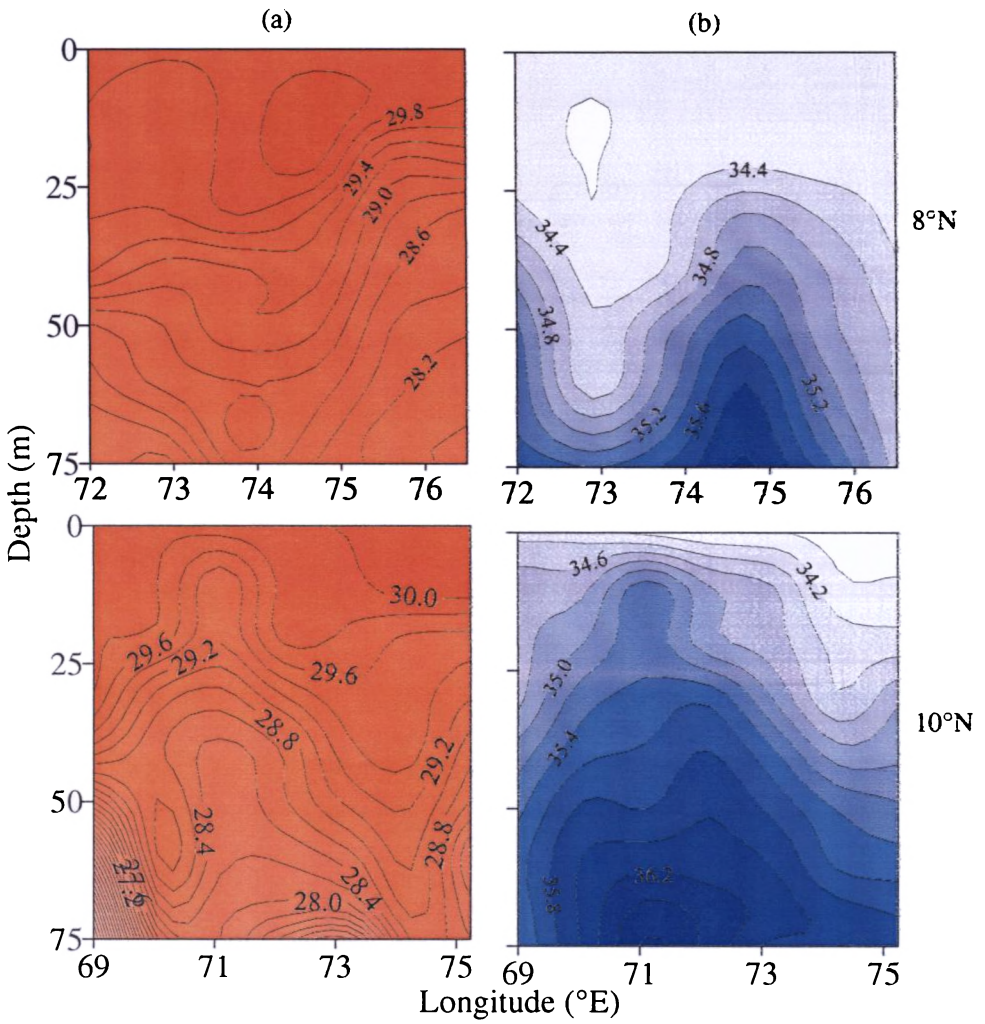

Fig. 5.4. Vertical distribution of (a) Temperature (b) Salinity

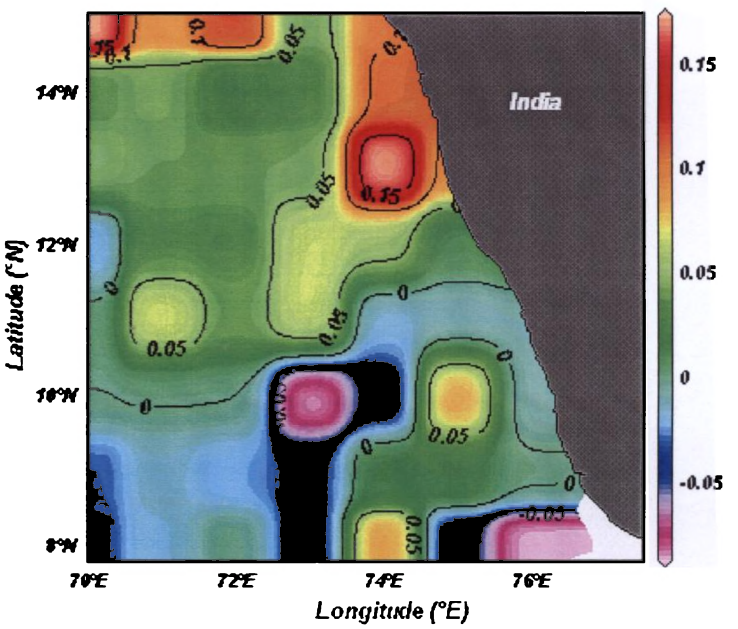

Fig.5.5. Temperature tendency in Mixed Layer (x 10-5) integrated over the entire mixed layer depth. Units are in °C m s^{-1}.

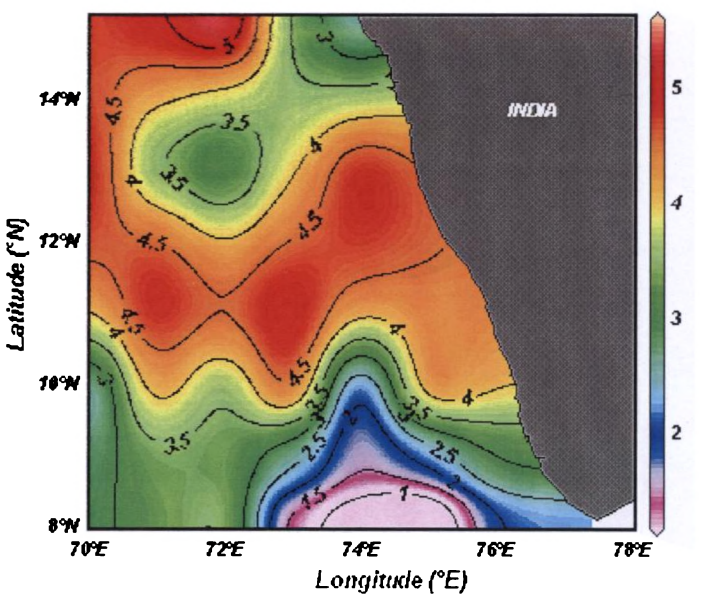

Fig.5.6. Surface Flux ($x10^{-5}$) from the observations. Positive means heat flux into the ocean. Units are in °C m s^{-1}

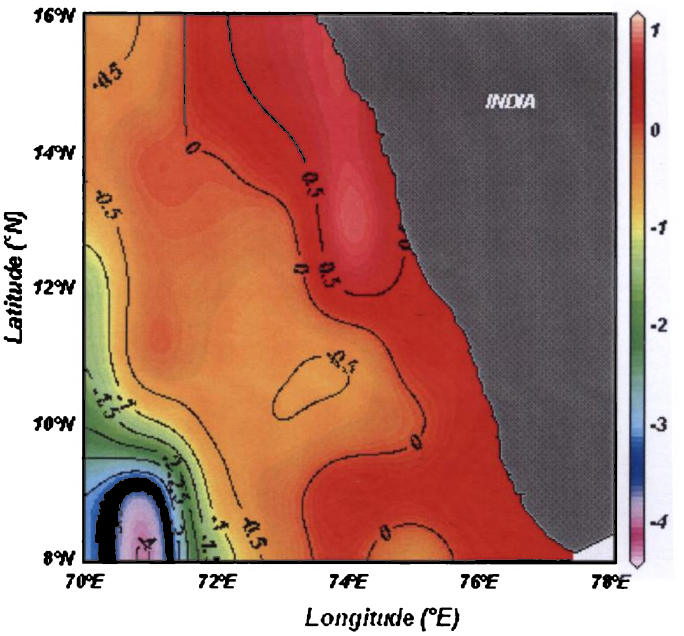

Fig..5.7. Horizontal advection integrated over the mixed layer ($x10^{-5}$) Units are in °C m s^{-1}

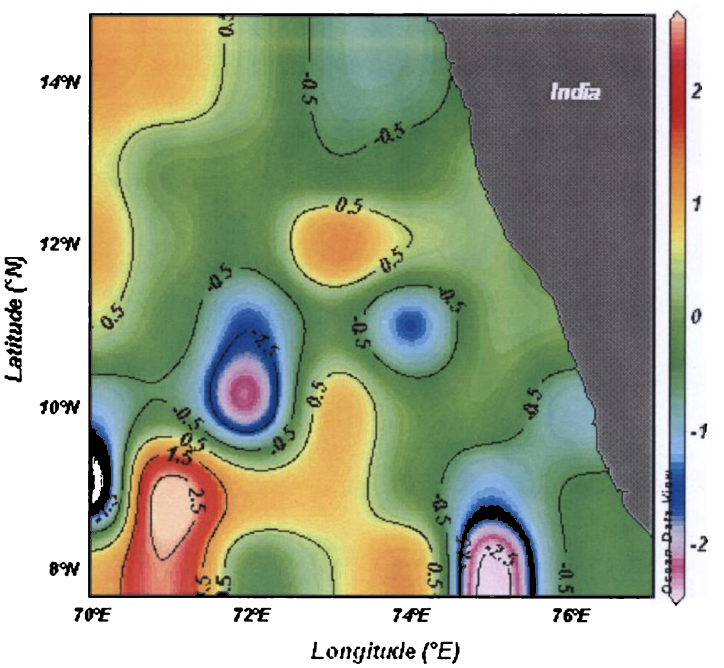

Fig.5.8. Diffusion term ($x10^{-5}$) vertically integrated over the mixed layer. Units are in °c m s-1.

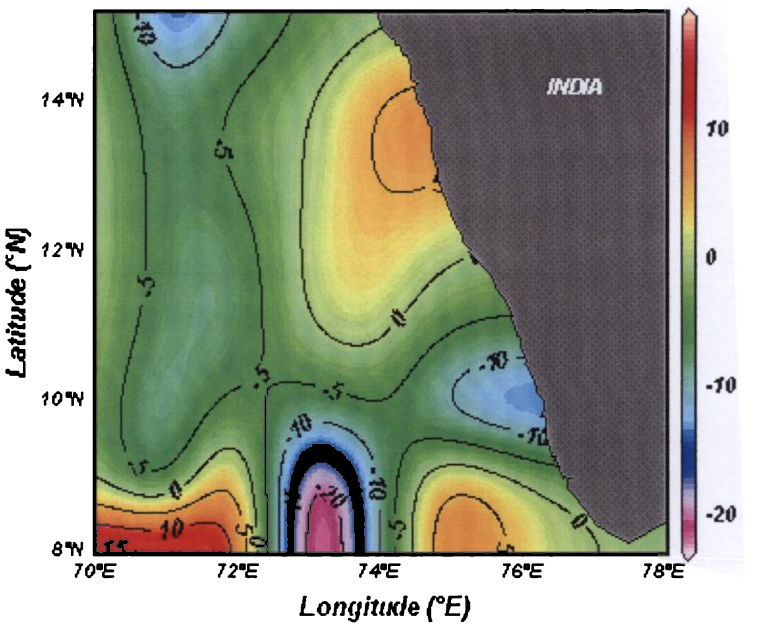

Fig.5.9. Mixing term ($x10^{-5}$) vertically integrated over the mixed layer. Units are in °C.m s^{-1}

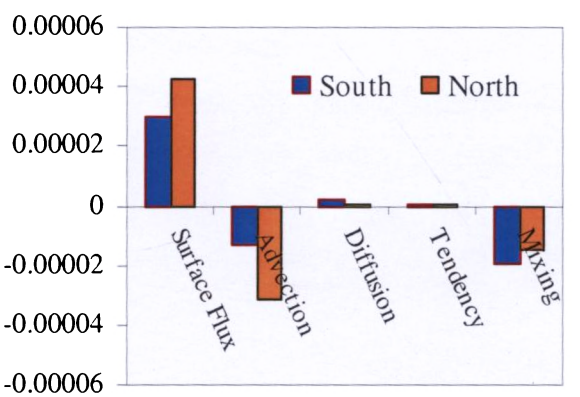

Fig.5.10. The heat budget averaging over B_N and B_S of the study region

****

Chapter 6

Heat Budget of the Arabian Sea Warm Pool during the Collapsing Stage

Contents

Heat budget of the upper ocean is an important factor to understand the various atmospheric and oceanic processes that controls the mixed layer temperature. The relative importance and contribution of various processes in the total heat budget of the mixed layer of ASWP were also studied during the collapsing stage of the warm pool (May-June, 2005) and discussed.

6.1 Theory

The mixed layer temperature tendency of the upper ocean is controlled by the surface heat fluxes, horizontal advection, eddy diffusion, vertical mixing and entrainment. The evolution of mixed layer temperature (T) can be written as,

$$\partial T/\partial t + [u_1 \partial T/\partial x + v_1 \partial T/\partial x] + w\partial T/\partial z =$$

$$[Q/h\rho C_p] + \partial/\partial z(K_h.\partial T/\partial z) + A_h(\partial^2 T/\partial x^2 + \partial^2 T/\partial y^2)$$

The individual terms in the mixed layer equation and method of computation are described in section 1.1.1.

The horizontal velocity components $u_T(u_g + u_e), v_T(v_g + v_e)$ include the geostrophic and Ekman velocity. Computation of geostrophic currents is described in section 2.2.1. The Ekman components are computed from observed winds using the equation,

$$u_e = V_0 \cos(\Pi/4 + ((\Pi/D_E).z)\varepsilon^{(\Pi/DE.z)}$$

and

$$v_e = V_0 \sin(\Pi/4 + ((\Pi/D_E).z)\varepsilon^{(\Pi/DE.z)}$$

where $V_o = 0.79\times10^{-5}(W^2/D_E.f)$, W is the wind speed (ms^{-1}) and D_E $(\Pi\sqrt{2.(A_z/f)})$ is the Ekman depth, f is the magnitude of the Corilois force and A_z is the eddy viscosity. The effect of wind and subsequent Ekman current is computed and included with the geostrophic currents. It has been found the magnitude of the Ekman velocity is higher during this time.

Four stations near the coast are avoided from the present analysis because they yielded unreasonably large values in the heat budget terms. Also the coastal stations are found having difficulty in resolving the processes well.

6.2 Results and Discussion

During May, the winds were southwesterly in the open ocean region (2 m/s) but became strong northwesterly winds in the coastal region of SEAS. During June, strong southwesterly winds (>10 m/s) were observed in the open ocean region and northwesterly winds in the coastal region (Fig.3.13a). The winds show a rapid increase in magnitude from May to June (Fig.3.13b). With the onset of the SEM, steady winds prevail over the north Indian Ocean. The wind blowing parallel to the coast generates an offshore transport.

The SST is varied from 30.2° C to 31.4° C, with meridionally aligned isotherms having higher temperatures in the northwest (Fig.6.1a). Many studies have reported that during late May and early June. The SST is > 30° C in the offshore areas and tends to decrease towards the coast (Ramsey Babu et al., 1991). The surface isothermal layer was warmer towards north than the south. The thermal structure, north of 10°N was vertically homogenous with a temperature greater than 30°C and below 30 °C in the top 25m. In regions south of 10°N, the temperature below 30°C was observed during this season. The surface salinity exhibited zonally aligned isohalines in the south and relatively high saline waters (>35.8) in the north (Fig.6.1b). The isothermal layer and thermocline along 8°N and 10°N transects were shifted towards the coast where the ILD was 30m. The 20°C isotherm was also shifted to shallower depth along 8°, 10 ° and 11.5°N but was observed in deeper depths (Fig.3.11 (a) & (b)). During this time, MLD greater than 30 m was observed in the north and comparatively shallow (25m) in the southern SEAS (Fig.6.2)

6.3 Heat Budget of the Mixed Layer

6.3.1 Surface flux

The variation of the surface flux in the SEAS is related to the monsoon system. Before the onset of the southwest monsoon, the sky over the SEAS is relatively clear with less cloud cover and thus more shortwave radiation can penetrate into the upper layer of the ocean. On the other hand, an increase in cloudiness due to the onset of the southwest monsoon significantly decreases the shortwave radiation.

The surface heat fluxes, which is a sum of downward shortwave radiation, upward long wave radiation, sensible and latent heat fluxes show that there is a net heat gain in the northern part of the domain while

there is a net cooling in the southern part (Fig.6.3). The mixed layer temperature tendency shows a slight warming in the northern part of the domain, while cooling in the south except in a small region in the southeast of the domain (Fig.6.4). Thus the mixed layer temperature tendency generally follows the surface heat flux in the mixed layer.

6.3.2 Horizontal Advection

The advection shows that there is a slight warming by the horizontal transport of heat in the northeastern part of the domain (6.5). The surface heat fluxes show a warming of maximum amplitude at the central northern part of the domain, whereas the tendency shows a warming oriented mainly in the northeastern part. The advection has a moderate warming effect in this area and thus may equally influence in the mixed layer temperature tendency term. The central and southern part of the domain shows a general cooling by the advective heat transport.

6.3.3 Vertical Mixing

The vertical heat dissipation in the mixed layer shows a general cooling centered on the 74°E and 10°N (Fig.6.7). This resembles the location where the net surface cooling by the heat loss to the atmosphere is a maximum. Thus the surface cooling in this region of the mixed layer resulted a mixed layer depth deepening (greater than 30 m) and heat dissipation in the surface mixed layer in this region. The western part of the domain, however, shows vertical heat dissipation with a warming effect.

6.3.4 Diffusion

The horizontal heat dissipation, the diffusion term, shows a warming in the southern and a cooling in the northern part of the domain (Fig.6.6). The magnitude of individual mixed layer heat budget terms are compared with an

area average carried out over a box of northern (11°-15°N) and southern part (8°-11°N) the domain separately and is shown as a bar diagram (Fig.6.8). It can be seen that there is a general balance exist between the individual terms in the heat budget of the surface mixed layer. The northern part of the domain has net heat gain which is balanced by a net heat loss in the vertical mixing term. However the horizontal advection plays a moderate role to bring heat into the mixed layer of the domain and is resulted in a net positive tendency in the mixed layer temperature. The horizontal diffusion however has a slight cooling effect in the mixed layer.

6.4 Conclusion

In the southern part of the SEAS, all the terms looked opposite in sign compared to its north. The surface heat flux has cooling effect while the vertical mixing, as an area average of the entire southern domain, has a net warming effect. The advection term has a surface cooling effect while diffusion has negligible role. This is in contrast with the heat budget observations during March-April in the same region where the diffusion had a significant warming effect in the mixed layer which is not found equally in the present set of data. Thus the magnitude of eddy diffusion depends up on the presence of meso-scale features in the study region.

Thus from the analysis it is clear that, the SEAS has two distinct regions in terms of surface heat budget. In the northern part, the dominant mechanism of mixed layer warming is the surface heat fluxes while in the southern part the advective, diffusive and vertical mixing redistributes the surface heat fluxes and evolves a resultant tendency in the mixed layer temperature.

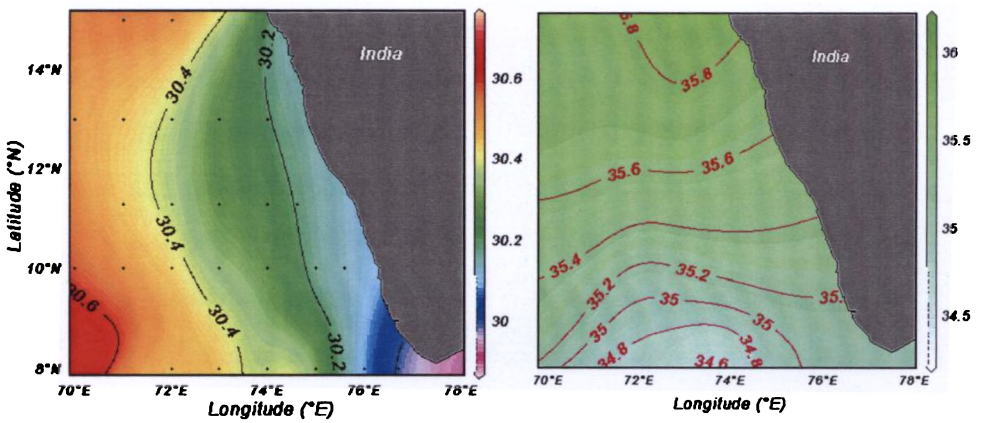

(a) **(b)**

Fig.6.1. Distribution of **(a)** Temperature (°C) and **(b)** Salinity during the observation period

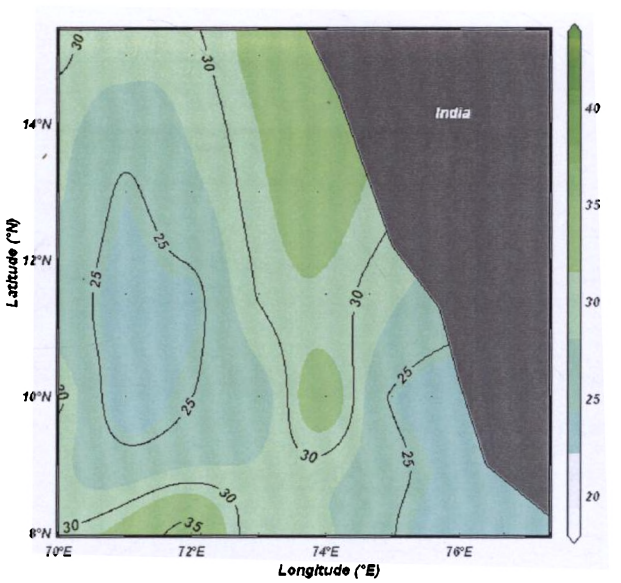

Fig.6.2. Mixed Layer depth (m) of the study region

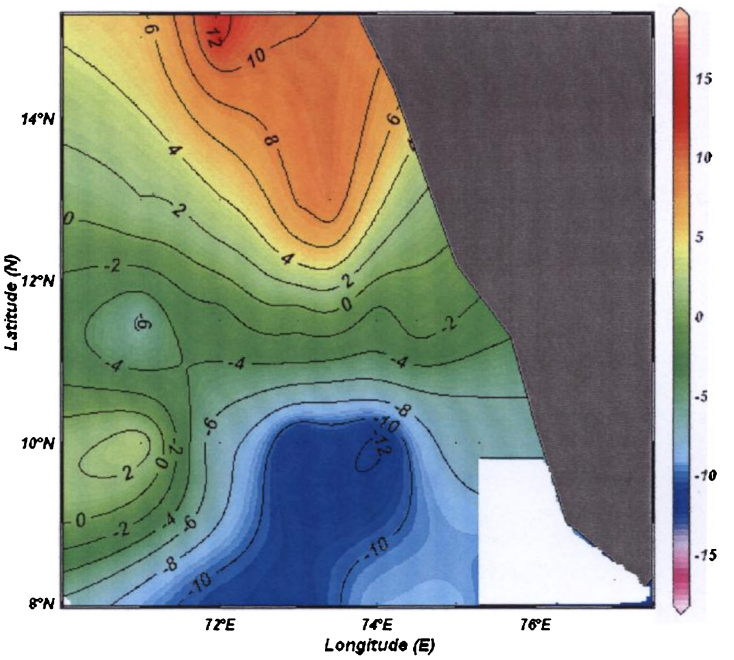

Fig.6.3. Surface Flux ($x10^{-5}$) from the observations. Positive means heat flux into the ocean. Units are in °C m s^{-1}

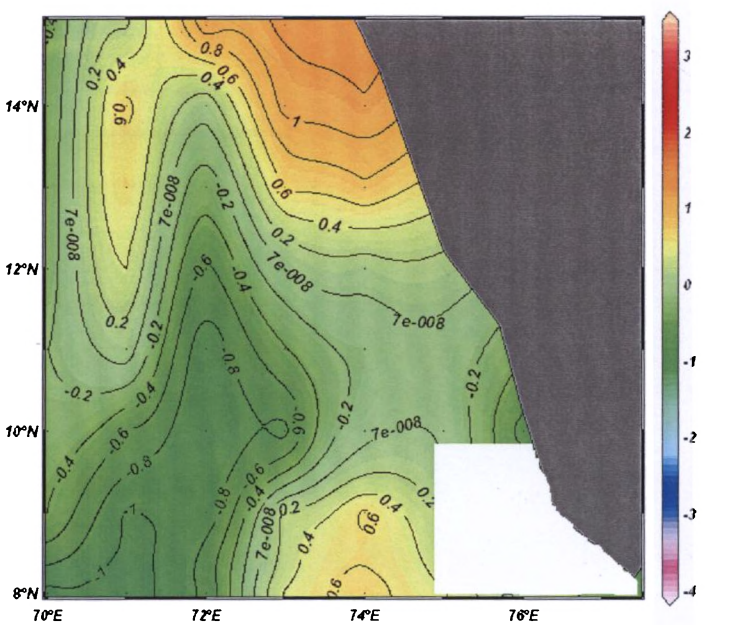

Fig.6.4. Temperature tendency in Mixed Layer (x 10-6) integrated over the entire mixed layer depth. Units are in °C m s^{-1}.

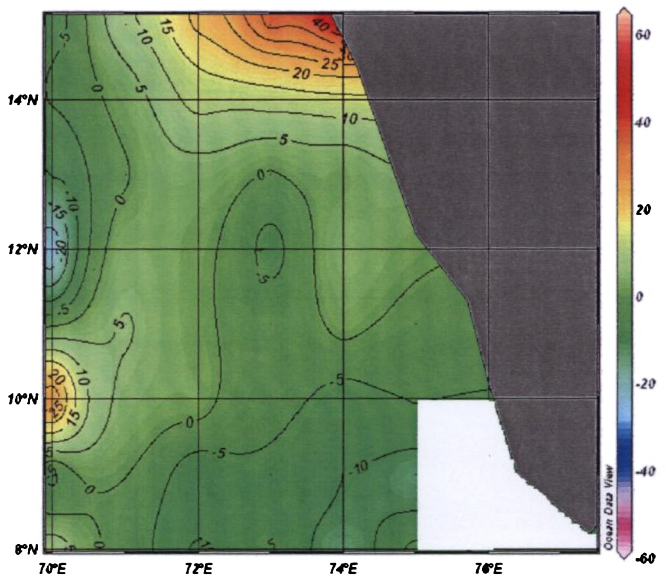

Fig.6.5. Horizontal advection integrated over the mixed layer ($x10^{-6}$) Units are in °C m s^{-1}

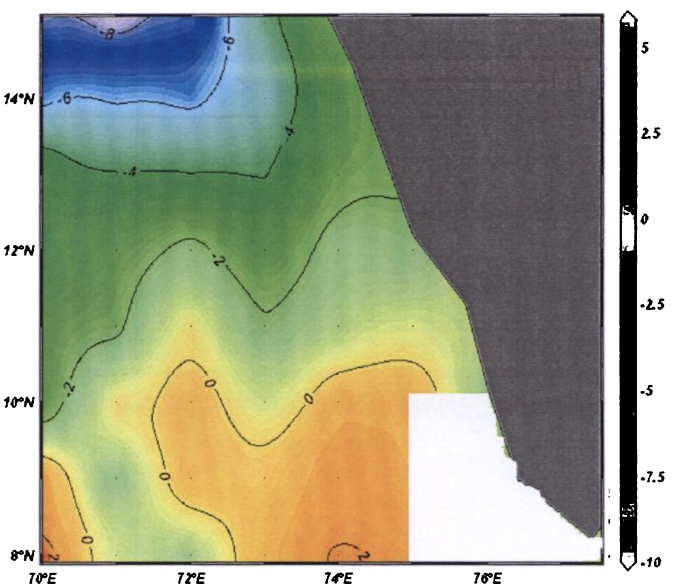

Fig.6.6. Diffusion term ($x10^{-6}$) vertically integrated over the mixed layer. Units are in °c m s-1.

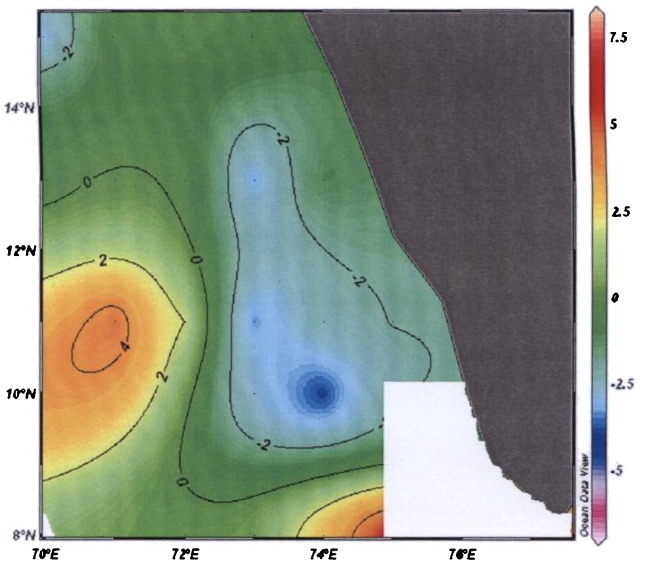

Fig.6.7. Mixing term ($x10^{-5}$) vertically integrated over the mixed layer. Units are in °C.m s^{-1}

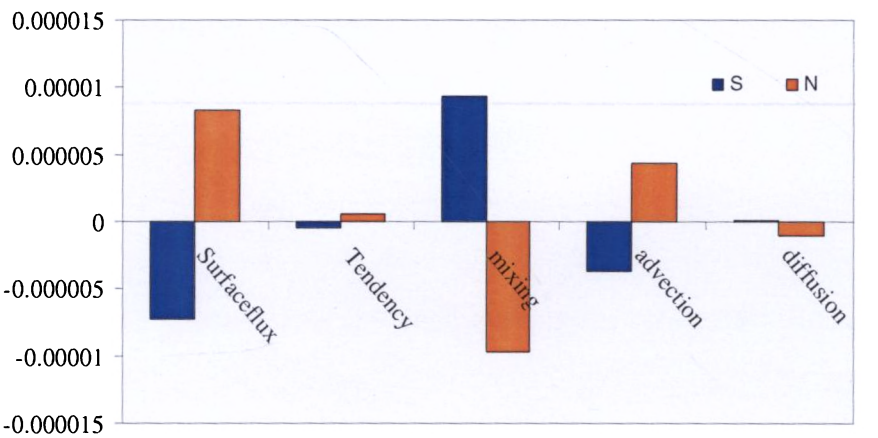

Fig.6.8. The heat budget averaging over the south and north of the SEAS

****

Chapter 7

Summary and Conclusion

Heat budget of the ASWP and the associated hydrography of the region were investigated using *in situ*, satellite and climatological data sets. The theoretical approach for the present work is that, the mixed layer temperature tendency (change) of the upper ocean is mainly controlled by the surface heat fluxes, horizontal advection, eddy diffusion, vertical mixing and entrainment. Based on this, mathematical form of mixed layer temperature evolution is developed and applied in the ASWP region. Temperature tendency in the mixed layer is computed from satellite SST. Horizontal advection of heat including the geostrophic and Ekman components was computed (Centered Finite Difference Scheme) using in situ data on wind, temperature and salinity. The eddy induced diffusion is computed from Topex/Poseidon SSHA data. The SSHA is the deviation from the mean geopotential height (dynamic height) and thus it is assumed that the removal of the mean flow remains the fluctuation of the mean flow primarily driven by eddies. A vertical mixing coefficient (K_h) of the mixed layer is estimated using K-Profile parameterization (KPP).

Hydrography and circulation of the SEAS during different stages of the ASWP were studied. Most of the features and structure of the temperature and salinity in the SEAS evidenced in an *in-situ* observation similar to that from the climatology. The salient features in the hydrography of the SEAS include the presence of warm pool during March-May, intrusion of low-salinity and high-salinity waters, presence

of thick barrier layer and the thermal inversion during December. The SEAS has a seasonal cycle in salinity, with high-salinity water in the subsurface depth and low saline water in the surface during December to April. Upwelling starts in May-June and downwelling during December-March, in accordance with the eddies and circulation. The upwelling promotes the annihilation of warm pool in the SEAS. The circulation in the SEAS is characterized by the presence of seasonally reversing coastal current and westward propagation of anticyclonic eddies, which are driven by local and remote forcings. Present study explains the mechanism by which the low salinity water enters into the SEAS during December and March-April.

Air sea fluxes and hydrography of the NEAS and SEAS are discussed, and explained the role of salinity in the evolution of ASWP. Cold dry northeasterly winds, which cause extensive cooling over NEAS, remain very week over the SEAS during the entire winter. Weak winds caused due to the orographic effects of Western Ghats considerably decrease the loss of heat from the SEAS and keep it warmer. As a result SST in the SEAS was warmer (~ 2°C) than NEAS due to the net heat gain during December-January. Thus the initial warming in the SEAS is due to the weak winter cooling and no direct influence of salinity is evidenced in the observation. But the low saline waters from the BoB may provide favorable condition for the intensification of SST. During March-April, NEAS receives comparatively large amount of heat than the SEAS, but the progressive warming is higher in the SEAS. The presence of low saline water and the thick BL (25m) in the SEAS has a major role in the warming. The interesting feature is that the spatial extension and thickness of the warm water exactly coincides with the low saline patch,

again pointing to the significance of low saline water in the formation of warm pool.

The southern part of the SEAS is an eddy prominent region, with horizontal dimensions in the range of 200 to 300 km and vertical extent of few hundreds of meters. These eddies present in the southern part of the region may play a major role on the evolution of ASWP. The relative importance and contribution of various processes to the total heat budget in mixed layer of ASWP were studied during spring intermonsoon (March- April, 2004). In the northern part of the ASWP, the surface heat flux is dominant in mixed layer warming while advection plays a role in spreading the warm water from coastal regions to far offshore. In the southern part of the ASWP, the eddy induced horizontal mixing provides substantial amount of heat spreading, which influences the mixed layer temperature evolution. Thus observations carried out in the present study suggest that a detailed 3-Dimensonal model is necessary for the thorough description of the mixed layer processes in the ASWP. The study also categorizes various regions in the ASWP according to the significance of each mixed layer process.

In the collapsing stage, surface heat fluxes are dominant and controls the mixed layer temperature tendency in the northern part. The temperature tendency shows a slight warming in the region, while cooling in the south except for a small region of warming in the southeast. Thus, in the north the mixed layer temperature tendency is generally defined by the surface heat flux. In the southern part of the SEAS, the surface heat flux has cooling effect while the vertical mixing, has a net warming effect. The advection term has a surface cooling effect while diffusion has negligible role. This is in contrast with the heat budget observations

during March-April in the same region where the diffusion had a significant warming effect in the mixed layer. Thus the magnitude of eddy diffusion depends up on the presence of meso-scale features.

In conclusion, "SEAS has two distinct regions in terms of surface heat budget. In the northern part the dominant mechanism of mixed layer warming is the surface heat fluxes while in the southern part the advective, diffusive and vertical mixing redistributes the surface heat fluxes and evolves a resultant tendency in the mixed layer temperature".

Concluding Remarks

The SEAS has several distinguishing features that make it a unique and dynamic region in the north Indian Ocean. For a prospective study on the dynamics and thermodynamics of the SEAS and the ASWP, there is a need for continuous monitoring of oceanic as well as atmospheric parameters. Only with such comprehensive observed datasets, the processes during winter, spring and the monsoon onset period can be described precisely. Moreover, such datasets would be useful in evaluating regional models in Indian Ocean. Also, Mesoscale processes (eddies) in the upper layers of the SEAS strongly influence the mixed layer processes of the ASWP. Thus it is suggested that, only high resolution models embedded with mesoscale features could precisely explain the mixed layer processes of the ASWP.

****

References

Abram, N.J, M.K. Gagan, M.T. McCulloth, J. Chappell, and W.S. Hantoro (2003) Coral reef death during the Indian Ocean Dipole linked to Indonesian Wildfires.Sci., 952-955.

Ananthakrishnan, R., V. Srinivasan, A. R. Ramakrishnan, and R. Jambunathan (1968) Synoptic features associated with onset of southwest monsoon over Kerala. Forcasting Manual, FMU Rep., Tech. Rep. IV-18.2, India Meteorological Department, Pune, India.

Anonymous (2001) Arabian Sea Monsoon Experiment (ARMEX): Science plan. Department of Science and Technology, New Delhi.

Antonov, J. I., R. A. Locarnini, T. P. Boyer, A. V. Mishonov, and H. E. Garcia (2006) World Ocean Atlas 2005, Volume 2: Salinity. S. Levitus, Ed. NOAA Atlas NESDIS 62, Tech. rep., NODC, U.S. Government Printing Office, Washington, D.C., 182pp, Available online at http://www.nodc.noaa.gov/OC5/WOA05/pr woa05.html.

Antony, M. K., G. Narayana Swamy, and Y. K. Somayajulu (2002) offshore limit of coastal ocean variability identified from hydrography and altimeter data in the eastern Arabian Sea. Cont. Shelf Res., 22(17), 2525–2536, doi: 10.1016/S0278-4343(02)00100-0.

Ardnuy, P., Cuddapth. P, and H. L Kyle (1987) Remote sensing of water vapor convergence, deep convection and precipitation over the tropical Pacific Ocean during 1982-83 El Nino. J. Geophys.Res., 92 14204-14216

Banse, K. (1968) Hydrography of the Arabian Sea Shelf of India and Pakistan and effects on demersal fishes. Deep–Sea Res. and Oceanogr. Abstr., 15(1), 45–48, doi:10.1016/ 0011-7471(68)90028-4.

Bauer, S., Hitchcock, G.L., Olson, D.B., 1992. Response of the Arabian Sea surface layer to monsoon forcing. In: Desai, B.N. (Ed.), Oceanography of the Indian Ocean. Oxford & IBH, New Delhi, pp. 659–672.

Borqne, R.L., R.T Barber, T. Delcroix, H.Y. Inoue, D.J. Mackey, and M Rodier (2002) Pacific warm pool and divergence: temporal and zonal variations on the equator and their effects on the biological pump. Deep Sea Res. I, 2471-2512.

Bruce, J. G., D. R. Johnson, and J. C. Kindle (1994) Evidence for eddy formation in the eastern Arabian Sea during the northeast monsoon. J. Geophys. Res., 99(C4), 7651–7664.

Clark, C.O., J.E.Cole, and P.J. Webster (2000), Indian Ocean SST and Indian Summer rainfall: Prdictive relationships and their decadal variability,J.Climate, 13(14),2503-2519

Darbyshire, M. (1967) The surface waters off Kerala, southwest India. Deep Sea Res., 14(3), 295–320, doi:10.1016/0011-7471(67)90073-3.

Deepa, R., P. Seetaramayya, S. G. Nagar, and C. Gnanaseelan (2007) On the plausible reasons for the formation of onset vortex in the presence of the Arabian Sea mini warm pool. Curr. Sci., 92(6), 794–800.

Doval, M.D. and D. A. Hansell (2000) Organic carbon and apparent oxygen utilization in the western South Pacific and the central Indian Oceans. Mar. Chem., 249-264.

Durand, F., D. Shankar, C. de Boyer Mont'egut, S. S. C. Shenoi, B. Blanke, and G. Madec (2007) Modelling the barrier-layer formation in the South–Eastern Arabian Sea. J. Climate, 20(10), 2109–2120, doi:10.1175/JCLI4112.1.

Durand, F., S. R. Shetye, J. Vialard, D. Shankar, S. S. C. Shenoi, C. Ethe, and G. Madec (2004) Impact of temperature inversions on SST evolution in the South–Eastern Arabian Sea during pre–summer monsoon season. Geophys. Res. Lett., 31, L01305, doi: 10.1029/2003GL018906.

Fairall, C.W., E.F. Bradley, J.S. Godfrey, G. A. Wick, J. B. Edson, and G.S. Young (1996) Cool skin and warm layer effects on sea surface temperature. J. Geophys Res. 101, 1295-1308.

Findlater, J. (1969) A major low-level air current near the Indian Ocean during the northern summer. Quarterly Journal of Royal Meteorological Society, 95, 362-380.

Gent, P.R and J.C. MC Williams (1990) Isopyncal Mixing in Ocean Circulation Models. J. Phys. Oceanogr. 20,150-155.

Godfrey, J. S., A. Alexiou, A.G. Ilahude, D.M. Legler, M.E. Luther, J. P. McCreary, Jr., G.A.Meyers, K. Mizumo, R. R. Rao, S. R. Shetye, J. H.Toole, and S. Wacogne (1995) The Role of the Indian Ocean in the Global Climate System: Recommendations Regarding the Global Observing system. Report of the Ocean Observing system Development Panel, Texas A&M University, College station, TX, USA, 89pp.

Godfrey, J. S., R. A. Houze Jr., R. H. Johnson, R. Lukas, J. L. Redelsperger, A. Sumi, and R. Weller (1998) Coupled Ocean-Atmosphere Response

Experiment (COARE): An interim report, J. Geophys. Res., 103(C7), 14,395–14,450

Gopalakrishna, V. V., Z. Johnson, G. Salgaonkar, K. Nisha, C. K. Rajan, and R. R. Rao (2005) Observed variability of sea surface salinity and thermal inversions in the Lakshadweep Sea during contrast monsoons Geophys. Res. Lett., 32, L18605, doi:10.1029/ 2005GL023280.

Gopalakrishna, V.V, R.R.Rao, K.Nisha, M.S.Gireesh Kumar, T.Pankajakshan, M.Revichandran Z. Johnson, K. Girish, N. Aneeshkumar, M. Srinath, S. Rajesh and C. K. Rajan Observed anomalous upwelling in the Lakshadweep Sea during the summer monsoon season of 2005. J. Geophy Res, 113 C05001, doi:10.1029/ 2007JC004240, 2008.

Grotzner, A., M. Latif, and T. P. Barnett (1998) A decadal climate cycle in the North Atlantic Ocean as simulated by the ECHO coupled GCM. J. Climate, 11, 831-847.

Halliwell, G. R., Jr. (1998) Simulation of North Atlantic decadal/ multidecadal winter SST anomalies driven by basin-scale atmospheric circulation anomalies. J. Phys. Oceanogr., 28, 5–21.

Hareesh Kumar P.V, K.V. Madhu Joshi, A. D. Sanilkumar, P. Rao, K.Anand, C.V. K Anilkumar, Prasada Rao (2008) Growth and decay of the Arabian Sea mini warm pool during May 2000: Observations and simulations, Deep Sea Res. I, doi:10.1016/j.dsr.2008.12.004

Hareesh Kumar, P. V, and B. Mathew (1997) On the heat budget of the Arabian Sea. Meteorol. Atmos. Phys., 62(3-4), 215–224, doi:10.1007/BF01029703.

Hareesh Kumar, P. V., and N. Mohan Kumar (1996) On the flow and thermohaline structure off Cochin during pre–monsoon season. Cont. Shelf Res., 16(4), 457–468.

Johannessen, O. M., G. Subharaju, and J. Blindheim (1981) Seasonal variation of the oceanographic conditions off the southwest coast of India during 1971–75. Fisk Dir. Skr. Ser. Hav Unders., 18, 247–261.

Joseph, P. V. and P. V. Pillai (1984) Air–sea interaction on a seasonal scale over north Indian Ocean–Part I: Inter-annual variations of sea surface temperature and Indian summer monsoon rainfall. Mauasam., 35, 323–330.

Jossia Joseph, K., M. Harikrishnan, G. Rajesh, and K. Premkumar (2005) Moored buoy observations in Arabian Sea warm pool. Mausam, 56(1), 161–168.

Kara, A.B., P.A Rochford, and H.E.Hurburt, 2000. An optimal definition for ocean mixed layer depth. Journal of Geophysical Research, 105, 16,803-16,821.

Kershaw, R. (1985) Onset of the southwest monsoon and sea surface temperature anomalies in the Arabian Sea. Nature., 315(6020), 561–563, doi:10.1038/315561a0.

Kershaw, R. (1988) The effect of sea surface temperature anomalies in a prediction of the onset of southwest monsoon over India. Quart. J. Roy. Meteorol. Soc., 144(480), 325–345.

Kitoh, A. (2002) Effects of large–scale mountains on surface climate – A coupled ocean–atmosphere general circulation model study. J. Meteorol. Soc. Japan, 80(5), 1165–1181.

Krishnamurti, T. N., P. Ardanuy, Y. Ramanathan, and R. Pasch (1981) On the onset vortex of the summer monsoon. Mon. Weather Rev., 109(2), 344–363.

Kurian, J., and P. N. Vinayachandran (2007) Mechanisms of formation of the Arabian Sea mini warm pool in a high–resolution Ocean General Circulation Model. J. Geophys. Res., 112, C05009, doi:10.1029/ 2006JC003631.

Large, W. G., J. C. McWilliams, and S. C. Doney (1994) Oceanic vertical mixing: A review and a model with a nonlocal boundary layer parameterization. Rev. Geophys., 32(4), 363–403.

Lau Ka-Ming and P.H. Chan (1986) The 40-50 day oscillation and ENSO: a new perspective. Bull.Am.Meterolol.Soc.67 533-534.

Lau, Ka-Ming and Chan Paul, H. (1988) Intraseasonal and interannual variations of Tropical Convection: A possible Link between the 40-50day Oscillation and Enso? J. Atmos. Sci, 506-521.

Li, T., Y. Zhang, C. P. Chang, and B. Wang (2001) On the relationship between Indian Ocean Sea surface temperature and Asian summer monsoon. Geophys. Res. Lett., 28(14), 2843– 2846.

Locarnini, R. A., A. V. Mishonov, J. I. Antonov, T. P. Boyer, and H. E. Garcia (2006) World Ocean Atlas 2005, Volume 1: Temperature. S. Levitus, Ed. NOAA Atlas NESDIS 61, Tech. rep., NODC, U.S. Government Printing Office, Washington, D.C., 182pp, Available online at http://www.nodc.noaa.gov/OC5/WOA05/pr woa05.html.

Luis, A. J., and H. Kawamura (2000) Wintertime wind forcing and sea surface cooling near the south India tip observed using NSCAT and AVHRR, Remote Sens. Environ., 73, 55–64.

Luis, A. J., and H. Kawamura (2002b) A case study of sea surface temperature-cooling dynamics near the Indian tip during May 1997, J. Geophys. Res., 107(C10), 3171, doi: 10.1029/2000JC000778.

Luis, J. A., and H. Kawamura (2003) Seasonal SST patterns along the west India shelf inferred from AVHRR. Remote Sens. Environ., 86(2), 206–215, doi:10.1016/S0034-4257(03) 00101-9.

Madhupratap, M., Gauns, Mangesh, Ramaiaha, N., Prasanna Kumar, S., Muraleedharan, P.M., De Sousa, S.N., Sardessai, S., Muraleedharan, Usha, 2003. Biogeochemistry of the Bay of Bengal: Physical, chemical and primary productivity characteristics of the central and western Bay of Bengal during summer monsoon 2001. Deep-Sea Research II 50, 881–896.

Masson, S., J. J. Luo, G. Madec, J. Vialard, F. Durand, S. Gualdi, E. Guilyardi, S. Behera, P. Delecluse, A. Navarra, and T. Yamagata (2005) Impact of barrier layer on winter spring variability of the southeastern Arabian Sea. Geophys. Res. Lett., 32, L07703, doi:10.1029/ 2004GL021980.

McCreary, J. P., P. K. Kundu, and R. L. Molinari (1993) A numerical investigation of dynamics, thermodynamics and mixed–layer processes in the Indian Ocean. Prog. Oceanogr., 31(3), 181–244.

Mittelstaedt, E. (1986) Upwelling regions. Landolt Bornstein, Group V, Vol.3, Sub volume, C, J.Sundermann, ed., Springer-Verlag, 349.

Nicholls, N. (1983) Predicting Indian summer monsoon rainfall from sea-surface temperature in the Indonesia-north Australia area. Nature (London) 306 576-577.

Nowlin Jr., W.D.and H.J. McLellan (1967) A characterization of the Gulf of Mexico waters in winter. J. Mar. Res. 25., 29-59.

Pankajakshan, T., and D. V. Rama Raju (1987) Intrusion of Bay of Bengal water into Arabian Sea along the west coast of India during north east monsoon, in Contributions in Marine Sciences, edited by T. S. S. Rao, R. Natarajan, B. N. Desai, G. N. Swami, and S. R. Bhat, Dr. S. Z. Qasim Sastyabdapurti felicitation volume, pp. 237–244, National Institute of Oceanography, Dona–Paula, Goa, India.

Prasad, T. G., and M. Ikeda (2002) The winter-time water mass formation in the northern Arabian Sea: A model study. J Phy Oceanogr, 32, 1028-1040.

Prasanna Kumar, S., and T. G. Prasad (1999) Formation and spreading of Arabian Sea high–salinity water mass, J. Geophys. Res., 104(C1), 1455–1464.

Prasanna Kumar, S., J. Narvekar, A. Kumar, C. Shaji, P. Anand, P. Sabu, G. Rijomon, J. Josia, K. A. Jayaraj, A. Radhika, and K. K. C. Nair (2004) Intrusion of the Bay of Bengal water into the Arabian Sea during winter monsoon and associated chemical and biological response. Geophys. Res. Lett., 31, L15304, doi: 10.1029/2004GL020247.

Qiu, B and S. Chen (2004) Eddy-induced heat transport in the subtropical North Pacific from Argo, TMI and Altimetry measurements. J. Phys. Oceanogr. 35, 458-473.

Qiu, B. (2002) The Kuroshio Extension system. Its large-scale variability and role in the midlatitude ocean-atmosphere interaction. J. Oceanogr. 58, 57-75.

Ramesh Babu, V., J. S. Sastry, V. V. Gopalakrishna, and D. V. Rama Raju (1991) Premonsoonal water characteristics and circulation in the east central Arabian Sea, Proc. Indian Acad. Sci. (Earth Planet. Sci.), 100(1), 55–68.

Ramesh Babu, V., M. J. Varkey, V. Kesava Das, and A. D. Gouveia (1980) Water masses & general hydrography along the west coast of India during early March. Indian J. Mar. Sci., 9(1), 82–89.

Rao, K. G., and B. N. Goswami (1988) Interannual variations of sea surface temperature over the Arabian Sea and the Indian monsoon: A new perspective Mon. Weather Rev., 116(3), 558–568.

Rao, P. S., and D. R. Sikka (2005) Intraseasonal variablity of the summer monsoon over the north Indian Ocean as revealed by the BOBMEX and ARMEX field programs, Pure Appl. Geophys., 162, 1481–1510, doi:10.1007/s00024-005-2680-0.

Rao, R. R., and R. Sivakumar (1999) On the possible mechanisms of the evolution of a mini-warm pool during the pre-summer monsoon season and the onset vortex in the southeastern Arabian Sea. Q. J. R. Meteorol. Soc., 125, 787–809.

Rao, R. R., and R. Sivakumar (2003) Seasonal variability of sea surface salinity and salt budget of the mixed layer of the north Indian Ocean. J. Geophys. Res., 108(C1), 3009, doi:10.1029/ 2001JC000907.

Rasmusson E. M., and T. H. Carpenter (1982) Variations in tropical sea surface wind fields associated with the southern Oscillation / El Nino; Mon.Weath.Rev., 110,354-384.

Reynolds, R. W., and T. M. Smith (1994) Improved global sea surface temperature analyses using optimum interpolation. J. Climate, 7(6), 929–948.

Saji, N.H., B.N. Goswami, P.N Vinaychandran, and T. Yamagata, (1999). A dipole mode in the tropical Indian Ocean. Nature, 360-363.

Sarma,V.V.S.S. (2006) The influence of Indian Ocean Dipole (IOD) on biogeochemistry of carbon in the Arabian Sea during 1997-1998. J.Earth Sys Sci., 433-450.

Sanilkumar, K. V., P. V. H. Kumar, J. Joseph, and J. K. Panigrahi (2004), Arabian Sea mini warm pool during May 2000, Curr. Sci., 86(1), 180–184.

Schott, F. A., and J. P. McCreary (2001) The monsoon circulation of the Indian Ocean. Prog. Oceanogr., 51(1), 1–123.

Schott, F., J. Reppin, J. Fischer, and D. Quadfasel (1994) Currents and transports of the Monsoon Current south of Sri Lanka, J. Geophys. Res., 99(C12), 25,127–25,142.

Schott, F (1983), Monsoon response of the Somali Current and associated upwelling.Prg.Oceanogr.,12(3), 357-381.

Seetaramayya, P., and A. Master (1984) Observed air–sea interface conditions and a monsoon depression during MONEX–79. Arch. Met. Geoph. Biocl., A 33(1), 61–67, doi: 10.1007/BF02265431.

Shankar, D., and S. R. Shetye (1997) On the dynamics of the Lakshadweep high and low in the southeastern Arabian Sea. J. Geophys. Res., 102(C6), 12,551–12,562.

Shankar, D., P. N. Vinayachandran, and A. S. Unnikrishnan (2002) The monsoon currents in the north Indian Ocean. Prog. Oceanogr., 52(1), 63–120.

Shankar, D., V. V. Gopalakrishna, S. S. C. Shenoi, F. Durand, S. R. Shetye, C. K. Rajan, Z. Johnson, N. Araligidad, and G. S. Michael (2004) Observational evidence for westward propagation of temperature inversions in the southeastern Arabian Sea. Geophys. Res. Lett., 31, L08305, doi:10.1029/2004GL019652.

Shenoi, S. S. C., D. Shankar, and S. R. Shetye (2004) Remote forcing annihilates barrier layer in southeastern Arabian Sea. Geophys. Res. Lett., 31, L05307, doi: 10.1029/2003GL019270.

Shenoi, S. S. C., D. Shankar, V. V. Gopalakrishna, and F. Durand (2005a) Role of ocean in the genesis and annihilation of the core of the warm pool in the southeastern Arabian Sea. Mausam, 56(1), 147–160.

Shenoi, S. S. C., D. Shankar, G. S. Michael, J. Kurian, K. K. Varma, M. R. Ramesh Kumar, A. M. Almeida, A. S. Unnikrishnan, W. Fernandes, N. Barreto, C. Gnanaseelan, R. Mathew, K. V. Praju, and V. Mahale (2005b) Hydrography and water masses in the southeastern during March-June 2003,J.Earth Syst.Sci.,114 (5),475-491.

Shenoi, S. S. C., P. K. Saji, and A. M. Almeida (1999a) Near–surface circulation and kinetic energy in the tropical Indian Ocean derived from Lagrangian drifters. J. Mar. Res., 57(6), 885–907.

Shenoi, S.S.C., Shankar, D. and Shetye, S.R. (1999b) On the sea surface temperature high in the Lakshadweep Sea before the onset of the southwest of monsoon. J. Geophys.Res., 104, 15703-15712.

Shetye, S. R (1984) Seasonal variability of the temperature field off the southwest coast of India, Proc. Indian Acad. Sci. (Earth Planet. Sci.). 93(4), 399–411.

Shetye, S.R. and S.S.C.Shenoi (1988). The seasonal cycle of surface circulation in the coastal North Indian Ocean. Proc.Indian.acad.Sci. (Earth planet.Sci.).97, 53-62

Shetye, S. R. (1993) The movement and implications of the Ganges – Brahmaputra runoff on entering the Bay of Bengal Curr. Sci., 64(1), 32–38.

Shetye, S. R., A. D. Gouveia, S. S. C. Shenoi, D. Sundar, G. S. Michael, A. M. Almeida, and K. Santanam (1990) Hydrography and circulation off the west coast of India during the Southwest Monsoon 1987, J. Mar. Res., 48(2), 359–378.

Shetye, S. R., A. D. Gouveia, S. S. C. Shenoi, G. S. Michael, D. Sundar, A. M. Almeida, and K. Santanam (1991a) The coastal current of western India during the northeast monsoon, Deep-Sea Res. Part A, 38(12), 1517–1529.

Shetye, S. R., S. S. C. Shenoi, A. D. Gouveia, G. S. Michael, D. Sundar, and G. Nampoothiri (1991b) Wind–driven coastal upwelling along the western boundary of the Bay of Bengal during the southwest monsoon. Cont. Shelf Res., 11(11), 1397–1408.

Shetye, S.R., A.D.Gouveia, D.Shankar, S.S.C.shenoi, P.N.Vinaychandran, D.Sundar, G. S.Michel and G.Nampoothiri (1996). Hydrography and circulation in the western Bay of Bengal during the Northeast Monsoon.J.Geophys.Res., 101(C6), 14011-14025.

Shetye, S. R., and A. D. Gouveia (1998) Coastal circulation in the north Indian Ocean (14,S– W), in The Sea, The global coastal ocean: Regional studies and syntheses, vol. 11, edited by A. R. Robinson and K. H. Brink, chap. 18, pp. 523–555, John Wiley & Sons, Inc., New York, USA.

Shetye, S. R., and G. S. Michael (1988) Satellite-tracked drifting buoy observations in the south equatorial current in the Indian Ocean. Proc. Indian Acad. Sci. (Earth Planet. Sci.), 97(2), 149–157.

Singh, O. P., and H. R. Hatwar (2005) Response of sea state to the monsoon onset. Mausam, 56(1), 59–64.

Smyth, W. D., D. Hebert, and J. N. Moum (1996), Local ocean response to a multiphase westerly wind burst, 2, Thermal and freshwater responses. J. Geophys. Res., 101(C10), 22,513– 22,534.

Sprintall, J., and M. Tomczak (1992), Evidence of the barrier layer in the surface layer of the tropics. J. Geophys. Res., 97(C5), 7305–7316.

Taylor, R. C.(1973) An atlas of Pacific island rainfall; Hawai Institute of Geophysics Report No.25.

Thadathil, P., and A. K. Ghosh (1992) Surface layer temperature inversion in the Arabian Sea during winter. J. Oceanogr., 48(3), 293–304.

Thadathil, P., P. M. Muraleedharan, R. R. Rao, Y. K. Somayajulu, G. V. Reddy, and C. Revichandran (2007) Observed seasonal variability of

barrier layer in the Bay of Bengal. J. Geophys. Res., 112, C02009, doi: 10.1029/2006JC003651.

Thompson, B., C. Gnanaseelan, and P. S. Salvekar (2006) Seasonal evolution of temperature inversions in the north Indian Ocean. Curr. Sci., 90(5), 697–704.

Tomczak, M., and J. S. Godfrey (2001) Regional Oceanography: An Introduction, 391 pp., Online PDF Version 1, available from http://www.es.flinders.edu.au/ _mattom/regoc/pdfversion.html.

Vinayachandran, P. N., and J. Kurian (2007a) Hydrographic observations and model simulation of the Bay of Bengal freshwater plume. Deep-Sea Res. Part I, 54(4), 471–486, doi:10.1016/ j.dsr.2007.01.007.

Vinayachandran, P.N., D.Shankar, J.Kurian, F.Durand and SSC Shenoi (2007b) Arabian Sea mini warm pool and the monsoon onset vortex. Curr Sci, 93, no 2,203-213.

Weare, B. C., P. T. Strub, and M. D. Samuel (1981) Annual mean surface heat fluxes in the tropical Pacific Ocean. J.Phys.Oceanogr.,11, 705-717.

Webster, P. J., and R. Lukas (1992) TOGA COARE: The Coupled Ocean–Atmosphere Response Experiment, Bull. Amer. Meteorol. Soc., 73(9), 1377–1416.

Webster, P. J., T. N. Palmer, V. O. Magana, J. Shukla, R. A. Tomas, T. M.Yanai, and A. Yasunari (1998) Monsoons: Processes, predictability and the prospects for prediction. J. Geophys. Res., 103, 14,451–14,510.

Weller, R. A., A. S. Fischer, D. L. Rudnick, C. C. Erikson, T. D. Dickey, J. Marra, C. Fox, and R. Leben (2002) Moored observations of

upper ocean response to the monsoon in the Arabian Sea during 1994– 1995. Deep Sea Res., (to appear).

Wiggert, J.D., R.R. Hood, K. Banse, J.C. Kindle (2005) Monsoon-driven biogeochemical processes in the Arabian Sea. Prog. Oceanogr. 65, 176–213.

Yang, S., and K. M. Lau (1998) Influences of sea surface temperature and ground wetness on Asian summer monsoon, J. Climate. 11(12), 3230–3246.

****

Publications

[1] S.Prasanna Kumar, Jayu Narvekar, Ajoy Kumar, C.Shaji, P.Anand, **P.Sabu**, G.Rijo, J.Josia, K.A.Jayaraj, A.Radhika and K.K.C.Nair, Intrusion of the Bay of Bengal water into the Arabian Sea during winter monsoon and associated chemical and biological response, *Geophysical Research Letters,* VOL. 31, L15304, doi: 10.1029/2004GL020247,2004.

[2] Satish Sahayak, R.Joythibabu, K.J.Jayalakshmi, H.Habeebrehman, **P.Sabu**, K. Prabhakaran, Rejomon George, P.Shaiju, Threisamma Joseph and K.K.C. Nair, Red tide of *Noctiluca miliaris* off south of Thiruvananthapuram subsequent to the 'stench event' at the southern Kerala coast, *Current Science*, VOL. 89, NO. 9, 10 November 2005.

[3] C.M.Laluraj, K.K.Balachandran, **P.Sabu** and U.P. Saramma, Persistent Volcanic Signature observed around Barren Isaland, Andaman Sea, India, *Marine Geophys Res,* doi 10.1007/s11001-006-9008-z, 2006.

[4] P.K.Karuppasamy, S.Balu, Simmy George, Vimala Persis, **P.Sabu** and N.G.Menon (2007). Distribution and abundance of the swarming crab *Charibdis (Goniohellenus) smithii* Macleay in the deep scattering layer of the eastern Arabian Sea. *Indian Hydrobiology, 10 (1)*: 165-170.

[5] R. Jyothibabu, C.R. Asha Devi, N.V. Madhu, **P. Sabu**, K.V. Jayalakshmy, Josia Jacob, H. Habeebrehman, M.P. Prabhakaran, T. Balasubramanian, K.K.C. Nair. The response of microzooplankton (20–200 μm) to coastal upwelling and summer stratification in the southeastern Arabian Sea, *Contnental Shelf Research* 28 (2008) 653–671.

[6] H. Habeebrehman, M.P. Prabhakaran, Josia Jacob, **P. Sabu**, K.J. Jayalaksmi, C.T. Achuthankutty, C.Revichandran, and P. Jasmine. Variability in biological responses influenced by upwelling events in the Eastern Arabian Sea, Journal of Marine Systems 74 (2008) 545–560.

[7] K.R.Muraleedharan, **P.Sabu,** K.A. Abdul Rasheed, S.P.Satheesh, C.Revichandran and K.K.C.Nair, Comparative study of the monsoonal air sea interaction of Arabian Sea and Bay of Bengal, *Presented in Asia Oceanica Geosciences Society (AOGS) 2nd Annual Meeting, Singapore.*

[8] **P. Sabu** and C.Revichandran, Role of various mixed layer processes on the evolution of Arabian Sea warm pool; A study based on insitu and satellite data *(International Journal of Marine systems).*

[9] C.M. Lalu Raj, **P. Sabu**, K.K.Balachandran, C.Revichandran, H. Habeebrehman, K.R. Muraleedharan. P.K.Dinesh Kumar and C.T. Achuthankutty, Biogeochemistry of the eastern Arabian Sea during spring intermonsoon (*Communicated to Estuarine Coastal & Shelf Science, Under Review).*

[10] P.K. Karuppasamy, **P. Sabu**, Josia Jacob, C.R. Asha Devi, H. Habeebrehman, M.P. Prabhakaran, Sumitha G, C.Revichandran, Rosamma Stephen and C.T.Achuthankutty. Plankton community associated with warm pool and upwelling regions of the southeastern Arabian Sea during the onset of summer monsoon (*Deep Sea Research-Part I, Under Review*).

[11] C. R. Ashadevi, R. Jyothibabu, **P. Sabu**, Josia Jacob, H. Habeebrehman, P.Prabhakaran, K. J. Jayalakshmi & C. T. Achuthankutty. Characterization of microzooplankton (20-200 μm) in the southeastern Arabian Sea from spring intermonsoon to

peak summer monsoon periods (*Communicated to Journal of Marine Systems, Under Review).*

[12] Pankajakshan, T., **P. Sabu**, PrasannaKumar, S., Murty, V.S.N., Muraleedharan, K.R., Bajish. C.C, Reddy, G.V., S.N. Gaonkar, M. Revichandran, Gopalakrishna, V.V., Revichandran, C., Muraleedharan, P.M., J. Antonoy, Suryanarayana, A., Sarma, M.S.S., Quality of Argo salinity data from the Indian Ocean (Communicated to Journal of Geophysical Research, Under Review).